The Nearby SuperNova Factory

G. Aldering, A. Howell, S. Loken, P. Nugent, S. Perlmutter
Lawrence Berkeley National Laboratory (LBNL)

P. Astier, D. Hardin, J.-M. Levy, K. Schahmaneche, R. Pain
Laboratoire de Physique Nucléaire et des Hautes Energies (LPNHE)

P. Antilogus, Y. Copin, G. Smadja
Institut de Physique Nucléaire de Lyon (IPNL)

G. Adam, R. Bacon, E. Pecontal
Centre de Recherche Astronomique de Lyon (CRAL)

SNFactory-GEN/02-01

The Blue Book

DRAFT 1.1 - January 20, 2003

DO NOT DISTRIBUTE

Contents

1 Science goals **9**

1 Probing Dark Energy with Supernovae 9

2 The Need for Improved Statistics at Low-Redshift 11

3 Converting Systematic Uncertainties into Statistical Uncertainties 18

4 Constraining Ω_M with the **SNfactory** 20

5 Galaxies 21

6 Science goals summary 22

2 Program definition **24**

1 Baseline program 24

2 SNIa context 26

2.1 Target Redshift Range 26

2.2 SN rate from the Galaxy luminosity function 26

3 Discovery 27

4 Spectro-photometry and follow-up 30

4.1 Supernovæ template spectrum 30

4.2 Galaxy spectrum and surface brightness 30

4.3 Sky brightness 31

4.4 Signal-to-noise estimates 33

4.5 Survey efficiency 34
5 Complementary Observations 36

3 Instrumental setup **41**
1 *SNfactory* telescopes 41
2 NEAT 44
3 SNIFS 45
3.1 Overview 45
3.2 Technical design 45
3.3 Technical implementation 47
4 Complementary instruments 54

4 Calibration procedures **58**
1 Extinction Correction under Photometric Conditions 63
2 Extinction Correction under Non-Photometric Conditions 64
2.1 The role of a parallel imager 66
2.2 Multicolor field-star monitoring 68
3 The need to monitor system stability 73
3.1 Imager-to-Spectrograph scaling 74
3.2 Imager wavelength shifts and bandwidth changes 76
3.3 Location of photometric calibration sources 77
4 Multicolor imaging implementation 78

5 Operating mode **82**
1 Detection 82
1.1 Reference Image 83

1.2 Data Transfer from Palomar to LBL . . . 83
1.3 Data Reduction of Palomar Images . . . 85
1.4 Search Image . . . 87
1.5 Subtractions . . . 88
1.6 Automated Scanning . . . 89
1.7 Human Scanning . . . 89
1.8 Cross Checks . . . 89
1.9 Confirmation Image . . . 90
1.10 Supernovae found to date by this method . . . 90
2 Assessment of *NEAT* Data . . . 91
3 From Detection through Observation . . . 91
3.1 *A priori* Classification . . . 91
3.2 *A priori* Priority . . . 92
3.3 Scheduling . . . 93
4 SNIFS Observations . . . 94
5 Global monitoring and data flow . . . 96
5.1 *SNfactory* running . . . 97

6 Software and Data analysis 103

1 Computers and related hardware . . . 103
1.1 *NEAT* related computing . . . 103
1.2 *SNIFS* related computing . . . 103
2 Detection Software . . . 105
3 Scheduler software . . . 105
4 UH software . . . 105
5 SNIFS software . . . 105

6 Automated SN Classification 106
6.1 General Approach 107
6.2 Program specifics 108
6.3 SN templates 109
6.4 Galaxy templates 109
6.5 Weighting functions 110
6.6 Run time 110
6.7 Program output 110
6.8 Plotting the results 110
6.9 Limitations 111

7 Project Timeline and Management **113**
1 Timeline 113
2 Management 114

8 Conclusion **116**

The Nearby Supernova Factory will lay the foundation for the next generation of experiments to measure the expansion history of the Universe. It will discover and obtain lightcurve spectrophotometry for ~ 300 Type Ia supernovae in the low-redshift end of the smooth Hubble flow. The search capabilities and the follow-up instrumentation are described in this proposal; they include wide-field CCD imagers on two 1.2-m telescopes, and an integral-field-unit optical spectrograph on a 2.2-m telescope. The dataset will serve as the premier source of calibration of the SN Ia width-brightness relation and the intrinsic SN Ia colors used for correction of extinction by dust. This dataset will also allow an extensive search for additional parameters which influence the quality of SNe Ia as cosmological probes. The lowest redshift SNe Ia from this program can be used to measure galaxy peculiar velocities and thereby constrain Ω_M.

Overview

The Nearby Supernova Factory (SNfactory) is a project to discover and obtain detailed lightcurve and spectral observations for over 300 nearby supernovae during the period 2003—2007. This project has been initiated by scientist at Lawrence Berkeley National Lab (LBNL) in the United States; IN2P3 and Centre de recherche en Astronomie de Lyon in France; Stockholm University in Sweden; and Centro Multidisciplinar de Astrofisica at the Instituto Superior Tecnico in Portugal. The SNfactory will concentrate on Type Ia supernovae (SNe Ia), the type which have recently been used to determine that the expansion of the universe is accelerating (see Fig. 1.). Type II supernovae (SNe II) will also be developed as more reliable distance indicators. Several aspects of the SNfactory set it apart from other supernova projects. Foremost among these is that supernovae will be discovered using a blind wide-area CCD-based survey; other nearby supernova projects target known galaxies but there is now evidence that this approach misses an important subset of supernovae. In addition, the SNfactory will coordinate discovery and follow-up observations, eliminating the delays and spotty early lightcurve coverage which typically results from follow-up of supernovae listed in the IAU Circulars. It is expected that with the SNfactory detailed follow-up of supernova candidates can begin within as little as 12 hrs of the discovery observations. Finally, SNfactory follow-up observations will use an integral field unit spectrograph, data from which can be used to construct both detailed flux-calibrated spectra and broadband images. The regular photometric spectral time series for nearby supernovae the SNfactory will generate will revolutionize the study of supernovae. This dataset will also eliminate several limitations (bandpass mismatch, wavelength-dependent slit losses, etc.) of all other currently available instrumentation used to study supernovae.

The primary goal of the SNfactory will be to determine those properties of SNe Ia affecting their use for cosmology. The most critical of these will be the search for deviations or extra parameters not accounted for by the lightcurve width — brightness relations currently used to standardize SNe Ia for use as cosmological distance indicators. If such deviations are found, it is expected that exclusion criteria or improved standardization methods based on lightcurve shapes and/or spectral features will be found to ameliorate the effect of deviant SNe Ia on measurements of the cosmological parameters.

The SNfactory will search for supernovae using CCD images obtained by JPL's Near Earth Asteroid Team (NEAT). NEAT setup includes two 1.2-m telescope, one at the 10,000 ft summit of Haleakala, Hawaii) working 18 nights per month and the other operating at Mt. Palomar with a larger CCD camera. We expect to discover several supernovae per night. NEAT data will be transferred in near realtime via high-speed Internet connection to Lawrence Berkeley Nation Lab (LBNL. Once there, the images will be processed and searched using automated software. Candidate supernovae will be screened interactively and assigned a preliminary follow-up priority. An important aspect of the SNfactory is that the selection of supernova candidates will be quantitative and traceable, something current surveys completely lack and which makes calculations of supernova rates and peculiarity fractions extremely difficult.

The most revolutionary aspect of the SNfactory — aside from the huge numbers of supernovae it will find — is the coordinated follow-up using instrumention tailored to the study of supernovae. Candidate supernovae found in the NEAT images must first be screened with spectroscopy to confirm the supernovae and reveal its type (Ia, II, Ib, Ic) and redshift. The SNfactory will not only discover supernovae closer to explosion that other surveys do, with a 12 hr turn-around it will also begin the follow-up much much sooner. Typically candidate supernovae are confirmed with imaging on subsequent nights, then reported to the IAU Circulars, and then observed spectroscopically with regular – but infrequently — scheduled time or director's discretionary time (requiring a proposal for each supernova and the availability of the right instrumentation). This process can easily stretch on for a week or more after discovery. The SNfactory plans to have at least two telescopes with optimal instrumentation available every night, waiting to be fed by the stream of supernova candidates coming from the two NEAT sites.

Traditionally supernovae have been followed with $BVRI$ photometry, and spectra beyond the initial confirmation spectrum are rare. The SNfactory will change all that. Using a integral field unit on a two-channel (blue & red) optical spectrograph, the SNfactory's **S**uper**N**ova **I**ntegral **F**ield **S**spectrograph (**SNIFS**; under construction in France) equipped with LBNL's red-enhanced CCD's, will allow spectroscopy of supernovae at all epochs. Because these spectra will be spectrophotometric, $UBVRIZ$ photometry can be synthesized from these spectra, without the uncertainties due to photometric color terms and K-corrections (the latter usually based on non-spectrophotometric spectra). **SNIFS** will retain one advantage of the traditional approach, which allows surrounding field stars to be used for flux scaling when conditions are non-photometric, by also having an imager which integrates on the field immediately surrounding each supernova and having the exact same exposure as the integral field unit.

Chapter 1

Science goals

1. Probing Dark Energy with Supernovae

A coherent view of the universe is emerging in which a mysterious form of "dark energy" accounts for about 2/3 of the total energy density in the Universe. Direct evidence for this radical conclusion comes from distance measurements of Type Ia supernovae (SNe Ia; see Fig. 1) which indicate the expansion of the Universe is not slowing down as would be expected in a Universe filled with only matter and radiation Perlmutter *et al.* (1999), Riess *et al.* (1998). Further support for this result has come from recent measurements of the CMB indicating a flat universe, combined with determinations of $\Omega_M \sim 0.3$ from structure formation.

The most natural candidate for this dark energy was the cosmological constant, or vacuum energy, which exhibits the required large negative pressure with $w \equiv p/\rho = -1$. However, attempts to compute the energy of the quantum vacuum amount to 10^{55} times the observed density (or 10^{120} times, depending on the symmetry-breaking scale chosen). New physics is required to cancel this contribution either exactly or partially. In light of the incredible fine tuning problem that a partial cancellation over 55 orders of magnitude presents, complete cancellation seems to many theorists more likely — and a non-cosmological-constant dark energy would then be required at the small level observed. There are many other potential candidates for the dark energy which include but are not limited to quintessence (a rolling scalar field) Caldwell, Dave & Steinhardt (1998), Zlatev, Wang & Steinhardt (1999) and the effects of extra macroscopic dimensions Arkani-Hamed *et al.* (2000). Unfortunately, there is no current data that would help narrow the field among the myriad theoretical alternatives.

SNe Ia remain the most mature cosmological distance indicator, and therefore, offer the best means of experimentally probing the properties of the dark energy *now*. Their cosmological use was developed in the early 1990's by the Supernova Cosmology Project (SCP), paving the way

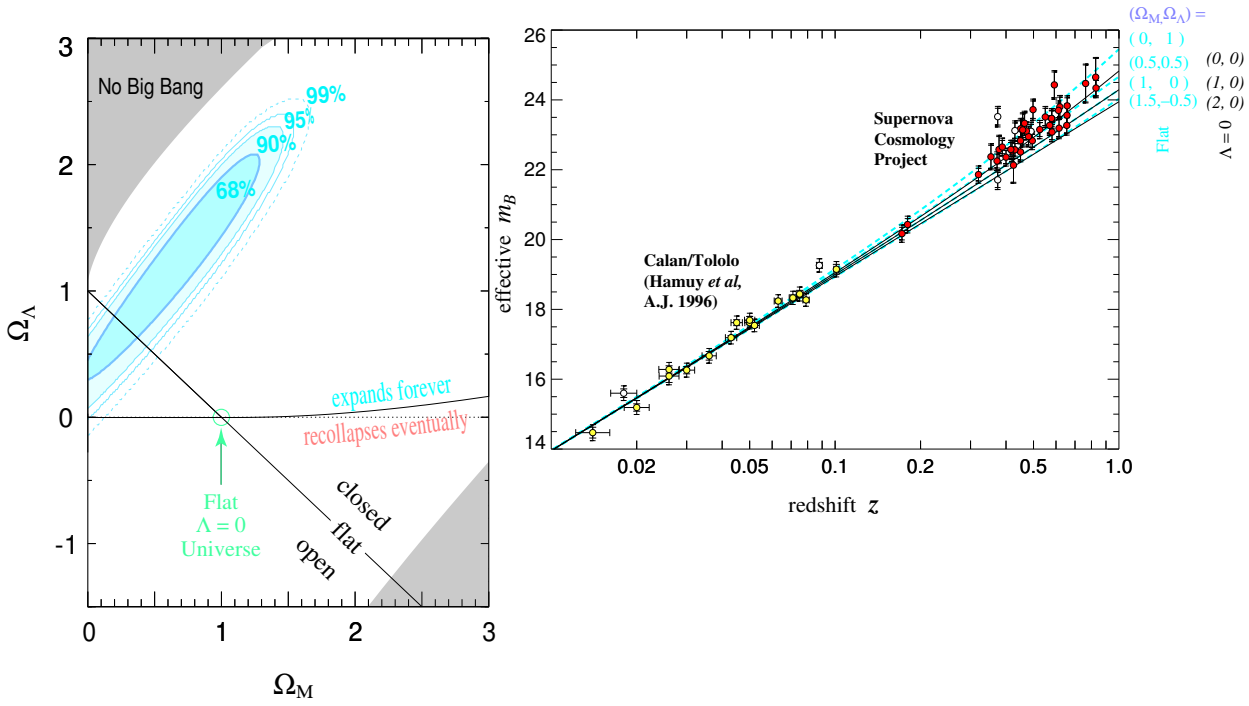

Fig. 1.— **Cosmological constraints from Type Ia supernovae:** Hubble diagram (brightness vs. redshift) and resulting constraints on Ω_M and Ω_Λ from 42 high-redshift Type Ia supernovae from Perlmutter *et al.* 1998b. At left, the 68%, 90%, and 99% confidence regions for an unconstrained fit for Ω_M and Ω_Λ are shown. For a flat universe only a cosmological constant or other form of dark energy can explain the data. Even without assuming a flat universe a cosmological constant is hard to avoid for any reasonable choice of Ω_M. At right, the Hubble diagram of the current SCP dataset of Type Ia supernovae is shown. The low-redshift SNe Ia shown are most of those currently available that are suitable for analysis using the same methods as used for the high-redshift SNe Ia.

for the discovery of dark energy Perlmutter *et al.* (1997), Perlmutter *et al.* (1998), Perlmutter *et al.* (1999). Now similar developmental efforts are needed so that the next order of magnitude improvement of the experimental constraints on the properties of dark energy can be made using SNe Ia.

Progress must be made on two fronts, at a level which cannot be pursued with existing programs alone: First a large number of *nearby* SNe must be observed in an appropriate fashion since they provide the fulcrum of the lever-arm needed to make cosmological inferences from high-redshift SNe observations. Furthermore, these SNe provide the critical empirical calibration of the SN lightcurve brightness-width relation, as well as providing the intrinsic SN colors needed to correct for dust extinction. At present half the statistical uncertainty in the dark energy measurements arises from the limited pool of low-redshift SNe; we propose to increase this pool to many hundreds of well-observed nearby SNe located in the smooth Hubble flow.

Second, the physics of the SNe Ia must be pushed to a deeper level of understanding.

Presently SNe Ia appear to be excellent standardized candles, but we do not understand the details of why this is so. The chief remaining loophole in the interpretation of the SN Ia results is the possibility of a conspiratorial evolutionary effect in the explosions themselves. There is already some empirical data that constrains such “conspiracies," but as we move to the next generation of experiments much tighter constraints will be needed. Low-redshift supernova data provide both the necessary empirical constraints, and the matching deeper physical understanding of the SNe Ia, and is therefore a necessary complement to the ongoing high-redshift work and future projects like the Canada-France Legacy Survey, the Cerro-Tololo Supernova Survey, the Large Synoptic Survey Telescope (LSST) and the SuperNova/Acceleration Probe (SNAP). This work to constrain evolutionary effects requires that the low-redshift SNe Ia be observed over their entire lightcurves and across a wide range of environments (spanning stellar age and metal content).

In recognition of the importance and urgency of this work, we have begun a new experiment – the Nearby Supernova Factory (*SNfactory*) – designed to exploit the full potential of low-redshift SN studies. The *SNfactory* will concentrate on the discovery and follow-up of $\sim$300–500 SNe Ia; an order of magnitude larger than currently available samples. It will also work to develop Type II supernovae (SNe II) as more reliable distance indicators. Since the physics and measurement methods applicable to SN Ia and SN II are so different, they will serve as crucial cross-checks on each other. The lowest-z SNe also will be used to measure galaxy peculiar velocities and thereby independently measure Ω_M to better than 5%.

Our low-redshift SN observations will require especially tight coordination between experimentalists, theorists and phenomenologists. Newly discovered SNe must be examined by experts so that the rarest and most interesting SNe — those which sample the space of physical properties — are scheduled for the best follow-up observations. Access to phenomenologists ensures that interesting trends or theoretical concepts can be developed rapidly and fed back into the observational program. The optical (and hopefully near-infrared) observational database will be an unparalleled resource for the entire astrophysics community.

2. The Need for Improved Statistics at Low-Redshift

The recent measurements of Ω_M and Ω_Λ by the Supernova Cosmology Project (SCP) using 42 high-redshift SNe Ia (see Fig 1) excludes a simple $\Omega_M = 1$ flat universe, and presents strong evidence for the existence of a dark energy ($\Omega_\Lambda > 0$). Through further ground-based and space-based initiatives — such as the Hubble Space Telescope (HST) and the SuperNova/Acceleration Probe (*SNAP*) — the SCP is working to confirm this exciting result with observations of SNe Ia at even higher redshift. (Indeed, the SCP now has preliminary confirmation from an independent sample of high-redshift SNe Ia observed with HST Knop *et al.* (2002).) However, $\sim 50\%$ of the

statistical uncertainty in the current result stems from the small number of low-redshift SNe Ia which are suitable to serve as the zero-point for the SNe Ia Hubble diagram. These SNe Ia are apparent in Fig. 1; one can see that the nearby SNe Ia are actually outnumbered by the high-redshift SNe Ia!

A number of groups are planning much larger, more comprehensive, experiments using high-redshift SNe Ia to probe the nature of dark energy. The Canada-France Legacy Survey expects to discover and follow-up ~ 300 high-redshift ($0.3 < z < 0.7$) SNe Ia over five years beginning in 2003. It is also expected that a search of similar size will be conducted at the Cerro-Tololo Interamerican Observatory. Members of our *SNfactory* collaboration are involved in these upcoming efforts, and it is our expectation that these experiments have the potential to measure the effective time-averaged equation of state, $w = p/\rho$, of the dark energy, with a level of precision that will begin to test whether dark energy is due to something other than Einstein's cosmological constant (for which is $w = -1$ independent of time). Further down the road the SuperNova/Acceleration Probe will begin the hunt for time variations in the equation of state – the next generation of tests for dark-energy that differs from the simple cosmological constant. These experiments will rely very heavily on the existence of a dataset such as the one *SNfactory* intends to provide, as we will now describe.

Anchoring the Low-Redshift Hubble Diagram

The luminosity distance to a Type Ia SN is given by:

$$d_L(z) \equiv \sqrt{\frac{L}{4\pi f}} = \frac{c(1+z)}{H_o} \int_0^z \left[\Omega_M (1+z')^3 + \Omega_X^{w(z')}\right]^{-1/2} dz' \tag{1.1}$$

for a spatially flat universe (assumed for simplicity of exposition only). Here L and f are the intrinsic and observed SN fluxes, respectively, integrated over all wavelengths, Ω_M is the normalized mass-density, Ω_X is the normalized dark-energy density, and w is the dark energy equation of state, which may evolve with redshift. In the case of a cosmological constant, $w = -1$.

Observations provide the redshift, z, and a form of f (generally the flux over the wavelengths defined by the restframe B-band filter). Thus, Eq. 1.1 can be recast in a form convenient from an experimental viewpoint:

$$f = \frac{LH_o^2}{4\pi c^2 (1+z)^2} \left[\int_0^z \left[\Omega_M (1+z')^3 + \Omega_X^{w(z')}\right]^{-1/2} dz'\right]^{-2} \tag{1.2}$$

From a cosmological perspective, we are interested in Ω_M, Ω_X and $w(z)$, while the product LH_o^2 is an unknown nuisance parameter which must be marginalized over in order to extract the

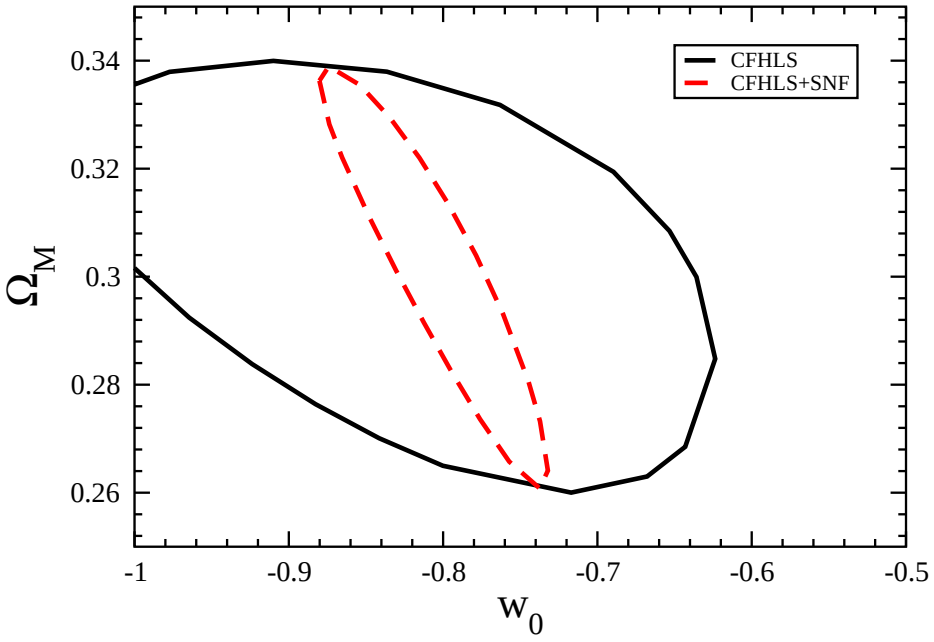

Fig. 2.— **The importance of low-redshift SNe Ia for near-future dark energy probes:** The impact of adding 300 *SNfactory* SNe Ia to a representative sample of 300 high-redshift ($0.3 < z < 0.7$) SNe Ia, such as the Canada-France Legacy Survey or the CTIO Supernova Survey might obtain over the next 5 years is demonstrated. The solid contour is the 68% projected confidence in the Ω_M—w_0 plane from the high-redshift survey alone, while the dashed contour is the 68% projected confidence when the *SNfactory* SNe Ia are added. In this example the addition of the *SNfactory* SNe Ia allows elimination of a cosmological constant model ($w_0 = -1$). A flat universe has been assumed, as has a prior of $\sigma_{\Omega_M} = 0.04$. When comparing to Fig. 3 note that here w_1 is set to zero and therefore contributes no uncertainty; if w_1 were allowed to float the uncertainty in w_0 would be much larger. Courtesy Eric Linder, Ramon Miguel, and Dragan Huterer.

cosmological parameters. However, for $z \sim 0$ Eq. 1.2 simplifies to:

$$f_{|z\sim 0} \sim \frac{LH_o^2}{4\pi(cz)^2} \tag{1.3}$$

Thus, observations of nearby supernovae can significantly improve the determination of the cosmological parameters by strongly constraining the nuisance product, LH_o^2.

This result is dramatically illustrated in Fig. 2 for the case of the Canada-France Legacy Survey, which is expected to have a sample of 300 SNe Ia with $0.3 < z < 0.7$. This survey will attempt to rule out a cosmological constant by examining the case of a constant effective equation of state, $w(z) = constant = w_0$; for a cosmological constant the effective equation of state is

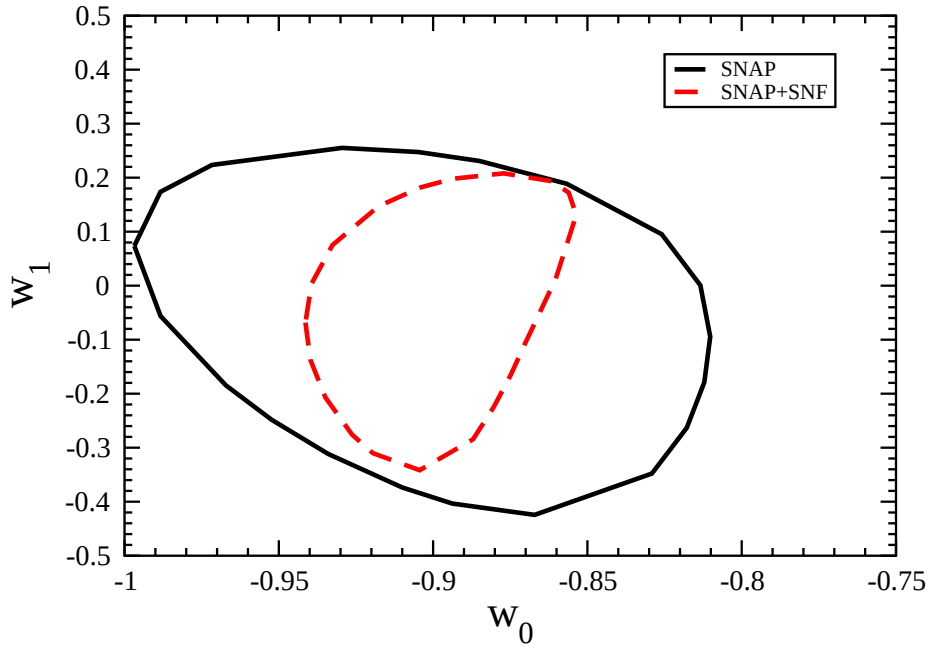

Fig. 3.— **The importance of low-redshift SNe Ia for next-generation dark energy probes:** The impact of adding 300 *SNfactory* SNe Ia to a more ambitious high-redshift SNe Ia experiment such as *SNAP* is demonstrated. The solid contour is the 68% projected confidence from *SNAP* alone, while the dashed contour is the 68% projected confidence when the *SNfactory* SNe Ia are added. In this example the addition of the *SNfactory* SNe Ia allows elimination of a cosmological constant model ($w_0 = -1$, $w_1 = 0$). A flat universe has been assumed and a prior of $\sigma_{\Omega_M} = 0.04$ has been imposed. Courtesy Eric Linder, Ramon Miguel, and Dragan Huterer.

$w_0 = -1$. In the example shown, for a nominal $w_0 = -0.8$ the high-redshift SNe Ia still allow $w_0 = -1$ at the 68% confidence level (solid contour). However, addition of 300 SNe Ia from the *SNfactory* allows a clear rejection of $w_0 = -1$ (dashed contour). This is the result of the *SNfactory* constraint on LH_o^2.

The *SNfactory* is also essential for getting the best statistical results for a *SNAP* measurement of $w(z)$. $w(z)$ is often expressed to linear order as $w(z) = w_0 + w_1 z$. The solid contours of Fig. 3 show the 68% confidence region in the w_0, w_1 plane for a *SNAP*-like dataset of 2000 SNe Ia with $0.3 < z < 1.7$. In this example, *SNAP* does not rule out $w_0 = -1, w_1 = 0$, that is, a cosmological constant is still allowed. However, addition of the *SNfactory* SNe Ia allows a clear rejection of a cosmological constant and significantly improves the measurement of w_0.

In the general case, typically the *SNfactory* halves the uncertainty in w_0 by measuring LH_o^2 to 1%. Thus, is it clear that the *SNfactory* is a necessity if the high-redshift supernova cosmology

experiments are to realize their full potential.

Calibration of the Luminosity—Lightcurve Width Relation

The slope, α, of the relation between SN Ia intrinsic luminosity and lightcurve width (see Fig. 4) has been determined from only a relatively small (~ 30) number of Hubble-flow SNe Ia. Each of these SNe Ia has an intrinsic peak-brightness uncertainty of about 10% and measurement errors which are comparable. Moreover, the lightcurve widths for these SNe Ia exhibit a nearly Gaussian distribution around a typical value, so the lever arm which determines the slope contains relatively few SNe Ia. As a result, α is determined to only about 25% Phillips *et al.* (1999). This doesn't effect individual SNe too greatly because most SNe are clustered around the typical lightcurve width. However, for the future large high-redshift SNe samples where the probative value comes from averaging there exists the potential for σ_α to become an important source of statistical uncertainty since it is a correlated uncertainty for all the SNe.

Calibration of Intrinsic Colors for Dust Extinction Correction

The standard method of correcting for extinction by dust in the galaxies hosting Type Ia SNe relies on the observed fact that dust scatters blue light more than red light. Thus, the colors of extincted objects are redder than they would be without extinction. Observations of stars of known color and brightness in the Galaxy, and the Large and Small Magellenic clouds suggests a fairly consistent relation between the amount of reddening and the amount of extinction. For restframe B-band light the amount of dimming is roughly $4\times$ the change in the flux ratio between the B-band and the V-band.

Correction of SN brightnesses for dust extinction involves a comparison of a measurement of the color at maximum light of a new SN with maximum light colors of SNe Ia which are extinction-free (e.g., those in elliptical galaxies, which are mostly free of dust). The change in color must be multiplied by the above factor of 4 to obtain the extinction-corrected brightness.

The current uncertainty in the intrinsic (dust-free) colors of SNe Ia is not negligible. Only about 10% of all host galaxies are ellipticals, so the number of calibrating SNe Ia is small. Moreover, few of those SNe Ia are in the smooth Hubble-flow, where the effects between SN color and brightness due to dust and intrinsic luminosity can be separated. As a result, the uncertainty in the intrinsic SN Ia colors is one of the dominant uncertainties in the current cosmology measurements. Note that this is a correlated uncertainty in the calibration of the intrinsic colors of all SNe Ia, so it does not average out as larger samples of high-redshift SNe Ia are obtained, unlike

the color measurement errors of each individual high-redshift SN Ia. The *SNfactory* measurements are designed to greatly improve this calibration of intrinsic colors, making it possible to take advantage of the large statistics from the next generations of high-redshift SN Ia projects.

K-corrections

Because SNe Ia will be at different redshifts, in the restframe of the SN any filter used to obtain an image will not exactly match the standard B-band filter. Therefore, the brightness of a SN Ia will be affected by spectral features which are either included or excluded due to filter mismatch. The correction for this effect — referred to as the K-correction — requires knowledge of the SN spectrum and the photon response of the instrument. For high-redshift SNe Ia the spectrum is usually only available from around the time of maximum light, whereas each photometry point along the SN lightcurve requires its own K-correction. Thus, the appropriate spectrum to be used for K-corrections at other epochs on the lightcurve must be inferred from the spectra of low-redshift analogs. The choice of the best analog relies on comparison of the maximum-light spectra and the colors of the low- and high-redshift SNe (it could also depend on additional inputs, such as the lightcurve shape). The better the analog, the better the accuracy of the K-correction.

For some types of SNe Ia observed at redshifts where the filter match to B-band is particularly bad, the errors in the K-corrections can alter the inferred corrected peak brightness by several percent. For the determination of SN colors, such errors will roughly add in quadrature (there will be some covariance since color is used to help choose the proper low-redshift analog), so the overall uncertainty in the standardized peak brightness after the color is used to correct for dust extinction can be $\sim 10\%$.

Thus, simple calibration uncertainties associated with dust extinction correction and K-corrections are both of order 10% after the application of the extinction correction. Each of these sources of uncertainty is as large as the intrinsic scatter among SNe Ia. In combination they increases the statistical uncertainty associated with each SN Ia by $\sim 1.7\times$. Also note that we have found extreme examples, such as SN1999aw in the I-band, where the K-correction at some specific epochs is uncertain by 10's of a percent.

With the spectral time series that the *SNfactory* will obtain for all 300 SNe Ia, the K-corrections for the low-redshift SNe will be **zero**, since the product of the B-band filter response and the SN spectrum can be calculated directly. This will allow excellent calibration of SNe Ia standardization relations. Moreover, the large *SNfactory* sample will vastly increase the number of analogs available for the K-correction of high-redshift SNe Ia. Thus, one can see that these

gains — although merely technical — have the power to significantly improve the results from supernova cosmology experiments.

These steps are needed for the proper application of the *current* standardization methods used by all the groups who do cosmology with Type Ia supernovae. Furthermore, the reader will have noted that these correction steps are not independent: K-corrections must be applied to get the SN color, which is then used to determine the dust extinction, after which α and LH_o^2 can be determined. Therefore a large homogeneous dataset is required to separate-out the contributions of these various effects. In particular, a large-scale search is necessary in order to find the rarer (elliptical host galaxies, large/small lightcurve width, etc.) events which provide leverage for the calibration.

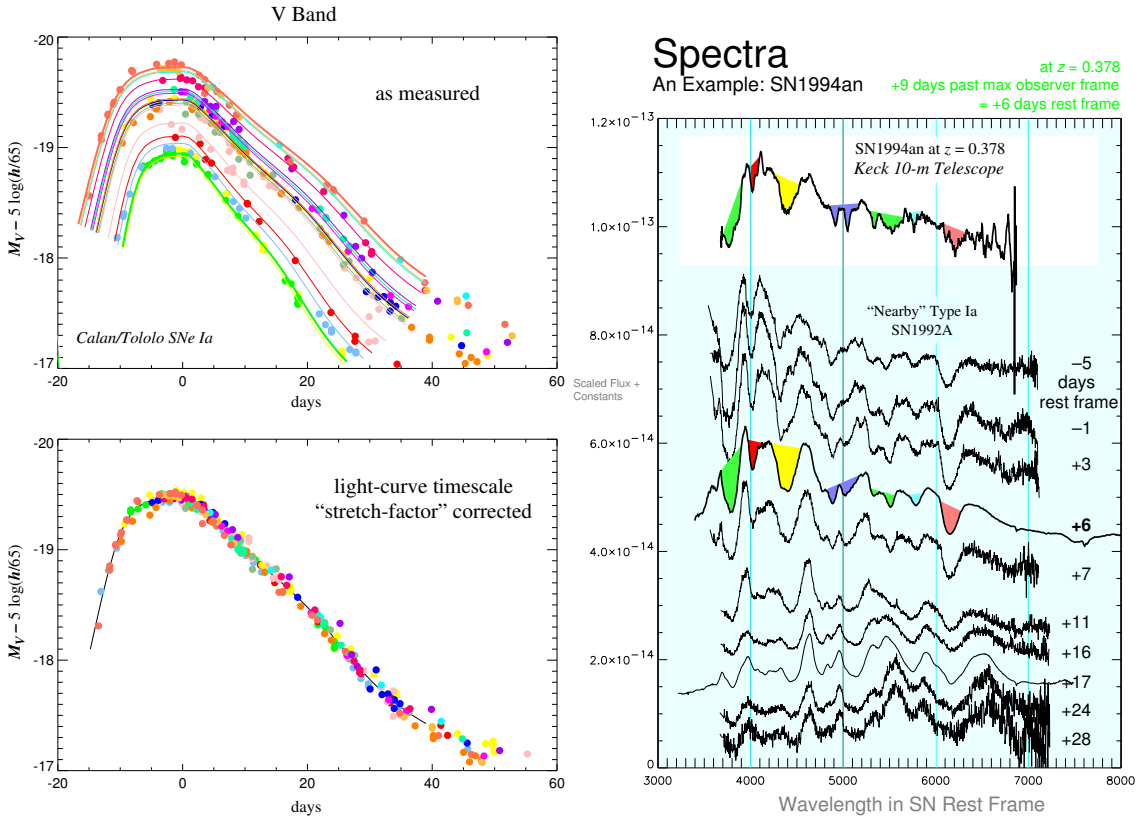

Fig. 4.— **Photometric and Spectral Time Evolution of Type Ia supernovae:** At left, lightcurves for nearby SNe Ia. The upper panel shows lightcurves for individual SNe Ia, corrected for relative distance using Hubble's law. Template lightcurves have been fit to the lightcurve for each SN and indicate that the brighter SNe have lightcurves which are broader and decline more slowly. The lower panel at left shows the superposition of these data after using a brightness correction derived from the lightcurve width. At right, the evolution of the spectrum of a Type Ia supernova as the explosion ages (constructed from different SNe Ia). The shaded regions highlight portions of the spectra which are seen to change with time; some of these are luminosity indicators. Both datasets offer important clues to the physics of SNe Ia.

3. Converting Systematic Uncertainties into Statistical Uncertainties

As we move to the next generation of supernova cosmology measurements with significantly improved target statistical uncertainties, it now becomes critical to improve the constraints on systematic uncertainties as well. In particular, we now want to scrutinize the SNe Ia closely enough that we can find second-order differences that are not parameterized by the lightcurve width vs. luminosity relation. Well-observed nearby SNe Ia, especially in host galaxies spanning a wide range in star-formation histories, are essential for hunting for such possible second-order systematic trends, and the observables that could constrain them. In addition, further study of nearby SNe will allow refinement of known SNe Ia luminosity indicators — and perhaps the discovery of more accurate or economical luminosity indicators — improving SNe Ia as tools for cosmology.

Supernova "Evolution"

Uncorrected "evolution" has also been proposed as one potential source of systematic uncertainty in the comparison of high- and low-redshift SNe Ia Umeda *et al.* (1999). Supernova behavior may depend on properties of its progenitor star or binary-star system. The distribution of these stellar properties is likely to change over time — "evolve" — in a given galaxy, and over a set of galaxies.

As galaxies age, generation after generation of stars complete their life-cycles, enriching the environment of their host galaxies with heavy elements. In a given generation of stars, the more massive ones complete their life cycles sooner, so the distribution of stellar masses also changes over time. Such statistical changes in the galactic environments are expected to affect the typical properties of supernova-progenitor stars, and hence the details of the triggering and evolution of the supernova explosions. Even the SNe Ia might be expected to show some differences that reflect the galactic environment in which their progenitor stars exploded, even though they are triggered under very similar physical conditions every time (as mass is slowly added to a white dwarf star until it approaches the Chandrasekhar limit).

Evidence for such galactic-environment driven differences among SNe Ia has in fact already been seen among nearby, low-redshift supernovae Hamuy *et al.* (1996). The range of intrinsic SN Ia luminosities seen in spiral galaxies differs from that seen in elliptical galaxies. So far, it appears that the differences that have been identified are well calibrated by the SN Ia lightcurve width-luminosity relation. The standard supernova analyses thus already are correcting for a luminosity effect due to galactic-environment-distribution evolution. There are likely to be additional, more subtle effects of changes in the galactic environment and shifts in the progenitor

star population, although it is not clear that these effects would change the peak luminosity of the SNe Ia. The *SNfactory* is designed to provide sufficient data to measure these second-order effects for nearby SNe Ia.

In this discussion it is important to recognize that each individual galaxy begins its life at a different time since the Big Bang. Even today, there are nearby galaxies forming, that have not yet gone through the life cycles of their high-mass stars, nor yet produced significant heavy element abundance. Thus locally there will be a large range of galactic environments present and the supernovae will correspondingly exhibit a large range of progenitor-star ages and heavy-element abundances.

It is only the relative distribution of these environment ages that will change with universal clock time. By identifying matching sets of supernova that come from essentially the same progenitor stars in the same galactic environments, between high and low redshift, we can then perform the cosmological measurements using SNe Ia having the same initial conditions. This only requires that the SN Ia sample sizes are sufficiently large and varied at each redshift that we can find matching examples in sufficient quantities. Indeed, this is another reason why the sample of nearby SNe Ia must be made much larger — to find low-redshift counterparts for each high-redshift SN Ia.

We have identified a series of key supernova features that respond to differences in the underlying physics of the supernova. By measuring all of these features for each supernova we can tightly constrain the physical conditions of the explosion, making it possible to recognize sets of supernovae with matching initial conditions. The current theoretical models of SN Ia explosions are not sufficiently complete to predict the precise luminosity of each supernova, but they are able to give the rough relationships between changes in the physical conditions of the supernovae (such as opacity, metallicity, fused nickel mass, and nickel distribution) and changes in their peak luminosities. We therefore know the approximate accuracy needed for the measurement of each feature to ensure that the physical condition of each set of supernovae is well enough determined so that the range of luminosities for those supernovae is well below the systematic uncertainty bound ($\sim$2% in total) for *SNAP*. The *SNfactory* will play a key role in empirically calibrating these relationships between changes in the physical conditions of the supernovae (as seen in the lightcurve and spectral features) and changes in their peak luminosities.

In addition to these features of the supernovae themselves, we will also study the host galaxy of the supernova. We can measure the host galaxy luminosity, colors, morphology, type, and the location of the supernova within the galaxy.

4. Constraining Ω_M with the SNfactory

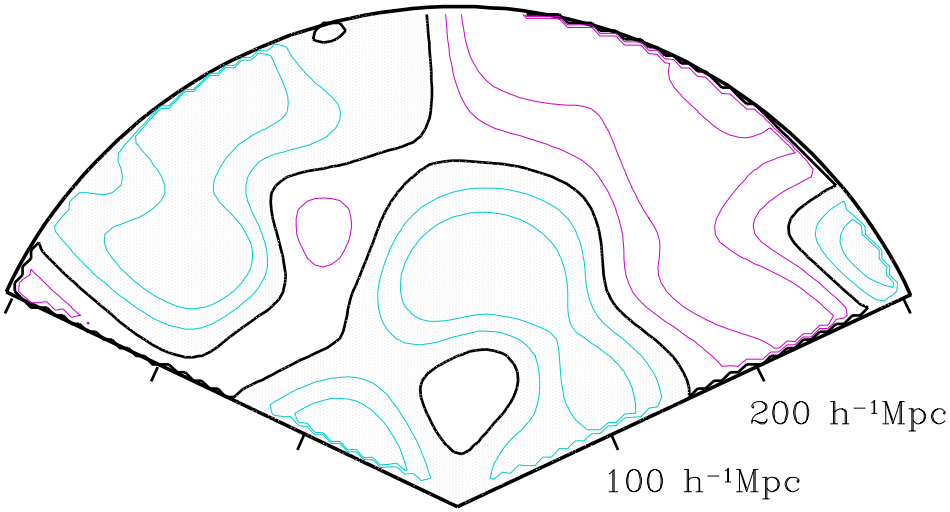

Fig. 5.— **Gravitationally-induced peculiar velocities:** The contours show a simulation of the radial component of peculiar velocities of the hosts of SN host galaxies, smoothed on a scale of $21h^{-1}$ Mpc. The shaded regions have positive radial peculiar velocities while the unshaded regions have negative radial peculiar velocities. The contours run from $-100 < v_r < 100$ km/s in steps of 50 km/s. From the Sloan Digital Sky Survey mock catalog of Colley *et al.* (2000)

The *SNfactory* will concentrate its intensive follow-up observations on Type Ia supernovae in the Hubble flow at $0.03 < z < 0.08$ so that the radial component of the peculiar velocities of the host galaxies (typically 300 km/s) is a minor portion of the overall error budget. For $z < 0.03$ these peculiar velocities will be measurable, and are proportional to the product of ${\Omega_M}^{0.6}$ and enclosed mass perturbations δ, i.e.

$$\nabla \cdot \mathbf{v} = -{\Omega_M}^{0.6}\delta.$$

The mean-square bulk velocity in a sphere of radius R is given by:

$$\left\langle v^2(R) \right\rangle = \frac{\Omega_M^{1.2}}{2\pi^2} \int_0^\infty P(k)\, \widetilde{W}^2(kR)\, dk$$

where $P(k)$ is the *matter* power spectrum and $\widetilde{W}^2(kR)$ is the Fourier transform of a spherical window function. A large all-sky sample of $z < 0.03$ supernova distance measurements will allow a purely dynamical measurement of Ω_M which is independent of Ω_Λ, and also independent of uncertainties in galaxy biasing which afflict galaxy redshift survey estimates of the mass power spectrum. Current constraints using the peculiar velocity method give $\Omega_M = 0.35 \pm 0.05$ for a flat universe with fixed H_o, Ω_b, n and COBE normalization Courteau & Dekel (2001), Silberman,

Dekel, Eldar & Zehavi(2001) using samples of various distance indicators having the statistical weight equivalent to roughly 100 SNe Ia. The *SNfactory* sample should help improve these constraints considerably. Including distance measurements from $z > 0.03$ *SNfactory* supernovae will allow determination of the spatial scale over which the velocity field converges. This in turn determines the spatial scale at which the universe becomes homogeneous. Due to the much smaller distance uncertainty associated with SNe Ia compared to, e.g. Tully-Fisher or Fundamental Plane techniques, systematic errors in the peculiar velocities for the *SNfactory* sample should be much smaller than for existing peculiar velocity samples. Thus the *SNfactory* will significantly advance the state of the art in this field Courteau & Dekel (2001). An example of what the peculiar velocity field might look like is shown in Fig. 5Colley *et al.* (2000).

5. Galaxies

v1, YC, 23/05

Besides these correlations, one can probe the connection between the SNe Ia and the host galaxy (age and metallicity, gas and dust contents, etc.), the *SNfactory* survey can shed new light on the low-redshift galaxies intrinsic properties. Indeed, the *SNfactory* galaxy sample – gathering the host galaxies of the observed SNe Ia – will not be selected according to any "traditional" criterion (total luminosity, surface brightness, morphology, distance, nuclear activity, etc.), but only on the fact of harboring an observed SN Ia. Therefore, *none* of the classic biases in action during the usual selection process – luminosity, surface brightness, color, cosmic environment – should affect the galaxy sample at any rate.

The "physical" selection criterion applied on the resulting galaxy sample is difficult to estimate. But under the assumption – to be validated – that the probability of a supernova is directly proportional to the stellar population density **(any good references?)**, the *SNfactory* galaxies will be selected according to their *total stellar mass*. However, a distinction must be made on the nature of the supernovæ: the thermonuclear SNe (SNe Ia) probe the *old* stellar population, while the gravitational SNe are related to the *young* stellar population. The *SNfactory* will only follow the SNe Ia along their light-curve, accumulating enough galactic signal for a spectroscopic analysis. As a result, the survey will provide two distinct very innovative samples of 300 nearby galaxies or more[1], but the complete study of the "young sample" would require complementary spectroscopic observations.

Besides the production of a new kind of local galaxy samples, the scientific topics that can be addressed by this aspect of the *SNfactory* are numerous (see the *Nearby Field Galaxy Survey* for a

[1]The exact size and characteristics of the samples still depend on the precise SNe discovery efficiency rate.

complete science case, Jansen *et al.* (2000)):

- establish the global galaxy luminosity function, and possibly of the luminosity-morphology relation (from both samples),
- connect various spectro-photometrically measured properties – age, metallicity, star formation, etc. – to the galaxy luminosity,
- serve as a *zero-evolution* benchmark for the interpretation of distant galaxy samples.

This last point is of particular interest considering the similarly tailored galaxy samples that the high-redshift supernoæ surveys to come (*SNLS, SNAP*) will provide: the comprison between the nearby and distant galaxies will be much facilited by a distant-independant selection criterion.

6. Science goals summary

The primary goal of the *SNfactory* is to provide a large sample of high-quality low-redshift SNe Ia, needed to establish the baseline against which the dimming of high-redshift SNe Ia can be measured and to determine those properties of SNe Ia affecting their use for the next generation of higher-statistics, lower-uncertainty cosmology measurements. A critical component of this work will be the search for second-order deviations and extra parameters beyond the lightcurve width-brightness relation current used to standardize SNe Ia. New exclusion criteria and standardization methods based on lightcurve shapes and/or spectral features (see Fig. 4) can then be developed using these high-quality low-redshift datasets to constrain these second-order deviations as we begin to use the higher statistics samples at high-redshift to make the next generation measurements of the cosmological parameters. These goals can be summarized as follows:

a) secure the low-redshift portion of the SNe Ia Hubble diagram (Figs 1, 2 and 3) which serves as the zero-point for high-redshift cosmological measurements.

b) acquire lightcurves at numerous optical (and, when possible, near-infrared) wavelengths beginning well before maximum — data currently available for only a handful of nearby SNe Ia, and needed to fit the lightcurves of high-redshift SNe Ia for which there is now extensive data prior to maximum (see 4a).

c) test and refine the lightcurve width vs. brightness relation used to standardize SNe Ia luminosities, for which a wide range of lightcurve widths is essential.

d) construct an ultraviolet (U-band) template lightcurve and an ultraviolet lightcurve width vs. brightness relation to allow restframe ultraviolet lightcurves of $z > 0.75$ SNe Ia observed with HST to be used.

e) obtain spectral coverage with lightcurve phase, and thereby determine accurate wavelength bandpass corrections (K-corrections) as a function of lightcurve width and time (see 4b).

f) determine intrinsic SNe Ia color-curves needed to establish the correct color zeropoints for host-galaxy dust extinction corrections.

g) test for the existence of abnormal host-galaxy dust extinction laws.

In principle, *SNAP* could conduct some of these studies itself. The measurements must be obtained in a fashion such that the technical measurements have little covariance with measurement of the cosmological parameters. This requires that the determination be made using a large sample of SNe Ia at very low redshift, which would be very difficult and inefficient for *SNAP* to get because the necessary areal coverage is thousands of times larger than the *SNAP* field of view. Thus, it is much more cost-effective and efficient to obtain these observations with the *SNfactory*. Furthermore, since the *SNfactory* data analysis can be completed well before *SNAP* flies, final details of the *SNAP* mission and analysis chain can be fine-tuned prior to launch rather than after *SNAP* has collected the data for these studies itself.

The resulting *SNfactory* dataset on SNe Ia will also allow detailed exploration of SNe Ia properties never before possible, which will almost certainly lead to a better understanding of SN physics, place strong constraints on progenitor models, and possibly allow improved luminosity estimates. It will enable us to determine

a) the intrinsic luminosity function of SNe Ia.

b) new relations between lightcurve shapes, spectral diagnostics (such as UV continuum slope, Si5180/Si6150 line ratios), etc., and luminosity.

c) SNe properties in different host galaxy environments (as a surrogate for progenitor age, mass, and metallicity).

d) the rates of SNe of all types, including rates as a function of host galaxy properties.

e) establish the color evolution of non-Ia SNe in order to refine ground-based and *SNAP* spectroscopy trigger criteria.

The large sample of *SNfactory* SNe will be important in recognizing the signature of any new supernova sub-types, which could in turn signal the existence of multiple progenitor scenarios. Indeed, the large number of SN and host-galaxy parameters whose exploration is of potential interest requires a large dataset covering the parameter space of initial conditions.

Chapter 2

Program definition

1. Baseline program

The baseline *SNfactory* factory program is to obtain spectrophotometric lightcurves covering 3200–10000 Å for a minimum of 300 nearby Type Ia SNe spanning as wide a range in SN parameter space as possible. These SNe Ia will be in the redshift range of $0.03 < z < 0.08$ – not so far as to require excessive amounts of telescope time (follow-up time goes as z^4), yet far enough so that host galaxy peculiar velocities will contribute little to the error budget. The goal is to discover the SNe Ia as soon after explosion as possible; for the *NEAT* flux limit and observing cadence we expect to easily find most SNe Ia 10-15 days before maximum light. SNe Ia spectra change noticeably on time-scales of 5–7 days, so we will attempt to obtain spectrophotometry every 3–5 days from -15 days through $+45$ days around maximum light. This follow-up cadence should yield roughly 15 spectra for each SN. Some of the nearer SNe also will be observed bimonthly in synthetic-photometry mode for several months after maximum light in order to better constrain positron escape models. Each spectrum will require 10–40 minutes to achieve adequate signal-to-noise, depending on SN brightness, atmospheric image quality, and sky brightness. Taking into account the overhead for screening of unsuitable SNe (e.g. those having the wrong type or redshift), acquisition, readout, calibration, and weather we expect to intensively study approximately 100 SNe Ia per year. Roughly a year after the initial observations a "final reference" spectrum will be obtained so that the host galaxy light superimposed on the previous year's SN light can be subtracted.

Several aspects of the *SNfactory* set it apart from other past and on-going nearby supernova projects. Foremost among these is that supernovae will be discovered using a blind wide-area CCD-based survey. Other blind surveys used less sensitive and badly calibrated photographic plates. Other nearby supernova projects using CCD's target known galaxies, generally at redshifts

less than 0.03. There is also now evidence that this approach misses an important subset of supernovae (such as the overluminous Type Ia, SN1999aw, or the hypernova, SN1999as, we discovered in the Spring 1999 Campaign). This is illustrated in Fig 1. In addition, the *SNfactory* will coordinate discovery and follow-up observations, eliminating the delays and spotty early-lightcurve coverage which is now typical. It is expected that with the *SNfactory* detailed follow-up of supernova candidates can begin within as little as 3 hrs of the discovery observations. Finally, *SNfactory* follow-up observations will use an integral field unit spectrograph, data from which can be used to construct both detailed flux-calibrated spectra and broadband images. The regular photometric spectral time series for nearby supernovae the *SNfactory* will generate will revolutionize the study of supernovae (see Fig 4). This dataset will also eliminate several limitations (wavelength bandpass mismatch, wavelength-dependent slit losses, etc.) of all other currently available instrumentation used to study supernovae.

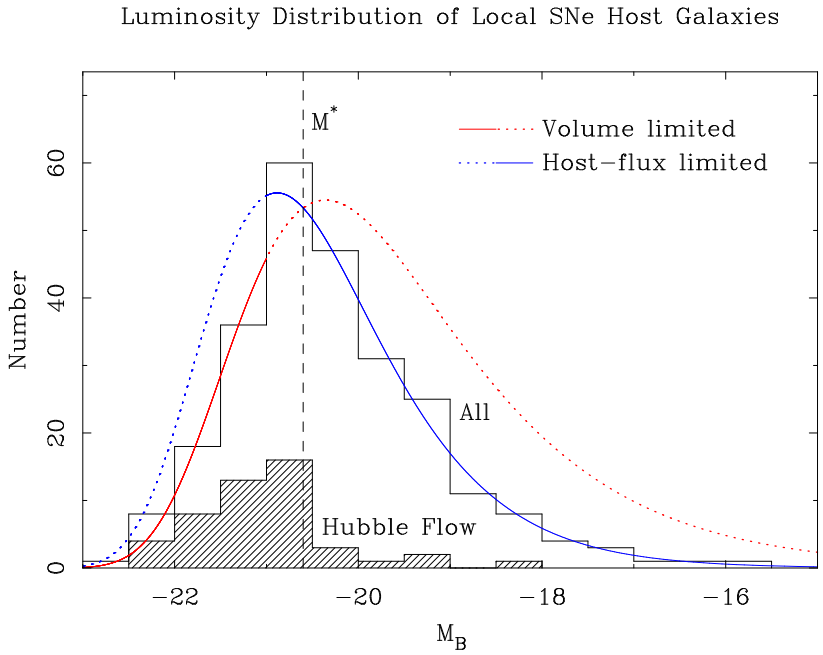

Fig. 1.— **Distribution of host luminosities for SNe Ia.** The open histogram shows the luminosity distribution of host galaxies for low-redshift SNe Ia in the Asiago SN catalog. The model curves show that for bright ($M < M^*$) galaxies the sample is volume-limited, whereas for fainter galaxies it is limited by the galaxy luminosity. Thus current SN Ia samples are biased against SNe Ia in lower-luminosity (low-metallicity) hosts. This is a direct result of the technique. The hashed histogram shows that this effect is even more pronounced among SNe Ia in the nearby smooth Hubble flow. It also illustrates the relative paucity of such SNe.

2. SNIa context

To be done: SNIa/SNII rate, galactic luminosity function, etc. **Resp.:** RP

2.1. Target Redshift Range

The *SNfactory* will be capable of finding SNe Ia at peak out to redshift $z \sim 0.2$ under the best conditions. However, since we wish to concentrateo on SNe Ia discovered well before peak, the upper redshift limit for the sample of interest is lowered to $z \sim 0.1$. Moreover, as noted earlier, the follow-up time goes roughly as z^4, so it is much more efficient for the *SNfactory* to concentrate on even lower-redshift SNe Ia provided they can be found in sufficient numbers. The very lowest redshift SNe Ia will be relatively rare in our sample; since their redshifts have a significant component due to the peculiar velocity of their host galaxy relative to the CMB they are not optimal for our main program (however they are key to constraining Ω_M from the *SNfactory* dataset.) Fig 2 illustrates this trade-off, and shows that the redshift range $0.04 < z < 0.08$ is optimal for our main program.

Fig 2 also illustrates the inherent advantage of the blind-search approach provided a wide-field camera is available. Namely, each pointing of a 1 $\square^\circ$ field contains 33 L^* galaxies whereas a pointed search will, by definition, contain only one L^* per image. In particular in the redshift range $0.04 < z < 0.08$, a luminosity density of $j_B = 2.16 \times 10^8$ h $L_\odot$ Mpc^{-3} Cross & Driver(2002) and a volume of 3.7×10^3 h^{-3} Mpc^3 deg^{-1} gives 8.0×10^{11} h^{-2} $L_\odot$ deg^{-1}; for $L^* = 2.4 \times 10^{10}$ h^{-2} $L_\odot$ this gives 33 L^* galaxies per $\square^\circ$. For a canonical rate of 1 SN Ia per L^* galaxy per hundred years, the expected yield is 330 SNe Ia for a region of 1000$\square^\circ$ monitored over the course of a year. This is more than enough to use the available observing time, thus verifying that $0.04 < z < 0.08$ is a good target redshift range for the *SNfactory*.

2.2. SN rate from the Galaxy luminosity function

The galaxy luminosity function for the simulations were taken from Marzke et al. 1998. It is a Schechter profile:

$$\Phi(M) = 0.4 \ln 10 \Phi_\star \left[A_\star(M)\right]^{1+\alpha} \exp\left[-A_\star(M)\right], \tag{2.1}$$

where

$$A_\star(M) = 10^{0.4(M_\star - M)}, \tag{2.2}$$

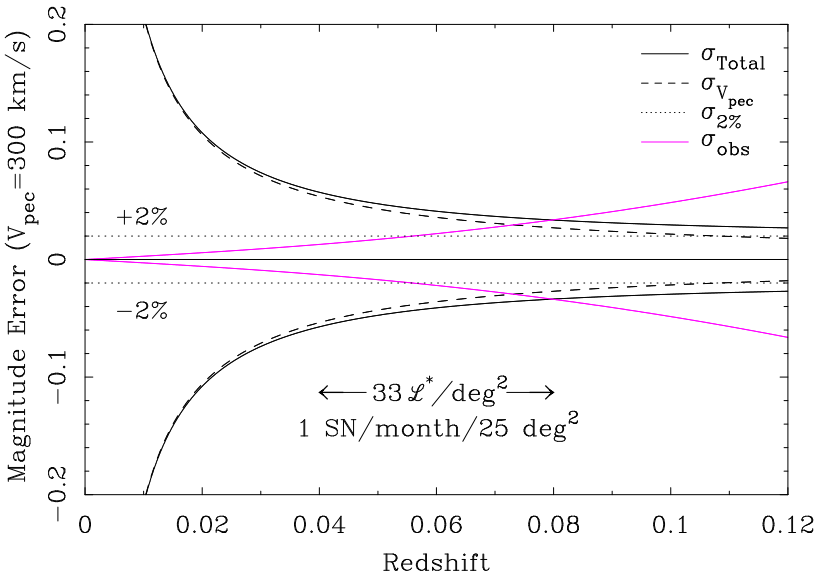

Fig. 2.— **Relative error contributions with redshift.** The size of the relative distance error due to galaxy line-of-sight peculiar velocities is illustrated. In order to test SNe Ia properties at the level of a several percent without being dominated by peculiar velocity errors requires working at $z > 0.04$. Also show is the relative cost in observing time as a function of redshift. This illustrates that the upper redshift limit should be lower as much as possible consistent with discovery of enough SNe Ia.

with $M_\star = -19.43$, $\alpha = -1.12$ and $\Phi_\star = 12.8$. Figure 3 (*left panel*) shows the corresponding luminosity function.

From this luminosity function, I compute the SN rate expected in a sphere of radius $z = 0.05$ assuming a SN rate of 0.5 per 10^{10} solar luminosities and per century (Pain et al. 1996). The rate per B magnitude and per square degree is displayed in Figure 3 (*right panel*).

The final SN rate per square degree is given by integrating this function on all the magnitudes: $2.15\,10^{-4}$ SN/day/deg^2. Adjusting this rate for the redshift range $0.04 < z < 0.08$ yields $7.7\,10^{-4}$ SN/day/deg^2. Assuming that *NEAT* effectively monitors 1000□°/year the discovery rate is 281 SNe Ia per year with $0.04 < z < 0.08$, consistent with our previous estimate.

3. Discovery

Discovery of SNe at low redshift operates in a different regime than SNe searches at high redshift because at high redshift a single wide field monitored over a year will contain many SNe, while at low redshift even the widest-field cameras will have substantially less than one SN per year. Thus, while at high redshift the search and follow-up can be combined to achieve a substantial multiplex advantage using one telescope and imager, at low redshift the optimal

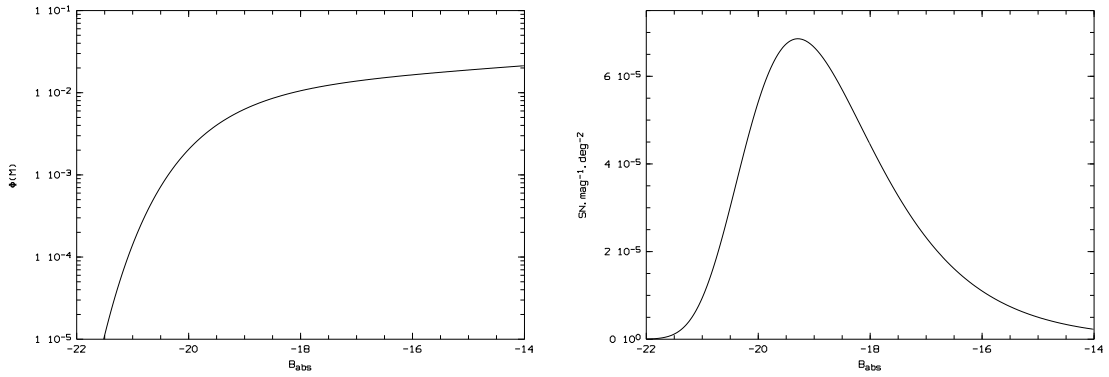

Fig. 3.— **Luminosity function and SN Ia rate.** *Left panel:* luminosity function for all types galaxies at $z \leq 0.05$ (Marzke et al. 1998). *Right panel:* SN Ia rate per B mag and per square degree within a sphere of radius $z = 0.05$.

telescopes and instrumentation for the discovery stage are very different than for the follow-up stage. Although requiring more instruments, on more than one telescope, this does allow better optimization for each stage.

Table 1: *NEAT* Search Facilities

Site	Haleakala	Palomar I	Palomar II
Aperture	1.2 m	1.2 m	1.2 m
Nights/Month	18 dark/gray	18 dark/gray	9 dark/gray
Imager Format	4k × 4k	3 × 4k × 3k	112 × 2.4k × 0.6k
Imager Scale	1.33″/pixel	1.01″/pixel	0.87″/pixel
Field of View	1.5°×1.5°	1.1°×3.4°	2.3°×4.0°
Filters	open	open	open
Exposures	3 × 20 s	3 × 60 s	TBD
Readout	20 s	20 s	40 s
Nightly Coverage	300 □°	500 □°	(1000 □°)
Start	Mar 2000	Apr 2001	∼Aug 2002
Data (compressed)	12 Gbyte/night	40 Gbyte/night	(80 Gbyte/night)

The *SNfactory* will search for supernovae using CCD images obtained by JPL's Near Earth Asteroid Team (*NEAT*). A proof-of-concept search conducted using two nights of *NEAT* data found 4 confirmed supernovae. *NEAT* has since expanded its operation to include a 1.2-m telescope (at the 10,000 ft summit of Haleakala, Hawaii) working 18 nights per month. In addition, since this search covers large portions of the sky irrespective of known galaxies, it will

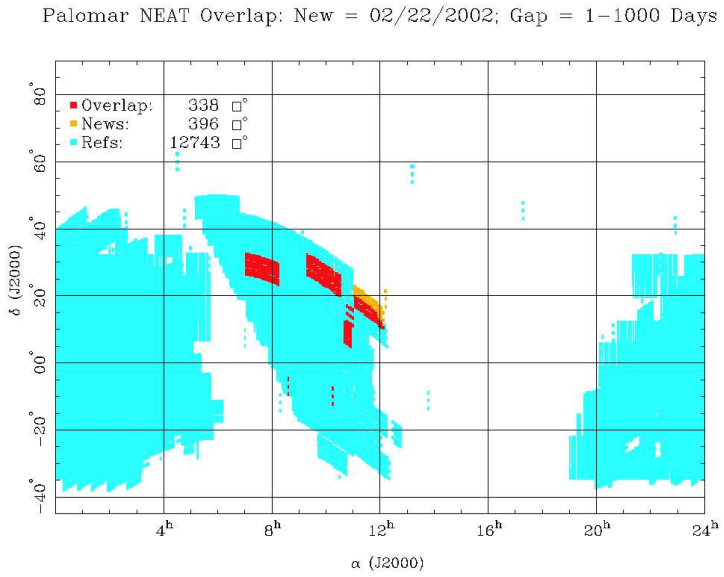

Fig. 4.— ***NEAT* sky coverage.** The total *NEAT* sky coverage prior to Feb 22, 2002 is shown in blue, while the coverage on the night of Feb 22,2002 is shown in orange; the overlap is shown in red.

be rid of the biases to which pointed searches are subject due to their reliance on existing galaxy catalogs. *NEAT* has recently quadrupled its capacity, with a second 1.2-m telescope operating at Mt. Palomar with a large CCD camera, so we expect to discover several supernovae per week. Each patch of sky will be revisited frequently (about every 6 days, since this is the "refresh rate" for NEA's). This will enable early discovery – and hence early lightcurve coverage – and help eliminate Malmquist bias. Table 1 provides technical details of the *NEAT* search facilities (also see § 1), while Fig. 4 shows the typical and cumulative nightly sky coverages attained with the current camera at Palomar Observatory.

As with the proof-of-concept search, *NEAT* data (up to 80 Gbyte/night) are being transferred in near realtime via high-speed Internet connections to LBNL/NERSC (including a custom-built wireless Internet connection to Palomar). Once there, the images are processed and searched on a PC cluster using automated software developed by the SCP and refined by the *SNfactory* (see § 2). An important aspect of the *SNfactory* is that the selection of supernova candidates will be quantitative and traceable, something current surveys completely lack and which makes calculations of supernova rates and peculiarity fractions extremely difficult.

4. Spectro-photometry and follow-up

To be done: galaxy and sky spectra, S/N estimate, survey performances **Resp.:** YC (+EP+SB) v2 YC 04/06

4.1. Supernovæ template spectrum

The SNe Ia simulated spectra are computed from the template of Peter Nugent. For a given input strech factor s, the absolute B magnitude of the supernova is computed following Perlmutter *et al.* (1997) and Hamuy *et al.* (1996):

$$\Delta m_{15} = 1.96(s^{-1} - 1) + 1.07 \qquad \text{and} \qquad M_B = -19.258 + 0.784(\Delta m_{15} - 1.1). \tag{2.3}$$

The templates of Peter Nugent are scaled to a magnitude $B = 0$, and are therefore easily scaled to any absolute magnitude M_B. The SN spectrum is then redshifted, and the apparent magnitude is simply computed using the input z.

4.2. Galaxy spectrum and surface brightness

The spectrum of the host galaxy is computed from the synthetic models of Rocca-Volmerange & Guiderdoni(1988) (which does not include any emission line). An Sc galaxy of 10 Gyrs is used as a benchmark, with the spectrum given in Figure 5 (*right panel*).

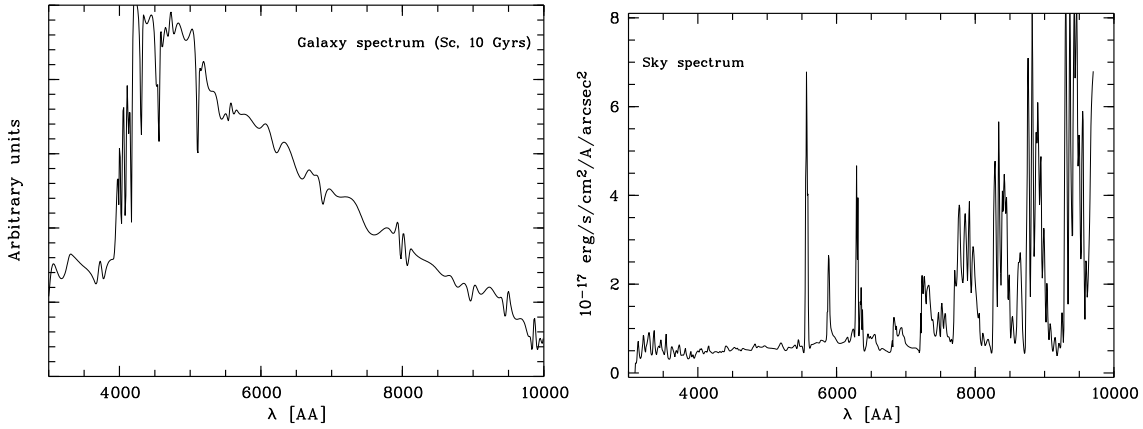

Fig. 5.— **Galaxy and sky spectra.** *Left panel:* synthetic spectrum of a 10 Gyrs Sc galaxy (Rocca-Volmerange & Guiderdoni(1988)). *Right panel:* sky brightness spectrum.

The luminosity of the underlying galaxy is the main uncertainty in these simulations, as there is a wide range of possible values. As a first try, we use the following methodology: Baggett et

al. 1998 give an analytical luminosity profile fit (in V) for a relatively large sample of 659 spiral and lenticular (bright) galaxies (the luminosity histogram is given in figure 6).

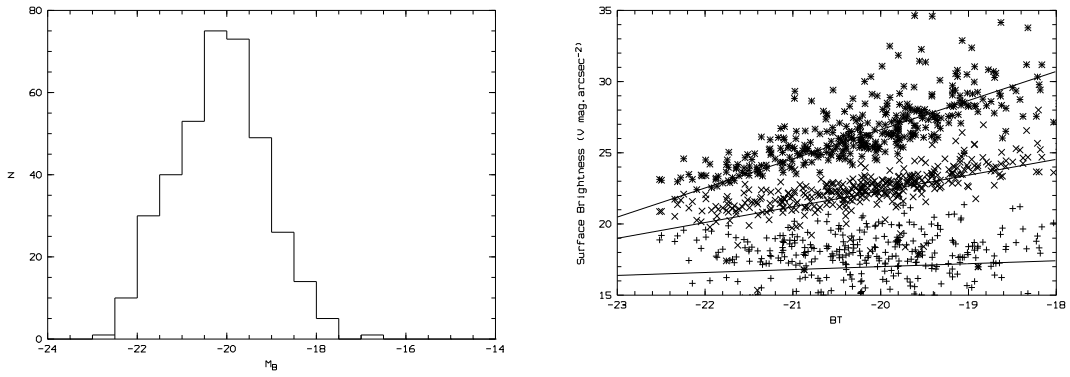

Fig. 6.— **Galactic surface brightness.** *Left panel:* Histogram of absolute luminosities in the sample of Baggett et al. 1998; *Right panel:* surface brightness μ_V *vs.* absolute magnitude B_T for the Baggett et al. 1998 sample at 1 arcsec ($+$), 5 arcsec ($\times$) and 15 arcsec ($\star$).

The analytical profile for all the galaxies of this sample have been computed for $z = 0.05$, and then convolved with a 0.8 arcsec gaussian seeing. The surface brightness was measured at different radius from the nucleus: Figure 6 shows the plot of the V surface brightness at different radius (1, 5, 15 arcsec) *vs.* B_T absolute magnitude (from `http://leda.univ-lyon1.fr/`) for the whole sample.

One can see that the V surface brighness of the galaxy will be $\sim$20 or fainter for a radius larger than 5 arcsec whatever the brightness of the host galaxy. On the contrary, due to seeing spreading, for radius between 1 and 5 arcsec, the background galaxy may be much brighter even for intrinsically faint galaxies.

As a first approach, we consider the typical underlying V surface brightness to be $\mu_V \simeq 18$ mag/arcsec^2. However, this parameter appears to be one of the most critical in the computation of the mean signal-to-noise spectrum and of the survey efficiency.

4.3. Sky brightness

The sky brightness spectrum from 3200 to 10000 Å was built by merging two spectra from the ING (blue part) and the CFHT (red part), (Fig. 5, *left panel*).

However, this moonless spectrum appears to be particularly dim, and an *ad-hoc* additive correction has been applied to match the *UBVR* Mauna-Kea sky brightness given in `http://www.gemini.edu/sciops/ObsProcess/obsConstraints/ocSkyBackground.html`.

These spectra (Fig. 7) correspond to an average over all the observing conditions (lunar phase, target-moon angular separation, ecliptic latitude, zenith angle, phase of the solar cycle) and is therefore probably pessimistic, as one can probably set up the observation strategy to meet sky conditions better than average. The cumulative probability distribution of sky brightness can be split in four:

The darkest sky occurs 20% of the time, and corresponds roughly to an observation less than 3 nights from new moon;

The dark sky is the modal sky (50%-ile), obtained for an observation less than 7 nights from new moon;

The grey sky corresponds to the 80%-ile (less than 7 nights from full moon);

The bright sky occurs the rest (20%) of the time (less than 3 nights from full moon).

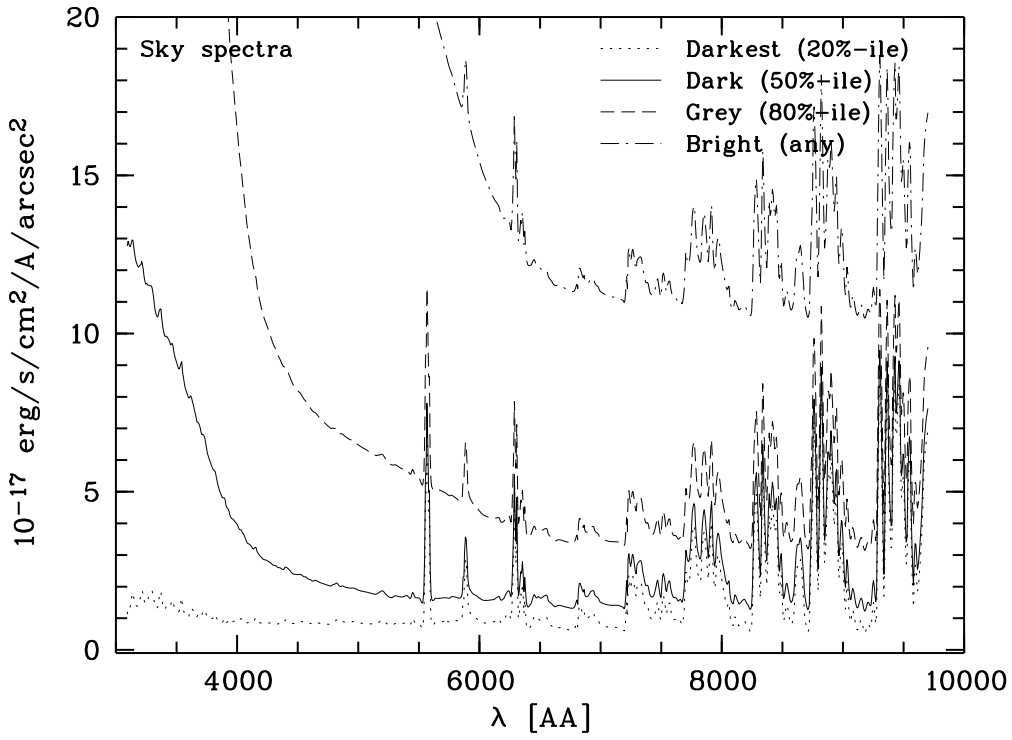

Fig. 7.— **Sky spectra for different observing conditions:** darkest night (*dot*), dark night (*full*), grey night (*dash*) and bright night (*dot-dash*).

Hereafter, the benchmark simulation uses a typical dark sky spectrum (50% of the observing conditions will be *at least* as good).

4.4. Signal-to-noise estimates

The transmission of the IFS blue and red channels are presented in Chap. 3 (§ 3.3, p.47). The benchmark observing conditions are the following:

- the sky is dark (see spectrum in Fig. 7),
- the host galaxy is a 10 Gyrs Sc spiral (see spectrum in Fig. 5) with mean V surface brighness $\mu_V = 18$ mag/arcsec^2, at a redshift of $z = 0.07$,
- the SN Ia has a stretch factor $s = 1$ and is observed at maximum ($t = 0$),
- the integration time is $T = 900$ s,
- the SN Ia spectra extraction uses optimal weighting both in spatial and cross-dispersion directions (Horne 1986).

In these conditions, the *observed* spectra (in counts) and their relative contributions are presented in Fig. 8, and the reference SN Ia S/N spectrum is displayed as a *solid line* in the following figures.

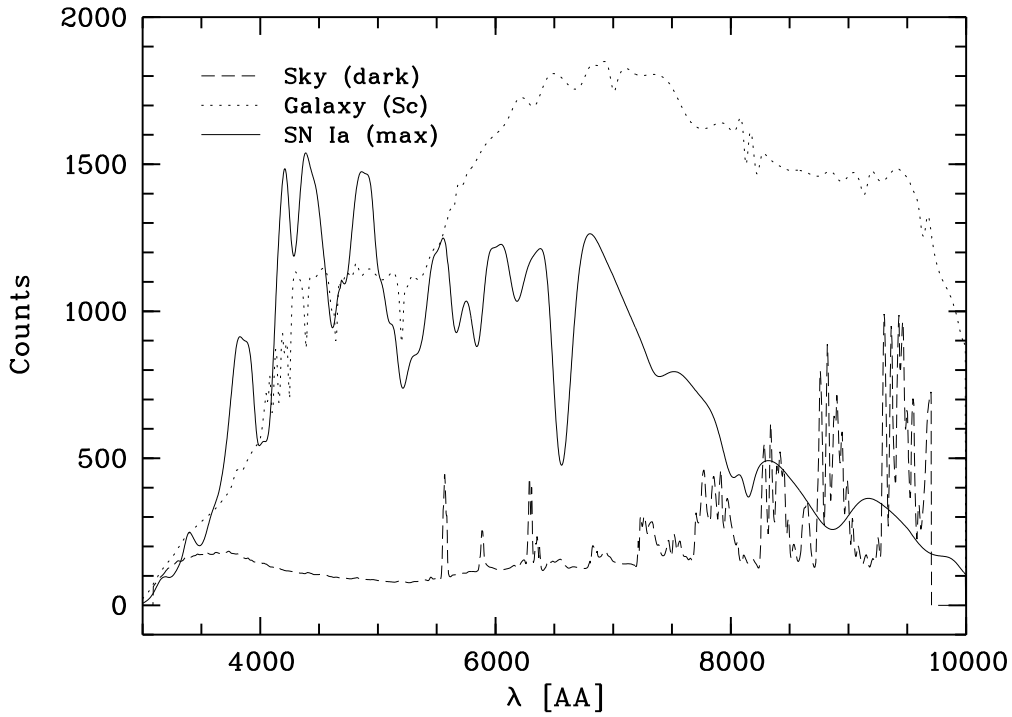

Fig. 8.— **SN Ia/galaxy/sky relative contributions** in the benchmark case (see text).

The influence of various parameters on the SN Ia S/N spectrum (all the other parameters being fixed to the benchmark values) is analysed in Fig. 9, 10 and 11:

- surface brightness and type of the host galaxy (Fig. 9),
- supernova age and stretch factor (Fig. 10),
- redshift (Fig. 10),
- exposure time and sky brightness (Fig. 11).

4.5. Survey efficiency

Observation strategies

The *SNfactory* spectro-photometric survey goals are the following:

- obtain 15 SN Ia exposures from $t = -15$ to $t = +45$ days,
- the supernova S/N per bin of 10 Å averaged over the full spectral range (3000–10000 Å) is $\langle \mathrm{S/N}_{10} \rangle \geq 10$ before $t = +35$ d, and ≥ 5 after,
- at maximum ($t = 0$), the S/N per bin of 10 Å is above 10 *everywhere* between 3500 and 9500 Å.

Tables 2 and 3 present possible strategies which attempt to balance these goals, using exposure times computed with the previous reference conditions (except of course for the SN Ia age). After $t = +35$ days, the exposures would have been longer that 1h, and lower S/N level had to be accepted.

These strategies correspond to a total exposure time on a supernova of ∼14400 s = 4h (strategy #1) and ∼21600 s = 6h (strategy #2). However, strategy #2 (Table 3) includes the fact that ∼ 75% of the nights are clear: one needs to plan 20 observations along the light-curve to indeed obtain the 15 required exposures. The effective exposure time is therefore ∼4h30 per supernova.

Survey efficiency

Given the observation strategy, one can estimate the spectro-photometric survey efficiency. Assuming:

Table 2: Spectro-photometric observation strategy #1 meeting the goals detailed in the text.

t (days)	$\langle S/N_{10} \rangle$ ($T_{exp} = 900$ s)	T_{exp} (s)	Comments
-14	3.4	900	screening spectrum
-10	10.6	840	
-6	18.7	360	
-3	21.6	300	
max	22.2	1200	
$+4$	20.6	300	
$+8$	17.4	360	
$+13$	12.8	600	
$+17$	10.8	780	
$+21$	9.7	960	
$+25$	8.4	1200	
$+29$	6.7	1800	
$+34$	5.1	900	$S/N_{10} = 5$
$+40$	3.6	1560	$S/N_{10} = 5$
$+46$	2.8	2520	$S/N_{10} = 5$

- a mean night duration of 9h (actually 9h17 of astronomical night in 2003),
- an available fraction of 20% of the UH telescope time,
- 75% of clear nights (Bely 1987),
- a total overhead[1] of 25%,

one gets $365\ \mathrm{d/yr} \times 9\mathrm{h} \times 20\% \times 75\% \times 75\%/4\mathrm{h} = 92$ SN Ia/yr for strategy #1 and 82 SN Ia/yr for strategy #2. This yields close to the number of SNe Ia described in the baseline program

[1]This overhead might be optimistic, as it will include:

- target acquisition,
- pre- and post-observation calibration exposures (arcs),
- spectro-photometric standards,
- all the SN that will be screened but not kept for further analysis.

Typical observing overheads (not including the last point, specific to the *SNfactory*) for major telescopes are around 30% (`http://www.ing.iac.es/~crb/wht/overheads.html`).

Table 3: Spectro-photometric observation strategy #2 meeting the goals detailed in the text.

t (days)	$\langle \mathrm{S/N}_{10} \rangle$ ($T_{\mathrm{exp}} = 900$ s)	T_{exp} (s)	Comments
-15	2.5	900	screening spectrum
-12	6.3	1980	
-10	10.6	840	
-7	17.1	360	
-5	20.1	300	
-2	22.0	240	
max	22.2	1200	
$+3$	21.1	300	
$+5$	19.8	300	
$+8$	17.4	360	
$+10$	15.5	480	
$+13$	12.8	600	
$+15$	11.6	720	
$+18$	10.5	840	
$+23$	9.1	1080	
$+28$	7.1	1800	
$+33$	5.4	2700	
$+38$	4.1	1320	$\mathrm{S/N}_{10} = 5$
$+45$	2.9	2400	$\mathrm{S/N}_{10} = 5$
$+48$	2.6	2700	$\mathrm{S/N}_{10} = 5$

(§ 1), althought it results in less S/N at late times than hoped for. Possible gains can come from a decrease in the overhead and from concentrating on SNe Ia at slightly lower mean redshift than $z = 0.07$.

5. Complementary Observations

Assuming our current low-redshift SN observing program with HST is extended through future proposal cycles, the *SNfactory* will have access to HST to obtain UV spectra of a subsample of the SNe Ia. This is invaluable for glimpsing the properties of SNe Ia at wavelengths which are redshifted into the visible at high redshift. The restframe UV contains important information on the metal content of the SN atmosphere. Further coordinated simultaneous multi-band near-infrared (*JHK*) imaging would allow the determination of the bolometric luminosity needed

to determine the total energy budget of the SNe, as well as providing a better determination of the amount of dust extinction suffered by each SN. Rest-frame near-infrared SN data are extremely scarce; our large sample of low-redshift SNe may reveal better SNe Ia standardization techniques which could be applied to high-redshift SNe Ia in the future using *SNAP* or the Next Generation Space Telescope (NGST). The *SNfactory* could also work to develop Type II supernovae (SNe II) as more reliable distance indicators. Since the physics and measurement methods applicable to Type Ia and Type II supernovae are so different, they will serve as crucial cross-checks on each other. With the current telescope resources support for the near-IR and Type II studies will be difficult, however, we are exploring ways to broaden the scope of the *SNfactory* to include such studies.

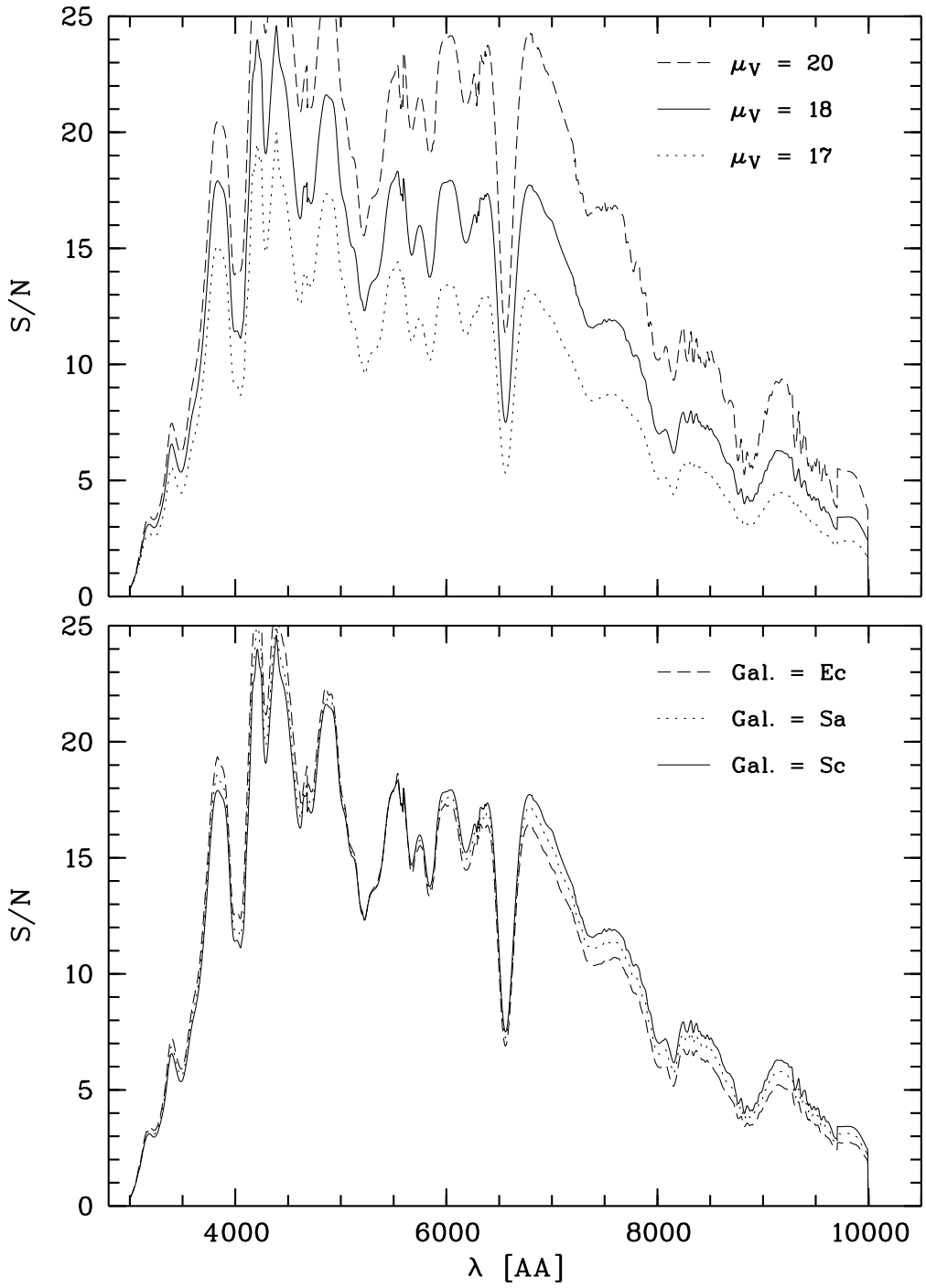

Fig. 9.— **Influence of the host galaxy characteristics on the SN Ia S/N.** *Upper panel:* influence of the underlying surface brightness (in V mag/arcsec^2); *lower panel:* influence of the host galaxy type (elliptical: *dash*, early-type spiral: *dot*). The *solid lines* correspond to the benchmark case.

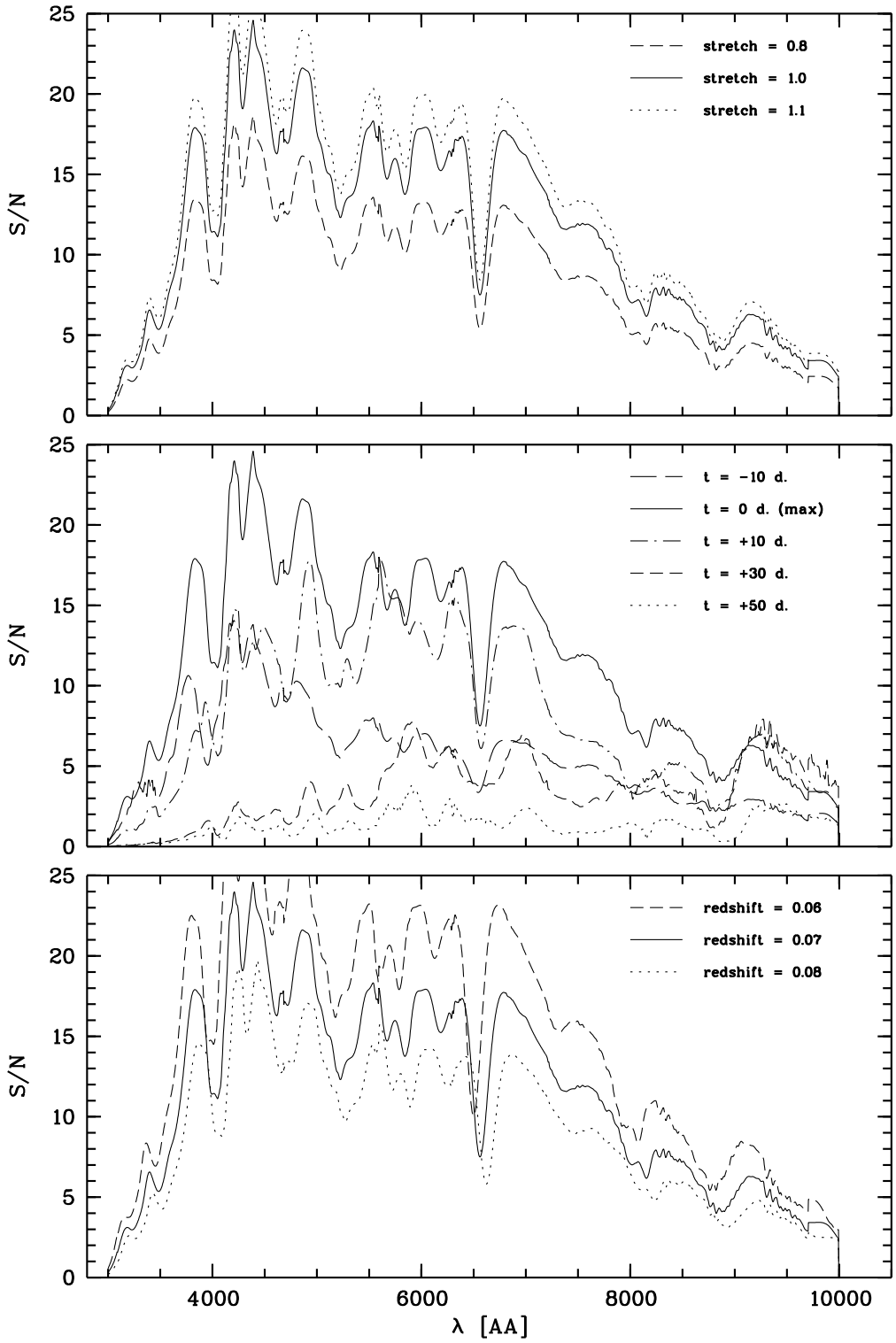

Fig. 10.— **Influence of the supernova parameters on the SN Ia S/N.** *Upper panel:* influence of the SN Ia stretch s ; *middle panel:* influence of the SN Ia age; *lower panel:* influence of the redshift z. The *solid lines* correspond to the benchmark case.

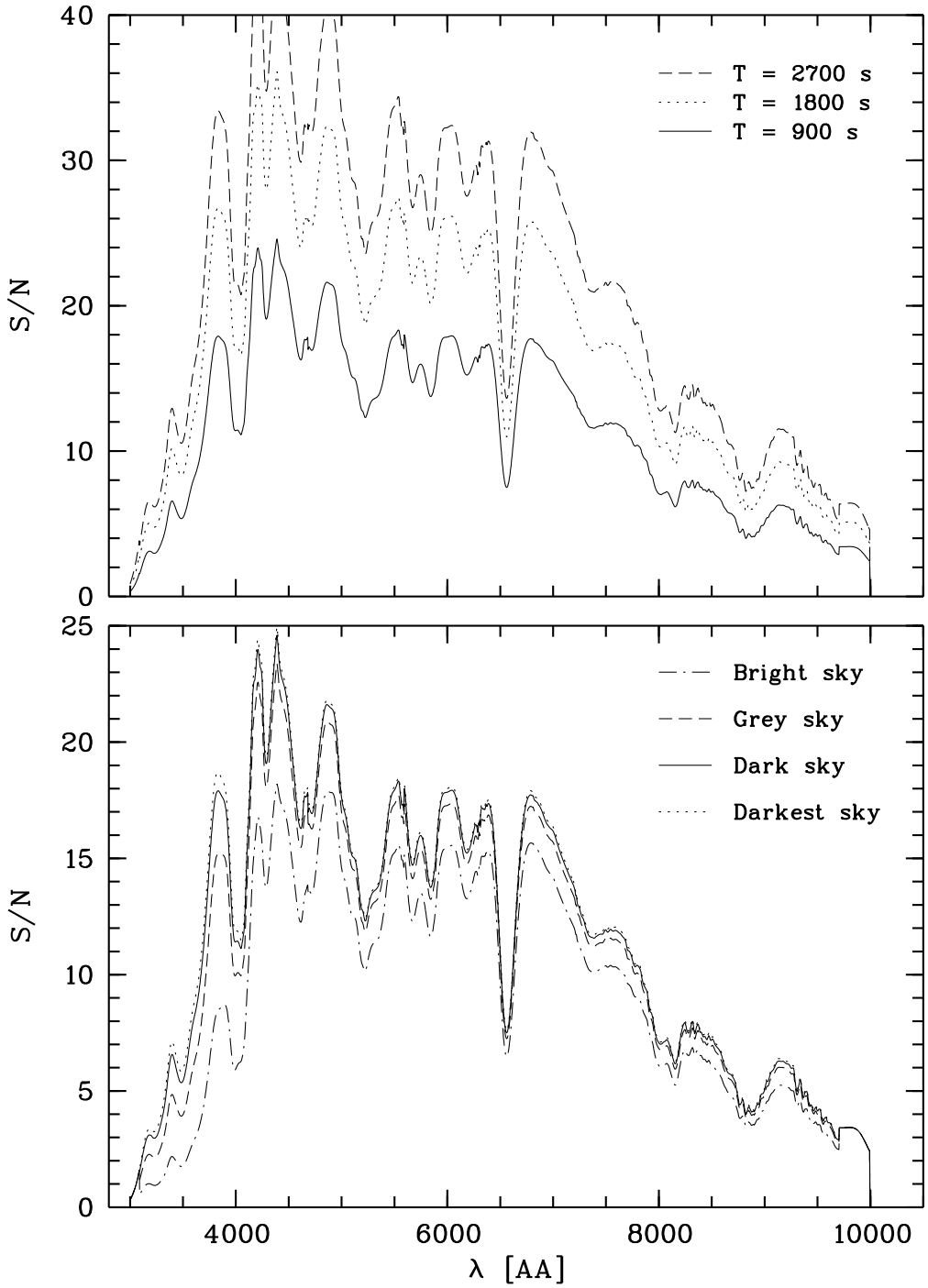

Fig. 11.— **Influence of the observing conditions on the SN Ia S/N.** *Upper panel:* influence of the exposure time; *lower panel:* influence of the sky brightness (see § 4.3 for definitions).

Chapter 3

Instrumental setup

1. *SNfactory* telescopes

The *SNfactory* relies on several existing telescopes to carry out its program. The *NEAT* program operates two telescopes to carry out its search for near-earth asteroids. The first of these is the 1.2-m telescope located at the Maui Space Survellience Station, operated at the Science City complex on the summit of Haleakala by the United States Air Force. *NEAT* operates a single 4k×4k thermoelectrically-cooled CCD behind a wide-field camera built by Boeing. The second *NEAT* telescope is the 1.2-m Oschin Schmidt on Palomar mountain, owned and operated by the California Institute of Technology. This telescope performed three famous photographic sky surveys: the Palomar Observatory Sky Survey, the Luyten proper motion survey, and the Second Palomar Observatory Sky Survey. Last April, work to upgrade the telescope to allow remote operation was completed. Currently a camera with three 4k×4k thermoelectrically-cooled CCD's is operating at the Oschin Schmidt; this summer Yale University will begin operating the QUEST II camera. *NEAT* has access to this telescope as part of the Jet Propulsion Laboratory's share in Palomar Observatory. This share of the Oschin Schmidt is currently 80%, but will decrease to 40% once the QUEST II camera is installed (with their former 40% going to Yale). Further details of the *NEAT* search cameras is given in Table 1 (Chap. 2, p.28). The *SNfactory* has access to the *NEAT* data from both of these telescopes through a MOU with JPL.

The primary follow-up for the *SNfactory* will be performed at the University of Hawaii's 2.2-m telescope, located on the summit of Mauna Kea. Mauna Kea is arguably the best astronomical site in the world, with excellent atmospheric stability producing some of the best image quality attainable from the ground. The *SNfactory* has arranged for collaborative use of 20% of the time on the 2.2-m, to be allocated as the 2nd half of the night on every first and third night of a five-night cycle. A near-infrared camera will be mounted at a second cassegrain

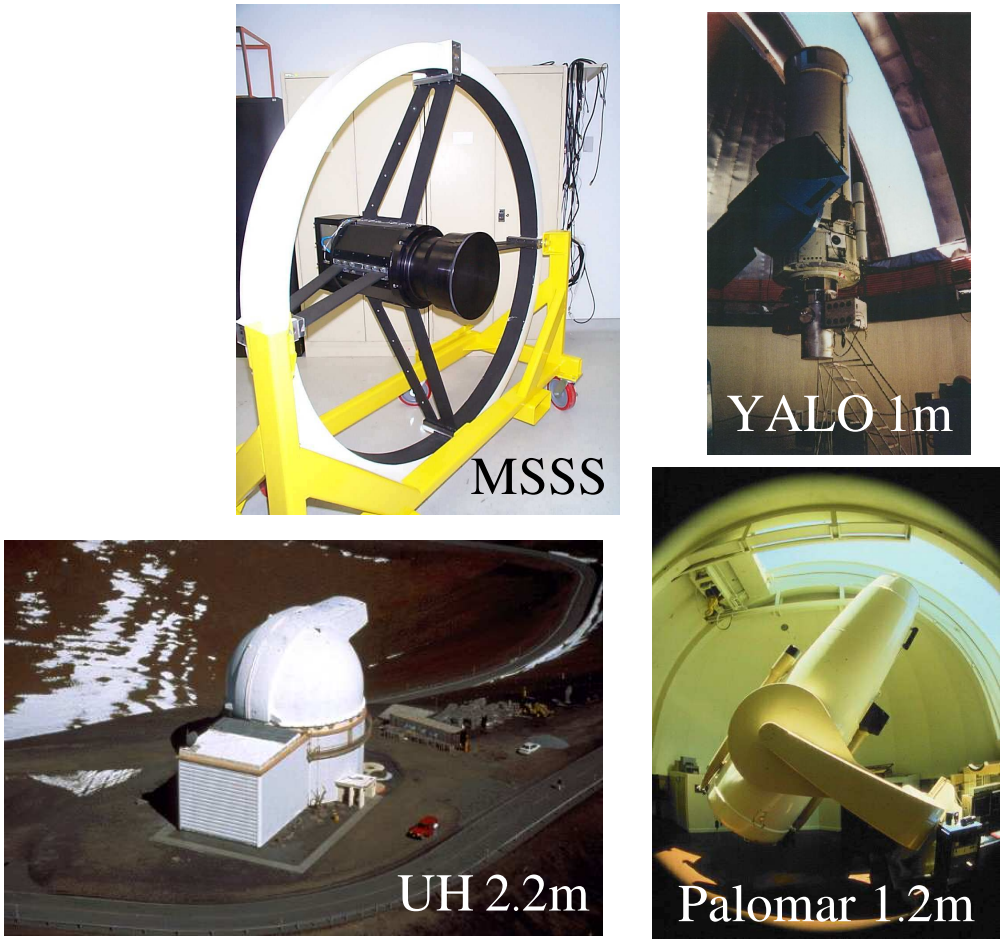

Fig. 1.— **Telescope Facilities Participating in the *SNfactory*:** Clockwise from upper left — the wide-field camera of the MSSS 1.2-m, the YALO 1.0-m telescope, the Oschin Schmidt telescope, and the University of Hawaii 2.2-m telescope. These telescopes are described more fully in the text.

port during bright time, in principle allowing us to obtain JHK photometry of the SNe Ia being followed with *SNIFS*. Access to time on this telescope is the rate-limiting step in the operation of this experiment. The typical losses due to weather and technical problems at the UH 2.2-m are provided in Table 1 (courtesy A. Pickles).

UH is working on completing implementation of remote telescope operations. This work has included an upgrade to the TCS to allow complete remote control of the telscope and dome. Further work will include installation of plumbing for cryo-coolers, the ability to remotely select the observing port, implematation of environmental monitoring and capabilities for remote instrument resets.

Since the *SNfactory* has some nights without access to the UH 2.2-m telescope we will need

Table 1: UH 2.2-m: Monthly Time Lost

Month	Weather (hrs/mon)	Technical (hrs/mon)
Oct 1999	34	2
Nov 1999	106	2
Dec 1999	122	6
Jan 2000	39	10
Feb 2000	12	2
Mar 2000	50	3
Apr 2000	62	1
May 2000	18	1
Jun 2000	17	10
Jul 2000	15	1
Aug 2000	22	1
Sep 2000	10	2

to obtain some imaging to screen potential SN candidates so that very rare events can be caught in a timely manner. We expect to obtain such imaging from the YALO I 1-m or the YALO II 1.5-m at the Cerro Tololo Interamerican Observatory in Chile. This access will come from a combination of United States national observatory time and Portugal time. Other possible sources of images may include LBNL's 80-cm telescope at Fenton Hill, New Mexico (under developement), the MAGNUM 2-m run by Japan on Haleakala, HI, or the ARC 3.5-m in New Mexico (if U. Chicago becomes involved in the *SNfactory*).

In addition to these ground-based facilities, the *SNfactory* has an on-going program on the Hubble Space Telescope (HST) to obtain ultraviolet spectroscopy of a limited number of nearby supernovae. The *SNfactory*'s ability to guarentee SN discoveries within a window of a few days eliminates the need for "target of opportunity" observations, which are very disruptive to the HST schedule and waste up to a day per SN of HST time. With input from the *SNfactory* the HST can observe twice as many SNe compared to the TOO mode other experiments require. Currently our program can observe about 5 SNe Ia per year, but we expect that as the *SNfactory* swings into full operation the HST will want to allocate more time to our program.

There is a great deal of interest by several groups in contributing in other ways to the *SNfactory* observations. As there is no other instrument in the world which can study SNe at optical wavelengths as effectively as *SNIFS* we are exploring complimentary observations, or

even the implementation of a second *SNIFS* at a second site. A second site has the great advantage of offering protection of against streaks of bad weather. Appropriately sited (e.g., at La Palma or Chile), a second *SNIFS* could allow the *SNfactory* to be "on sky" almost continuously. This would greatly improve our ability to respond to very rare events in need of quick observations.

2. NEAT

The SNfactory will search for supernovae using CCD images obtained by JPL's Near Earth Asteroid Team (NEAT). A proof-of-concept search conducted using two nights of NEAT data found 4 confirmed supernovae. NEAT has since expanded it's operation to include a 1.2-m telescope (at the 10,000 ft summit of Haleakala, Hawaii) working 18 nights per month. NEAT has agreed to examine supernova search fields three times during each month, giving the SNfactory the potential to find many supernova shortly after explosion. (Risetime — the time from explosion to peak brightness — is considered one possible parameter that could affect peak luminosity). In addition, since this search covers large portions of the sky irrespective of known galaxies, it will be rid of the biases to which pointed searches are subject due to their reliance on existing galaxy catalogs. NEAT will soon quadruple it's capacity, with a second 1.2-m telescope operating at Mt. Palomar with a large CCD camera, so we expect to discovery several supernovae per night.

As with the proof-of-concept search, NEAT data will be transferred in near realtime via high-speed Internet connection to Lawrence Berkeley Nation Lab (LBNL, where 1 Tb of NEAT data is already archived). Once there, the images will be processed and searched using automated software developed by the Supernova Cosmology Project (SCP) and further refined by the SNfactory. Candidate supernovae will be screened interactively and assigned a preliminary follow-up priority. An important aspect of the SNfactory is that the selection of supernova candidates will be quantitative and traceable, something current surveys completely lack and which makes calculations of supernova rates and peculiarity fractions extremely difficult.

The most revolutionary aspect of the SNfactory — aside from the huge numbers of supernovae it will find — is the coordinated follow-up using instrumention tailored to the study of supernovae. Candidate supernovae found in the NEAT images must first be screened with spectroscopy to confirm the supernovae and reveal its type (Ia, II, Ib, Ic) and redshift. The SNfactory will not only discover supernovae closer to explosion that other surveys do, with a 12 hr turn-around it will also begin the follow-up much much sooner. Typically candidate supernovae are confirmed with imaging on subsequent nights, then reported to the IAU Circulars, and then observed spectroscopically with regular – but infrequently — scheduled time or director's discretionary time (requiring a proposal for each supernova and the availability of the right instrumentation). This process can easily stretch on for a week or more after discovery.

3. SNIFS

Subsections, spec. table, transmissions.

Numbers have to be checked! V1 YC 04/06

3.1. Overview

Traditionally supernovae have been followed with *BVRI* photometry, and spectra beyond the initial confirmation spectrum are rare. The SNfactory will change all that. Using a integral field unit on a two-channel (blue & red) optical spectrograph, the SNfactory's **S**uper**N**ova **I**ntegral **F**ield **S**spectrograph (*SNIFS*, under construction at CRAL-Observatoire de Lyon) equipped with LBNL's red-enhanced CCD's (see Fig 2), will allow spectroscopy of supernovae at all epochs. Because these spectra will be spectrophotometric, *UBVRIZ* photometry can be synthesized from these spectra, without the uncertainties due to photometric color terms and K-corrections (the latter usually based on non-spectrophotometric spectra). *SNIFS* will retain one advantage of the traditional approach, which allows surrounding field stars to be used for flux scaling when conditions are non-photometric, by also having an imager which integrates on the field immediately surrounding each supernova and having the exact same exposure as the integral field unit.

3.2. Technical design

The opto-mechanical layout of *SNIFS* is shown in Fig. 3. The operation of *SNIFS* is intended to be fully automated. An observer/technician is needed to prepare the telescope for observing, point the telescope to targets designated by the SNfactory, close the telescope, and possibly ensure that the *SNIFS* dewars are supplied with LN2. *SNIFS* is intended to be capable of focusing the telescope, recognizing star fields near requested targets using it's own imager, adjusting the telescope pointing to place the desired target on the integral field unit, and acquire and guide on a suitable star. It will then execute an observing sequence for the spectrograph and imager, read out the date, determine the quality of the data, and take it's own calibration (afternoon dome flats may also be required on occasion). Moving parts on *SNIFS* are limited to a shutter, filter wheel, and pick-off mirror (feeding the spectrograph). The electronic components consist of detector readout (for 4 CCD's), a shutter, filter wheel, calibration lamps, and status-monitoring. Software interface to the telescope control system to execute pointing and focus adjustments, and to obtain information for the data headers and control software will be necessary. An additional software interface to the Internet is required to transfer the imager and spectrograph data (at most 64

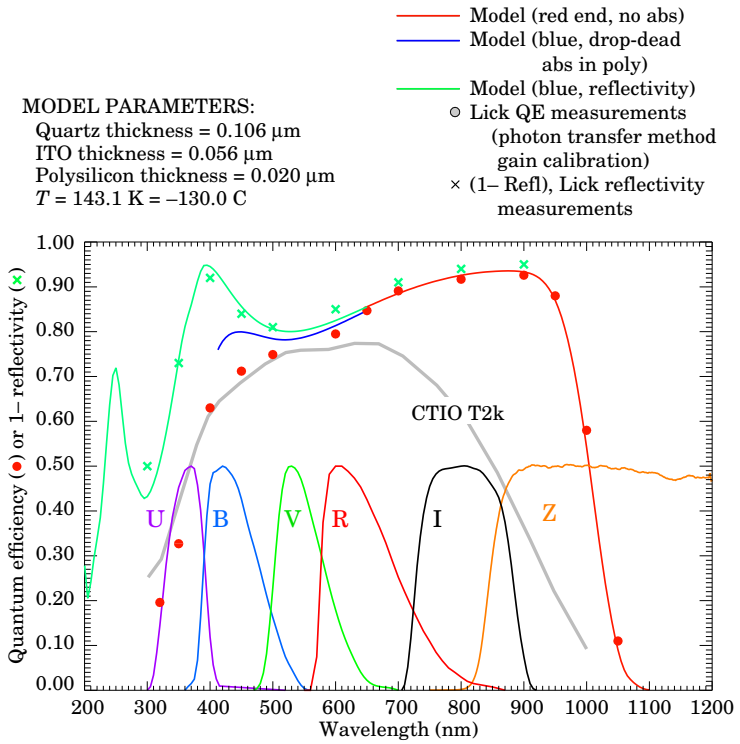

Fig. 2.— **Measured QE of LBNL red-enhanced CCD:** The black solid circles show the measured QE as a function of wavelength for a LBNL 2k×2k CCD. The red crosses show 1−reflectance as a function of wavelength for the same device. Overlaid on these measurements are model calculations derived from the known physical parameters of the CCD's. Also overlaid as a thick gray line is the QE for a good imaging CCD from Cerro Tololo Interamerican Observatory. The standard $UBVRIZ$ bandpasses are also shown for reference. Note that this CCD has enhanced QE in at longer wavelengths than conventional thinned CCD's due to it's greater thickness (300 μm, which is fully deleted). The anti-reflection coating is also optimized for red wavelengths. These devices are free of fringing, which plagues other CCD's at red wavelengths. The difference between 1−reflectance and the QE indicates losses in the polysilicon gettering layer. An anti-reflection coating optimized for blue wavelengths would improve the blue performance slightly. Alternatively, *SNIFS* may use an EEV CCD for the blue channel.

Mbytes every 10 minutes, and that only during the fraction of time *SNIFS* is operating) to Europe and the United States so that the observing program can be revised as needed based on the new observations.

3.3. Technical implementation

The *SNIFS* instrument consists of 3 parts:

- The spectrograph continuously covers a $6'' \times 6''$ field of view with a sampling of $0.4''$. It has blue and red channels, which are operated simultaneously, generating spectra on 2k×4k LBNL red-enhanced CCD's at resolutions of 4.5 Å and 6.6 Å, respectively.
- The imager consists of a 2k×4k LBNL red-enhanced CCD with 15 μm pixels, which views the sky surrounding the spectrograph pick-off mirror.
- The built-in guider/focuser consists of a second identical CCD. The imager and guider are used directly, without re-imaging optics.

IFS channel

The *SNIFS* IFS is a two-way optical spectrograph equipped with a microlense-array integral field unit (see Table 2). The blue channel will cover 3500–5700 Å at a fixed dispersion of ~ 2.2 Å/pixel, while the red channel will cover 5300–10500 Å at a fixed dispersion of ~ 3.0 Å/pixel. The nominal resolution is set by the pixel sampling, and is therefore $\delta\lambda/\lambda \sim 1200$. The two channels can be operated together or separately, and are split using a dichroic beam-splitter with a nominal half-power point at 5500 Å. The target system throughput is 30% or better over 50% of the spectral range, and no worse than 10% anywhere over the full spectral range. The integral field unit consists of a 15×15 array of fused silica microlenses, and will sample a $6'' \times 6''$ region around the target at a resolution of 0.4" per lenselet. The optics are all transmission elements, including the dispersive element which is a total internal reflection prism mated to a grism. The detectors will be LBNL high-resistivity fully-depleted CCD's, of size 2048×4096, with high-performance AR coatings. A conceptual drawing of the IFS is presented in Figure 3.

A computation of the global transmission of the IFS blue and red channels is presented in Fig. 4. This computation includes (see Fig. 5 for details):

- the typical Mauna-Kea atmosphere,

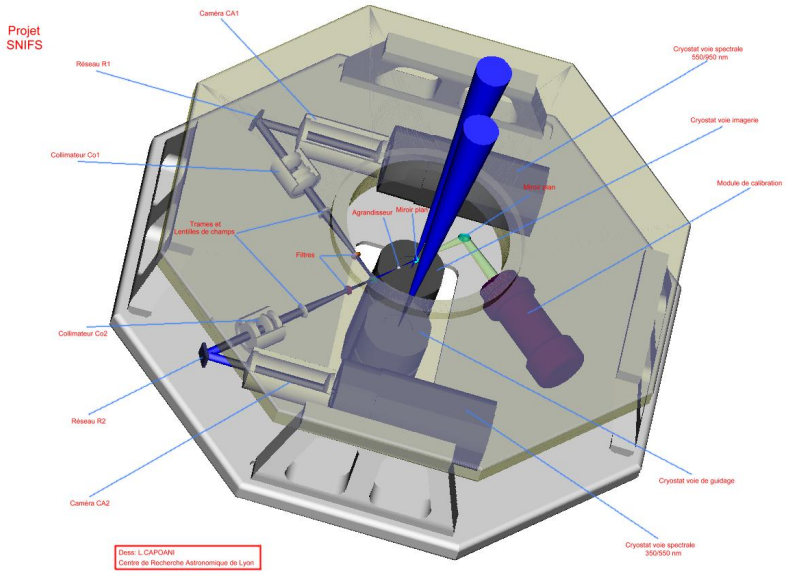

Fig. 3.— **Mock-up of *SNIFS* spectrograph for UH 88-inch telescope.** The on-axis f/10 beam from the telescope impinges on a total internal reflection pick-off prism which directs light into the two-channel spectrograph. The light is then split by a dichroic, sent through custom collimators, grism, camera, and CCD's for each of the two channels. Light not intercepted by the pick-off prism illuminates the photometry camera. The photometry camera and the spectrograph share a shutter. An off-axis beam illuminates the guider camera at all times, allowing fast guiding during spectroscopy, and focusing or offsetting between exposures (i.e. during readout of the spectrograph and photometry detectors).

- the 3 Aluminium-coated mirror telescope,
- the pick-off prism and the input enlarger,
- the dichroic, centered at 5300 Å,
- the field lens and the micro-lens array in each channel,
- the red and blue spectrographs, including the collimator, the grism and the camera,
- the CCD window and QE (see Fig. 2).

The total throughput of the spectrograph is $\sim 25\%$ in each channel.

Photometric channel

SNIFS includes a photometry camera run in parallel with the spectrograph (see Table 2). This photometry camera is designed to allow photometric normalization of the spectroscopic observations so that spectrophotometric observations can be obtained even under non-photometric sky conditions, as discussed in more detail in Chapter 4. The photometry camera and spectrograph will utilize the same shutter so that observations with both instruments are guaranteed to have identical observing conditions. The photometry camera will have one or more filters, probably fixed (TBD). Again, it is likely that an LBNL 2048×4096 CCD will be used.

A computation of the global transmission of the photometric channel is presented in Fig. 6. It includes (see Fig. 5 for details):

- the typical Mauna-Kea atmosphere,
- the 3 Aluminium-coated mirror telescope,
- the CCD window and quantum efficiency (see Fig. 2).

The total throughput is $\sim 50\%$ in in the V-band.

Auto-guider

SNIFS contains its own guider camera. Most likely a LBNL 2048×4096 CCD will be used as the detector. The guider obtains a panoramic image from which a suitable guide star is selected.

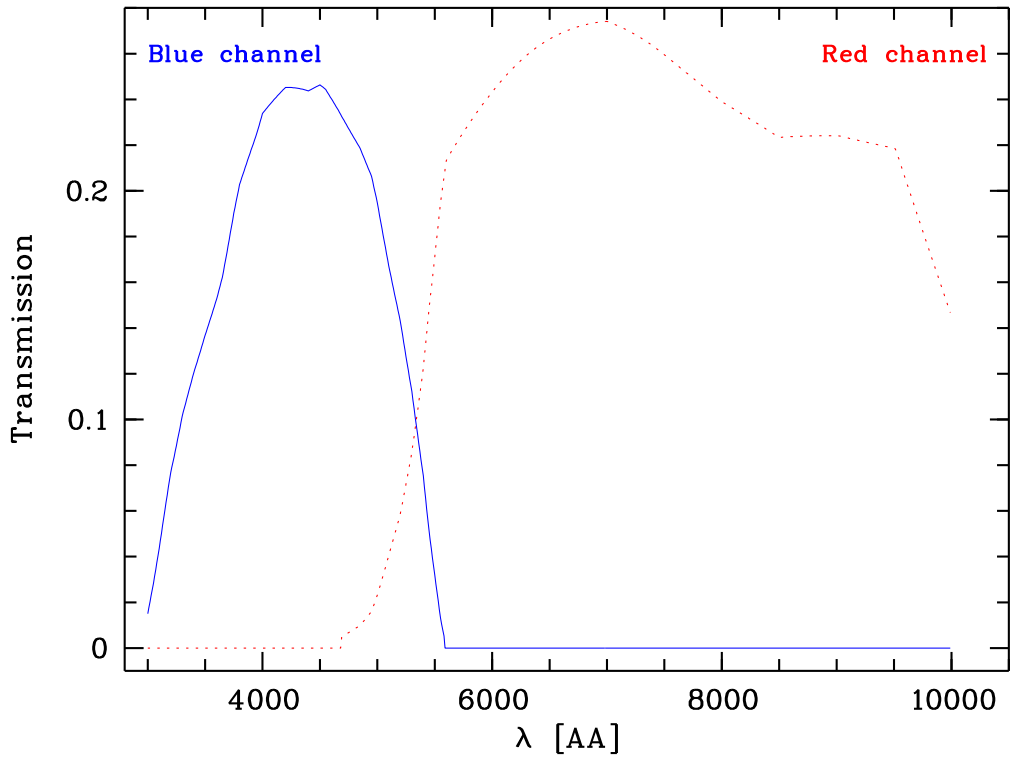

Fig. 4.— **Transmission of the *SNIFS* spectroscopic blue and red channels.**

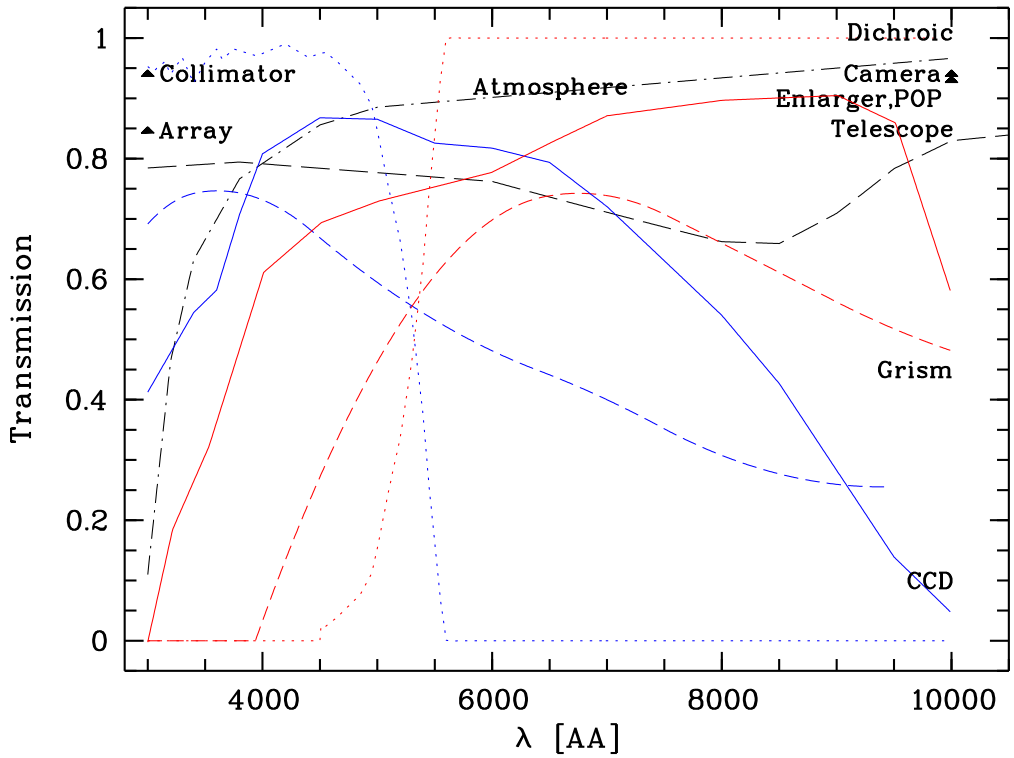

Fig. 5.— **Individual transmission of the *SNIFS* elements,** including atmosphere (*dash-dot*), telescope (*long dash*), dichroic (*dot*), grism (*dash*) and CCD (*full*), as well as other barely chromatic elements (POP, enlarger, field lens and micro-lens array, collimator, camera: *triangles*).

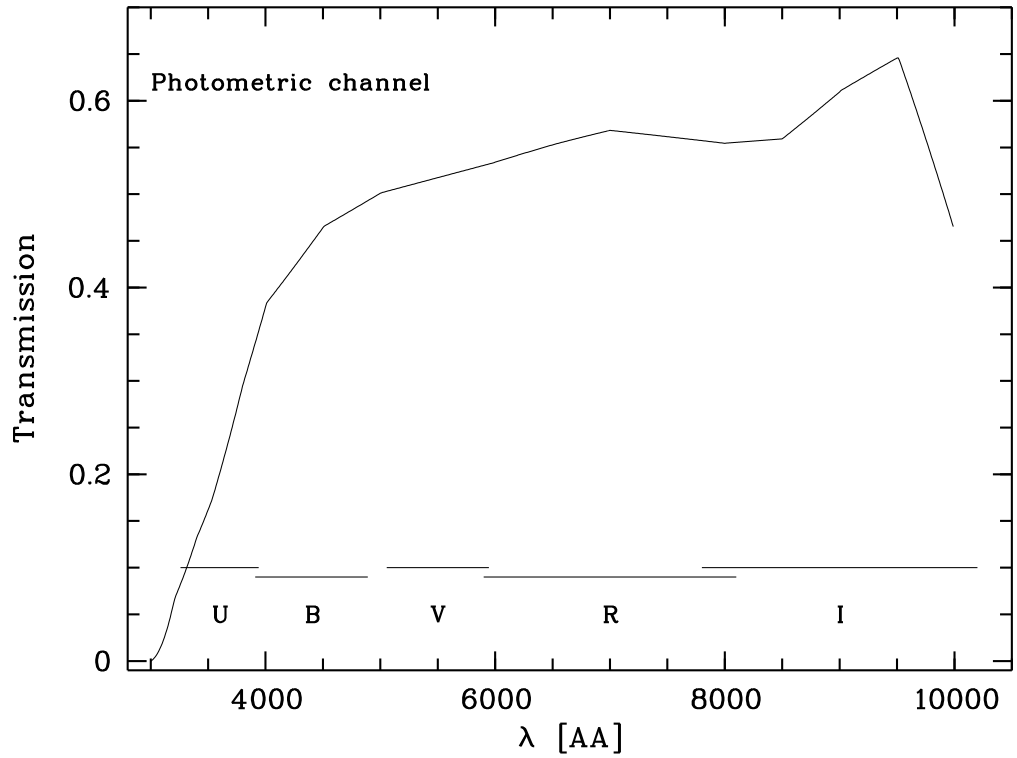

Fig. 6.— **Transmission of the *SNIFS* photometric channel.** The typical Bessel filters *UBVRI* are indicated.

Subsequently, a sub-region of the guider CCD centered on the guide star is read at a rate of several Hz and analyzed to provide a signal to the telescope guider motors. A portion of the guide camera is covered with a cylindrical lense or wedge to provide a signal for control of the telescope focus.

The guider FOV is the same as the *SNIFS* imager, 4.8′×9.6′∼0.013 deg^2. We have explored at what magnitude there will be an adequate number of guide stars in any randomly chosen field. First we determine the probability of finding no guide stars when the average expected number is N. That is, to ensure the presence of a star, the mean density must be some number N such that the probability, $P(k, N)$, of obtaining $k \equiv nstars = 0$ is less than some acceptable number (say P = 1/1000). $P(k, N)$ is given by the Poisson distribution $(N^k)e^{-N}$/k, which for $k = 0$ simplies to e^{-N}.

Let's try some values of N:

Here we see that if the mean number of guide stars per field is greater than 7 then blank guiding fields should be very rare (and never occur for our SNe). The required stellar surface density which will guarentee that necessary number of stars is therefore 7 stars/0.013 deg^2 ~ 550 stars/deg^2.

Star counts from my POSS I catalog of a high-latitude field are given in Table 3. A POSS I plate covers about 40 deg^2, so to reach a surface density of 550 stars/deg^2 we need 22000 stars per plate. From Table 3 we see that by $B = 17.75$ there are enough stars to guarentee the presence of a guide star. Even for 3 guide stars per field — a surface density which is reached at $B = 16.25$ — a failure results only 1 in 20 times. Since this failure can be predicted from existing catalogs, or the *NEAT* images themselves, the *SNfactory* can expect to work with brighter guide stars on average.

The next question is whether such stars will provide enough counts for guiding at a rate of 1 Hz or better. $B = 0$ yields 1461 ph/cm^2/s/Å, so in a 1000Å filter on a 2.2-m telescope with 40% efficiency a $B = 17.75$ mag star will provide 1765 counts/s. If the seeing has a dispersion of 1″/2.355 = 0.42″ then the centroid will be known to $0.42/\sqrt{1765} = 0.010''$ in each direction. (Note that the readout variance might be about 100 counts, summed over all the pixels in the fast-readout box.) This is for an integration of one second; faster guiding should be possible up until the point where readout noise becomes important, say 1/10 sec. Sky noise would only matter when the Moon is bright. At $B = 16.25$ we would obtain roughly 7026 cnts/sec, easily allowing guiding at a rate of 10 Hz.

If we extend the multi-filter over to the guider (rather than have a broadband filter over the guider), then the bandpasses might be only 400Å wide, in which case the count rate would be 40% of the above values. Still, the worst-case centroiding would be good to 0.016″in each direction for one second integration in this situation. In this arrangement the red bandpasses wouldn't be suitable for guiding if one were at high airmass, thus the guider's effective areal coverage would

be about 50% smaller assuming red filters cover about half of the field. This may be only a minor problem since fainter guide stars in blue filters could be used, and one has to be at high airmass with the only available guide star in a red filter. We could even mitigate against this by placing the red multi-filter bandpasses closer to the POP than the blue multi-filter bandpasses so red bandpasses could be used at high airmass. Of course some correction for atmospheric dispersion could also be built into the guider software.

The intended operational mode for *SNIFS* is quasi queue observing. Target coordinates and exposure sequences are generated automatically. It is anticipated that with the telescope close to the correct nominal coordinates, the photometry/guider camera will provide images from which a coordinate offset can be computed quickly, and sent to the telescope and the guider to execute.

Calibration unit

SNIFS is also equipped with a calibration unit for the spectrograph which will provide for spectral flats and arc exposures. Flat-field correction for the photometry camera will rely on dome flats and sky flats. Twilight flats will be useful for both the spectrograph and the photometry camera, and will be obtained when possible.

4. Complementary instruments

The *SNfactory* has an interest in obtaining observations in addition to those from *SNIFS*. One overriding concern will be to try to arrange for complementary data streams whose reduction and analysis can be automated. If is very common within the SN community to receive offers for a little help with one object or another, but if hand work is needed for each of these observations it may actually decrease the overall efficiency and effectiveness of the *SNfactory*.

The complementary observations of highest priority are JHK lightcurves for the *SNfactory* SNe Ia being followed with *SNIFS*. These can be obtained using the *SNfactory* time on the UH 2.2m for brighter SNe Ia. However, this would then impact the number of SNe Ia per year that the *SNfactory* could study in detail. Thus, other supplementary sources of this NIR data are being investigated, with an emphasis on queue-scheduled facilities. For instance there may be a niche for *SNfactory* NIR observations at telescopes like Gemini and VLT when the seeing is too poor for the faint sources typical of most other programs.

Since perhaps only 50% of all optical transients discovered in the *NEAT* search will be Type Ia SNe in our desired redshift range, and because we don’t currently have access to

the UH 2.2m every night, there might be a role for a telescope whose purpose would be to spectroscopically screen *SNfactory* candidates. Again, a queue-scheduled telescope with a spectrograph at the ready is called for since spectroscopy requires getting the object down a slit and we are unaware of any other spectrograph with the automated acquistion system planned for *SNIFS*.

Other complementary observations will included UV spectroscopy with HST, and very likely spectropolarimetry for bright SNe Ia at VLT. These are established programs by scientists at LBL, which could be brought under the umbrella of the *SNfactory*. NIR spectroscopy is another area in which the *SNfactory* may wish to partner with on-going studies.

Finally, it may prove useful to have the ability to obtain classical filter-photometry lightcurves. Certainly this should be the approach for very nearby SNe Ia which will be used for peculiar velocity studies. Such imaging may also help with candidate screening, possibly providing color-curves that may help distinguish SN types. LBL has for some time planned the automated operation of a 0.8-m telescope, and there is now good progress in getting this telescope working with a thermoelectrically cooled CCD at the DOE's Fenton Hill site in New Mexico. The *SNfactory* also has on-going discussions concerning the use of YALO-II imager at CTIO.

Table 2: Current specifications of *SNIFS* on the University of Hawaii 2.2 m $f/10$ telescope (Mauna Kea).

	IFS channel	
Microlens array	15×15	
Spatial sampling	$0\farcs4$	
Field of view	$6'' \times 6''$	
	Blue channel	Red channel
Wavelength range	3200 Å – 5400 Å	5400 Å – 1 μm
Spectral sampling	2.2 Å pix^{-1}	3.0 Å pix^{-1}
Instrumental dispersion ($\sigma_{\rm inst}$)	$\sim$130 km/s	$\sim$100 km/s
Cross-dispersion separation	$\sim$3.8 FWHM	$\sim$3.8 FWHM
Detector	Marconi 2k$\times$4k	LBNL/UCB 2k$\times$4k
Pixel size	15 μm	15 μm

	Photometric channel
Spatial sampling	$0\farcs14$
Field of view	$4\farcm8 \times 9\farcm6$
Detector	LBNL/UCB 2k$\times$4k
Filter	multi-chromatic
Spectral bands	U,B,V,R,I

N	k	$P(k,N)$
3	0	1/20
4	0	1/55
5	0	1/148
6	0	1/403
7	0	1/1096

Table 3: POSS I *B*-band Star Counts at High-Latitude

B mag	N	N(<B)
6.750	4	4
7.250	2	6
7.750	4	10
8.250	10	20
8.750	9	29
9.250	23	52
9.750	30	82
10.25	84	166
10.75	101	267
11.25	186	453
11.75	268	721
12.25	405	1126
12.75	564	1690
13.25	763	2453
13.75	1072	3525
14.25	1355	4880
14.75	1762	6642
15.25	2298	4060
15.75	2859	6919
16.25	3550	10469
16.75	4265	14734
17.25	5068	19802
17.75	5940	25742
18.25	6853	32595
18.75	6617	39212

Chapter 4

Calibration procedures

The baseline requirement for spectrophotometry for the SNfactory is an internally consistent extra-atmospheric flux calibration with systematic accuracy better than 1% under photometric conditions and better than 3% under non-photometric conditions. A knowledge of the flux calibration error on an internally consistent system is also required. A derived requirement is knowledge of whether conditions are photometric or non-photometric. The flux calibration systematics requirements apply over the spectral range where the total system throughput is greater than 20% of peak ($\sim$3500–10500Å), with the exception of the sharp atmospheric O_2 bands (6900Å and 7600Å).

The components necessary to determine the flux calibration include:

$$
\begin{aligned}
t &= \text{time} \\
\lambda &= \text{wavelength} \\
X &= \text{airmass} \\
k(\lambda, t, X) &= \text{atmospheric extinction, as a function of } \lambda, t, X \\
\phi(\lambda, t) &= \text{telescope throughput, as a function of } \lambda, t \\
\xi(\lambda, t) &= \text{instrument throughput, as a function of } \lambda, t \\
D(\lambda, t) &= \text{detector quantum efficiency, as a function of } \lambda, t \\
S(\lambda) &= \text{intrinsic standard star spectrum, as a function of } \lambda \\
s(\lambda, t, X) &= \text{observed standard star spectrum, as a function of } \lambda, t, X \\
F(\lambda) &= \text{intrinsic field star spectrum, as a function of } \lambda \\
f(\lambda, t, X) &= \text{observed field star spectrum, as a function of } \lambda, t, X
\end{aligned}
$$

$S(\lambda)$ is given by published spectrophotometry of standard stars. It is possible that these published

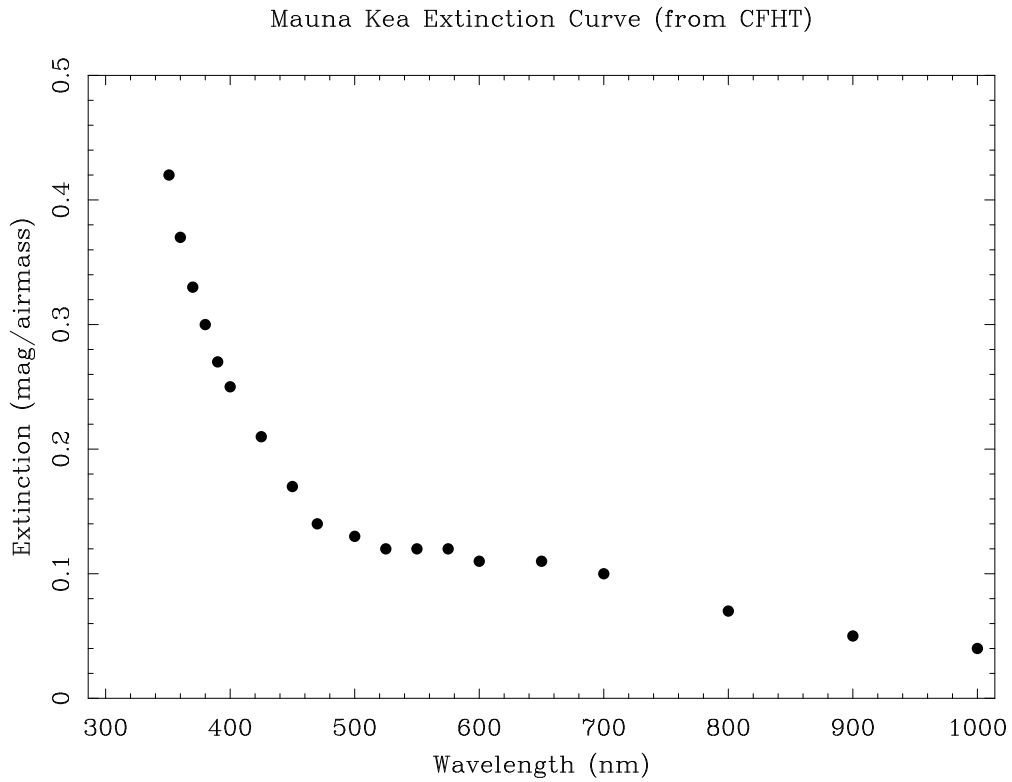

Fig. 1.— The extinction, in magnitudes per airmass, typical of Mauna Kea.

results contain systematic errors which exceed the desired SNfactory spectrophotometry absolute calibration budget. At this stage nothing can be done about this, thus only an internally consistent calibration budget is specified.

Atmospheric extinction can be decomposed into contributions from Rayleigh scattering, aerosol scattering, ozone absorption, molecular oxygen absorption, water absorption, and water scattering. None of these components can be considered constant, but a great deal is known about the typical spectral and temporal behavior of these components from calculations and monitoring. According to the GONG site survey (Hill, *et al.* 1994), the extinction at Mauna Kea is among the lowest and most stable of any astronomical site. The average optical extinction on clear days is 0.074, with a dispersion of only 0.015. The power spectrum of transmission variations measured by GONG during clear days follows the relation

$$(\Delta I/I_o)^2 = (\nu/10^{-6.80} Hz)^{-1.50} \tag{4.1}$$

where ν is the time frequency in Hz. This implies variations of 0.4% on timescales of one hour and variations of 1.7% over the course of a night. At La Silla, Burki, *et al.*, 1995 found that the total U-band extinction is correlated over a period of several days and that over one night the autocorrelation drops by only 5% (implying a typical 2.2% variation in extinction). These data

indicate that ∼1% extinction variations can be expected over the course of a clear night, even at the best astronomical sites.

A closer examination of the following extinction components is needed to help clarify the source and spectral characteristics of such extinction variations:

Rayleigh scattering: Extinction due to Rayleigh scattering, k_R, is known to follow $a_R\lambda^{-4+x}$, where $x \sim 0.04$ is a very small correction to the canonical law. Rayleigh scattering dominates the extinction at most wavelengths under photometric conditions. a_R depends on the molecular scale height (roughly 8 km) which depends on altitude, and on weakly varying parameters like temperature, T, and pressure, P.

Aerosols: Extinction due to aerosol scattering, k_a, is generally the second greatest contributor. k_a is often parameterized as $a_a\lambda^{\gamma}$ (Ångstrom 1961). γ can vary widely, as shown in Fig. 2, using observations from Mauna Loa. γ depends on the particle size distribution of the aerosols, which shows variation with the source of a given mass of air and can change appreciably after significant volcanic explosions. Burki *et al.* 1995 determined $\gamma = -1.39$ for La Silla using nights of low extinction. My modeling of the Mauna Kea extinction curve using libRadtrans indicates that a simple power law is inadequate to describe the aerosol scattering at that site. The aerosols on Mauna Kea are likely a mix of sea salt and volcanic dust from the summit and/or nearly islands ("vog," as it is known in Hawaii). The strong temperature inversion layer below the summit helps to keep a significant fraction of aerosols below the summit. Scattering (but not absorption) by suspended water droplets is generally included in the aerosol scattering budget.

Water vapor and ice: The extinction due to absorption by water vapor or clouds, $k_{H_2O,a}$ is generally absent or weak weak expect at a few wavelength intervals in the red. The night time scale height for H_2O is roughly 1 km. CSO monitoring indicates that $k_{H_2O,a}$ easily varies by factors of 2 over a few days (outer quartiles at 1.7 and 5.9 mm of water), and by several tens of a percent during a night on Mauna Kea (see Figs. 3 and 4). $k_{H_2O,s}$ only need be considered when clouds are present. It will be very time-variable as clouds pass through the field of view. $k_{H_2O,s}$ is spectrally neutral according to theory due to the large number of random scatters in large water droplets or ice crystals.

Oxygen: Extinction due to ozone absorption, k_{O_3}, sets the UV limit for terrestrial observations, but is generally smaller than Rayleigh scattering over most of the optical spectrum. k_{O_3} has a spectral shape which is well known, but it's amplitude has seasonal variations and it is also reported to vary on timescales of hours (Hayes & Latham 1975). Daily O_3 observations covering 1966—2000 from Mauna Loa have a dispersion of 7%, with peak-to-peak variations of 36% (see www.cmdl.noaa.gov/dobson). A histogram of daily Mauna Loa ozone column values is shown in Fig 5. O_2 also produces absorption, k_{O_2}, which results in the A and B band absorption features.

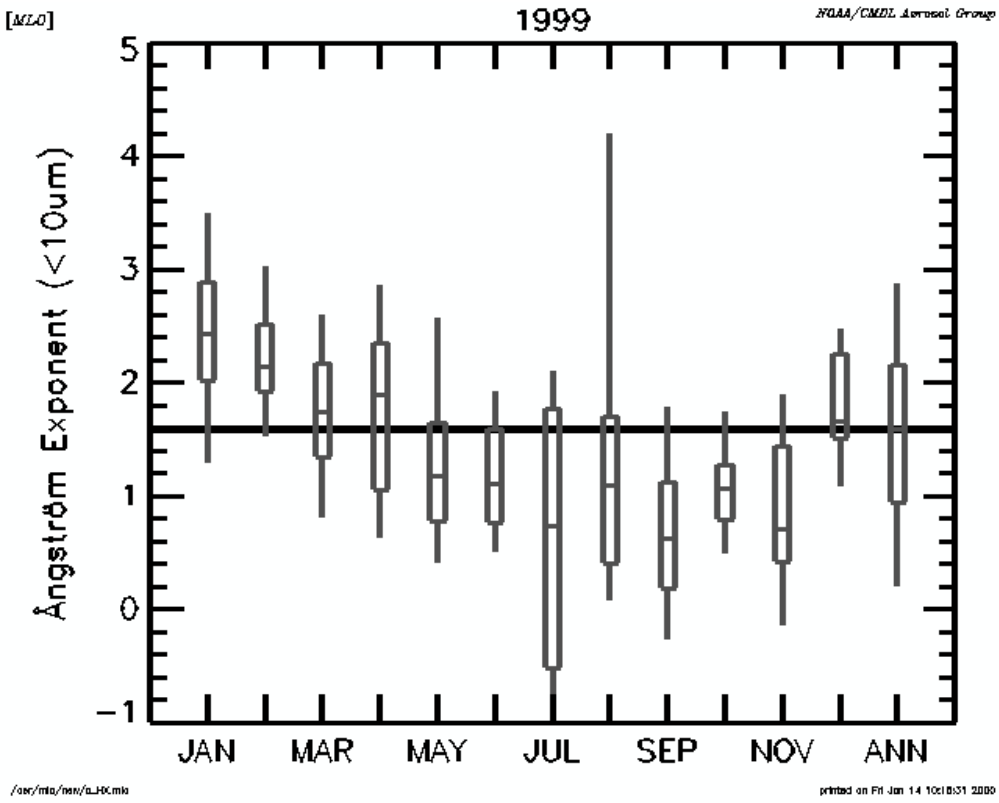

Fig. 2.— **The variation in the Ångstrom aerosol extinction parameter**, γ, measured over Mauna Loa in 1999. The central bar is the median, the boxes define the 25—75% range, and the outer whiskers denote the 5—95% range. Note that the Ångstrom exponent in this graph is equal to $-\gamma$. (From wwwsrv.cmdl.noaa.gov/aero/net/mlo/datacheck_mlo.html.)

These are strong but narrow, and their shape is well known.

It is generally assumed that extinction sources follow the Beers-Lambert relation:

$$I_{obs} = I_{true} e^{-kX} \tag{4.2}$$

so the relation between the true spectrum of a star, $S(\lambda)$, and its observed spectrum, $s(\lambda, t, X)$ is given by:

$$s(\lambda, t, X) = \phi(\lambda, t)\xi(\lambda, t)D_S(\lambda, t)S(\lambda)\ exp[-X \sum_{i}^{5} k_i(\lambda, t)] \tag{4.3}$$

Exceptions include k_{O_2}, which goes as $X^{0.55}$, but this contribution can be easily determined from spectroscopy since it is so spectrally isolated. Assuming that the Beers-Lambert relation holds,

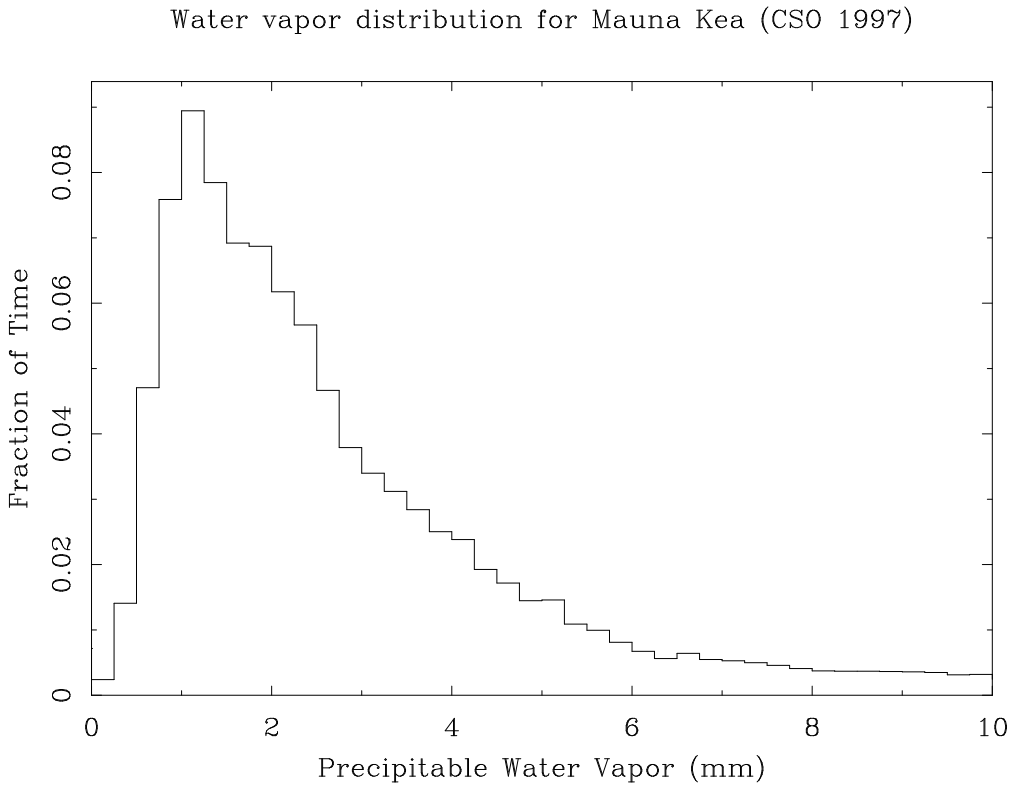

Fig. 3.— The frequency distribution of water vapor typical of Mauna Kea.

the total extinction can be written as:

$$k(\lambda,t) = k_R(\lambda) + k_a(\lambda) + k_{O_3}(\lambda) + k_{H_2O,a}(\lambda) + k_{H_2O,s}(\lambda) + k_{O_2}(\lambda)$$
$$= a_R(t)\lambda^{-4+x} + a_a(t)\lambda^{\gamma} + a_{O_3}(t)\tau_{O_3}(\lambda) + a_{H_2O}(t)\tau_{H_2O}(\lambda) + a_{cld}\tau_{cld}(\lambda)) + a_{O_2}(t)\tau_{O_2}(\lambda) \quad (4.4)$$

The functions $\tau_i(\lambda)$ represent the spectral properties of those extinction terms which are somewhat complicated, but which are known from external measurements. Note here I have separated the H_2O into a "normal" component which includes only absorption, and a "cloud" component. The scattering due to water vapor is not included in the "normal" component since it is is already accounted for in the aerosol-scattering term. The "cloud" term accounts for scattering by water and ice in clouds. τ_{cld} can change slightly depending on the ice/water fraction of the clouds, and further work is needed to characterize such changes. Additional absorption by water vapor in clouds is accounted for in the above scheme by the "normal" water component.

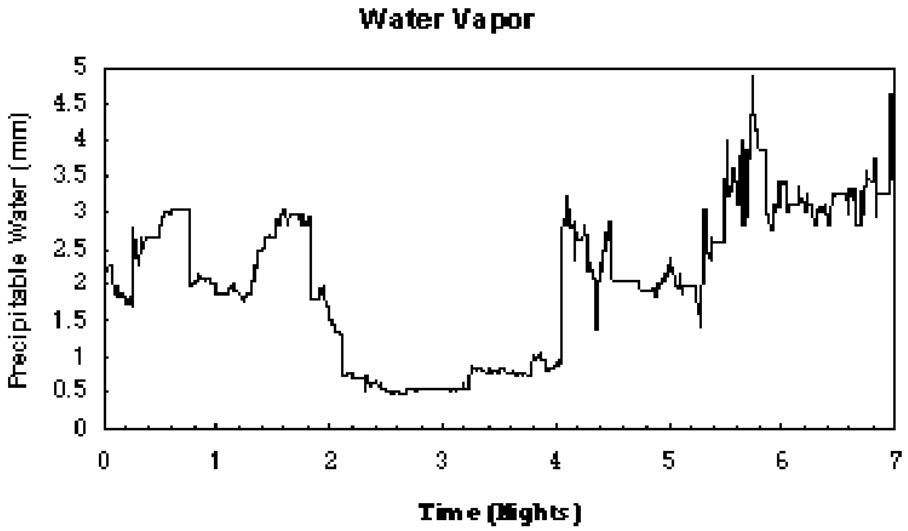

Fig. 4.— Representative Mauna Kea water vapor monitor readings, from CSO.

1. Extinction Correction under Photometric Conditions

When conditions are photometric, k is isotropic on the sky and has no time dependence. In this case $k(\lambda) = \sum_i^5 k_i(\lambda)$ can be solved for in Eqn. 2 by observing the spectrum, $s(\lambda, t, X)$, of at least two stars with known intrinsic spectrum, $S(\lambda)$. This statement implicitly assumes that the combined response of the telescope, instrumentation, and detector, given by:

$$C(\lambda, t) = \phi(\lambda, t)\xi(\lambda, t)D_S(\lambda, t) \tag{4.5}$$

is constant in time. That is, it is assumed that $C(\lambda, t) = \overline{C}(\lambda)$, an issue which will be discussed below.

If $k(\lambda)$ is solved for at each wavelength, it is not necessary to determine the individual $k_i(\lambda)$ values for each extinction component. However, if $k(\lambda)$ must be smoothed due to low S/N or other reasons, then the relative contributions of the smooth (k_R, k_a, k_{O_3},$k_{H_2O,s}$) and structured ($k_{H_2O,a}$, k_{O_2}) components must be determined separately. Most reduction methods do this in an approximate way by only separating $k_{H_2O,a}$ and k_{O_2} at wavelengths were they are very large, and including spectral regions where they are not so strong in the calculation of the smooth component.

It will be useful to verify the above parameterization of k by decomposition of the SNfactory observations of spectrophotometric standards. This is tractable because the relative contributions of the various components vary with wavelength. Table 1 gives the relative contributions to the total extinction (mostly from La Silla); several key wavelengths at which a given atmospheric component will be most easily separable have extinction values indicated in bold.

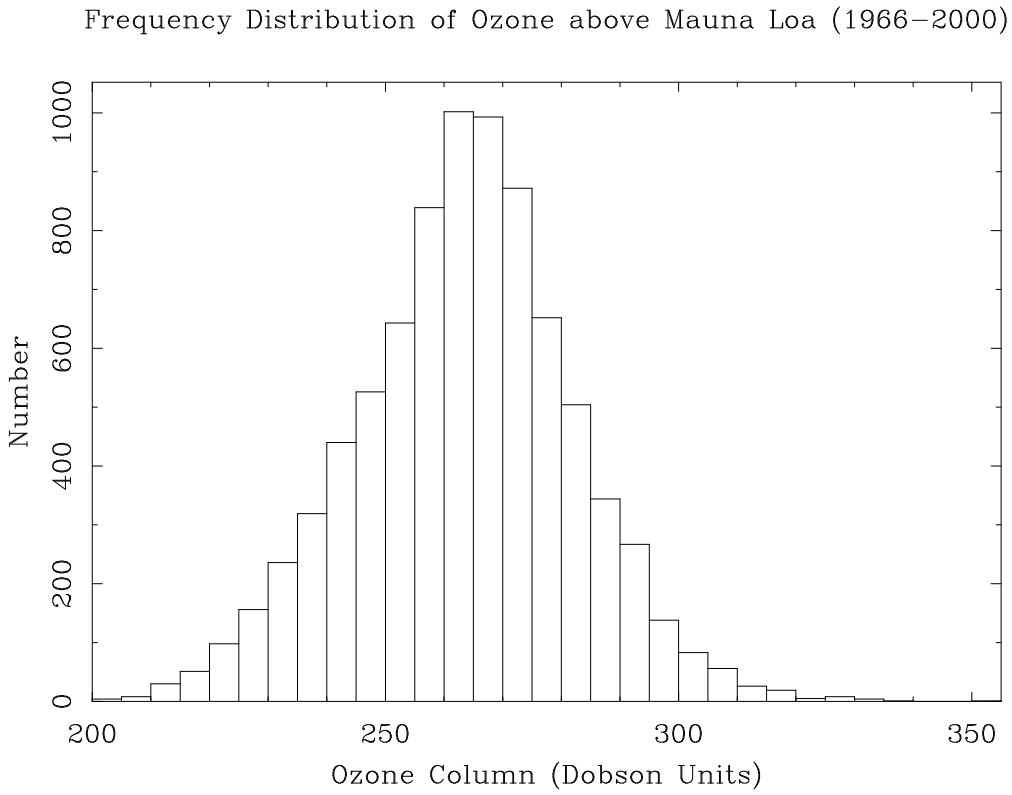

Fig. 5.— **Histogram of Ozone over Mauna Loa,** measured in Dobson units. Values are based on daily observations since 1966.

Table 1 is also useful for identifying the extinction components which must be well-determined to provide better than 1% flux calibration. For instance, at most wavelengths k_R dominates and must be well-determined. Fortunately the behavior of $k_R(\lambda)$ is well known. k_a must be determined to better than 10% (meaning constraints on both a_a and γ), while the amplitude a_{O_3} can be uncertain by 20%, before these sources cause any appreciable error. H_2O and O_2 must be determined very well (1%), but only at certain wavelengths where they are well isolated from the other components. A great advantage over existing work in this area is the large simultaneous wavelength coverage the SNfactory spectrograph will provide.

2. Extinction Correction under Non-Photometric Conditions

Two levels of non-photometric conditions can be defined:

Mildly non-photometric conditions are defined to occur when k is neither isotropic nor time

invariant, but before the formation of any visible clouds. These conditions can occur for a number of reasons, most notably a transition from one weather system to another during which the aerosol content and composition, water content, temperature, and pressure are changing. (Note that the arrival of a new weather system changes temperature and pressure, which should therefore be routinely monitored as a clue that conditions may be non-photometric.) These conditions can also occur due to sinking of the aerosol layer (whose scale-height is typically only $\sim$1.5 km), and to a lesser degree the molecular layer (having an 8 km scale-height), during the night as the atmosphere cools.

Strongly non-photometric conditions are defined to occur whenever clouds of any kind are present. Since efficiency decreases quickly with cloud optical depth, the only situation under which fruitful observations might proceed is for thin cirrus clouds. In this situation, the scattering properties of clouds enter into the extinction through $k_{H_2O,s}$. As mentioned before, $k_{H_2O,s}$ is fairly gray (spectrally neutral).

Under mildly non-photometric conditions where temporal and spatial variations in k consist of large pockets of air, as with different weather systems, then the observations of spectrophotometric standard stars close in time and sky location to the observation of program objects may allow localized correction for extinction. Unfortunately, the accuracy of this approach is difficult to verify, since the location and temporal variations in k are not known *a priori*. With sufficient observations, trends in the standard star observations can be examined for evidence of smooth changes or an isolated transition in time or sky location. Only under these very simple situations can calibration exclusively from spectrophotometric standards hope to be sufficiently accurate. Under strongly non-photometric conditions, observations of spectrophotometric standards is only of value of determining the relation between $k_{H_2O,a}$ and $k_{H_2O,s}$. Therefore, additional methods are needed in order for useful observations to be obtained under non-photometric conditions.

Table 1: Extinction components per airmass at various wavelengths

λ	Rayleigh Scattering	Aerosol Scattering	Ozone Absorption	Water Absorption	O2 Absorption
3460	0.500	0.049	0.020	0.000	0.000
4000	**0.275**	0.041	0.000	0.000	0.000
5800	0.062	0.025	**0.023**	0.000	0.000
7600	0.021	0.017	0.002	0.000	**0.6**
8500	0.013	**0.015**	0.000	0.000	0.000
9300	0.009	0.013	0.000	**0.35**	0.000

2.1. The role of a parallel imager

With the advent of CCD's, imaging follow-up of variable events such as supernovae has exploited the fact that over small fields of view non-photometric conditions tend to uniformly depress the flux from all objects in the field. Thus, non-variable objects in the field can be used as comparison objects, and once the brightness of such comparison objects is determined under photometric conditions, the relative brightness between the target object and comparison objects can be converted to an absolute flux. There are potential problems with this approach, namely the issues of whether the non-photometric conditions really are constant over a field, and whether the non-photometric conditions have a reasonably neutral spectrum so that the scaling does not depend on the spectrum of the comparison stars. The constancy of the non-photometric conditions across a field can be determined directly by comparing the variation in scaling determined using field stars observed during both photometric and non-photometric conditions. Thus, this uncertainty can be built directly into the error budget. For long exposures, a range of cloud patterns should be swept across the field of view, so most variations should be slowly varying across the field.

Most SNfactory supernova fields will be visited many times, and conditions can be expected to be photometric for some fraction of those visits. In particular, the visit during which a final reference spectrum is obtained can be chosen to occur during photometric conditions since it is not time-critical.

The imager will observe many stars surrounding each supernova. The intrinsic spectrum, $F(\lambda)$ of these stars is unknown and some fraction of them may be variable. The observation of star n, $f_n(\lambda_i, t, \alpha, \delta)$ can be presented as

$$f_n(\lambda_i, t, \alpha, \delta) = \int_0^{\infty} \int_t^{t+\Delta t} \phi(\lambda, t)\xi_{\lambda_i}(\lambda, t)D_I(\lambda, t)F_n(\lambda)\ exp[-X\sum_i^5 k_i(\lambda, t, \alpha, \delta)]d\lambda dt \qquad (4.6)$$

Where the imager instrument response, $\xi_{\lambda_i}(\lambda, t)$, is dominated by the response of a chosen filter, denoted by its central wavelength, λ_i. Since parallel imaging is only of value for photometric corrections of observations are obtained a precisely the same time as the spectroscopy, we assume that the interval t to $t + \Delta t$ is identical for both instruments and use t_j to label the observation at epoch j. This necessity leads to a derived requirement for common or synchronized shutters for the spectrograph and imager.

Assuming that the extinction is constant over a very small patch of sky surrounding the supernova and observed by the imager, and using the index x_k to label the field, one can write:

$$f_{n,\lambda_i,t_j,x_k} = f_{n,\lambda_i,t_j}(\alpha, \delta) \qquad (4.7)$$

Thus, for each star in a field the variation at a given wavelength during the course of j epochs is mapped out. Since some observations are obtained during photometric conditions, the absolute

brightness of each star can be determined and subtracted to give the absolute variation:

$$\Delta f_{n,\lambda_i,t_j,x_k} = f_{n,\lambda_i,t_j,x_k} - f_{n,\lambda_i,x_k,corr} \tag{4.8}$$

where $corr$ denotes a flux corrected for extinction under photometric conditions. The measurements for all the stars observed in one image can be combined, to give:

$$\overline{\Delta f}_{\lambda_i,t_j,x_k} = \frac{1}{N}\sum_{n=1}^{N} \Delta f_{n,\lambda_i,t_j,x_k} \tag{4.9}$$

Clearly these values of $\overline{\Delta f}_{\lambda_i,t_j,x_k}$ provide some indication of the extinction variations over the wavelength span of each filter, and for a set of wavelengths should give some information on the extinction which applied to the contemporaneous and nearly co-spatial supernova observation.

However, there are two problems here. First, note that without explicit knowledge of the λ-dependencies of the other terms in the integral of Eqn 6, $f_{n,\lambda_i,corr}$ can not be calculated using $\sum_{i=1}^{5} k_i(\lambda)$ determined from spectrophotometric standard star observations. Instead each field, x_k, would have to be followed as a function of airmass on a photometric night so that $f_{n,\lambda_i,corr}$ on the instrumental system of the SNfactory imager could be determined for each star in that field. Such observations could be done quite easily, but at some loss of observing efficiency on photometric nights.

Second, with a single filter, only the average extinction correction over one wavelength interval is being measured at the time of the supernova observation. Given the earlier discussion showing that extinction has multiple components which do not scale together, such a measurement could only provide an average correction for the portion of the spectrum covered by the imager filter. Extrapolating to other filters would be difficult, but not necessarily impossible. For instance, in the case of increased water vapor due to incipient cirrus, one could imagine monitoring a water absorption band to estimate the column of water. The scattering component due to water will only become gray once clouds actually form since multiple scattering is required, however, by spectrally monitoring a standard star under such conditions, a mapping between the water vapor absorption and the extinction should be found and used for correction purposes. (As discussed earlier, water scattering depends somewhat on whether water is in ice or liquid form, and on the circumstances of ice formation. Thus, any such relation would have an associated uncertainty whose expected size is not known at present.) Similarly, changes in aerosol content can be important contributors to non-photometric conditions and one could imagine monitoring one bandpass to detect changes Δa_a, in the aerosol content if water vapor and other contributors were stable. Of course k_a depends on a_a and γ, so it would be necessary to assume a value of γ in order to extrapolate to other wavelengths. A typical value (and dispersion) for γ would be known from spectrophotometric standards observed under photometric conditions, however, Fig. 2 shows

that this parameter isn't necessarily that stable. Knowledge of γ to ± 0.2 is sufficient to keep the calibration uncertainty below about 1%, for typical k_a.

Since extinction correction using monitoring one one wavelength is not necessarily sufficient, a solution for this and the field-star calibration problem will now be addressed.

2.2. Multicolor field-star monitoring

One might imagine simply expanding the above approach to include multiple filters. Since the observations must be taken simultaneously with spectroscopic observations, an imager would have to monitor different stars in a field using a single multicolor filter (e.g., a series of adjacent filters close to the focal plane). By covering the entire optical spectrum with filters, one would obtain the correct mean scaling for each portion of the simultaneous spectroscopic observations. However, even such full-coverage multicolor monitoring will not provide sufficient information to perfectly remove extinction since the different extinction components do not vary together. The uncertainty in this approach is difficult to predict because it depends on details of how much different extinction components can vary. In regions unaffected by water absorption, this approach might work rather well.

Table 1 and the previous discussion suggests a means of breaking the degeneracy amongst extinction components present in single-band or even full-coverage multicolor monitoring under non-photometric conditions. Namely, if $\overline{\Delta f}_{\lambda_i,t_j,x_k}$ is determined at wavelengths where each extinction component dominates, the parameterization of Eqn 4 could be used to determine the correct extinction to apply to the spectroscopic observations. Monitoring would have to occur at all λ_i at the same time in order to account for variations of all the extinction components. The parameters to be determined are $a_R(t_j)$,$a_a(t_j)$,$\gamma(t_j)$,$a_{O_3}(t_j)$, and $a_{H_20}(t_j)$. It is probable that a_{O_2} can still be determined using spectrophotometric standard star observations, even under non-photometric conditions, so it is not included here. Methods of this type are routinely used in remote sensing experiments.

Simulations indicate that the basic principle should work. Rick Kessler used χ^2 minimization with MINUIT, along with O_2 and H_2O templates (provided by G.Aldering) and an O_3 template from libRadtran v0.15 to simulate extinction retrieval from the *SNIFS* imager. The function to minimize within one field is

$$\chi^2 = \sum_s \sum_i \frac{\left[I_{s,\lambda_i} - \int d\lambda \mathcal{F}_s(\lambda)\xi_{\lambda_i}(\lambda)T_{\rm atm}(\lambda)\right]^2}{\sigma^2_{I_{s,\lambda_i}}} \tag{4.10}$$

where I_s is the observed flux of star "s" through filter "i", $\mathcal{F}_s(\lambda)$ is the flux vs. wavelength of the star as would be observed from above the atmosphere (but including the telescope collecting

area), $\xi_{\lambda_i}(\lambda)$ is the response of filter i centered at wavelength λ_i (including detector and telescope wavelength response) through which star s is measured, $T_{\rm atm}(\lambda)$ is the atmospheric transmission, which contains the a_i parameters that we want to extract, and $\sigma_{I_{s,\lambda_i}}$ is the uncertainty in the flux measurement.

The stellar spectra $\mathcal{F}_s(\lambda)$ are the only unknowns besides the a_i. We do not need precise knowledge of the star spectra, so we assume that at one photometric calibration epoch, the entire field is measured with the filter bands moved one step to the left and one step to the right. This gives the star fluxes in three neighboring filter bands, except for the stars at the edge which are measured in just two filters. With determination of $T_{\rm atm}(\lambda)$ from spectrophotometric calibration taken at the photometric calibration epoch, we can extract crude $\mathcal{F}_s(\lambda)$ for the field stars observed at the photometric calibration epoch. Another way to think of this is that all absolute quantities can be converted to ratios relative to a (spectro)photometric night.

A simple simulation is used to generate 50 stellar spectra (7 per filter) for one field of view. Each star is picked with a random temperature and a black-body spectrum is generated. The field of view filter data are simulated 50 times, and each time the a_i are randomly picked from a Gaussian centered at 1.0 with 5% width. The random a_i simulate the different atmospheric extinction for each measurement. For the first measurement, all of the a_i are set to 1.0, so that the goal is to find the relative changes in the a_i. Telescope properties are ignored and $X = 1$.

The result is given in Fig 8, which shows the precision (RMS) on the atmosphere transmission as a function of wavelength. The precision is well below the overall 1% error budget, except for wavelengths in the UV below 0.35 μm. Seven filters works better than five filters, particularly at higher λ; the strange 7-filter bump at 0.6 μm could be due to the Ozone uncertainty, or due to a strange fluctuation with the stars in that filter.

These preliminary simulations are encouraging, but the following caveats need to be addressed in future work.

- Within a filter band ($1.2' \times 5'$), are there really enough stars with sufficient magnitude to measure the average flux with a precision of $1\%/\sqrt{7} = 0.4\%$?
- Statistical fluctuations ... what happens when there are only 1 or 2 stars in a filter ?
- The "known" $k_i(\lambda)$ functions may not really be known exactly; additional parameters that describe the extinction functions may also have to float in the fit, and will reduce the precision. These extra parameters are likely to include γ for aerosols, and x for Rayleigh.
- How well do we [have to] know the reference a_i ?
- Stars are not black-bodies; realistic spectra should be used in the simulation.

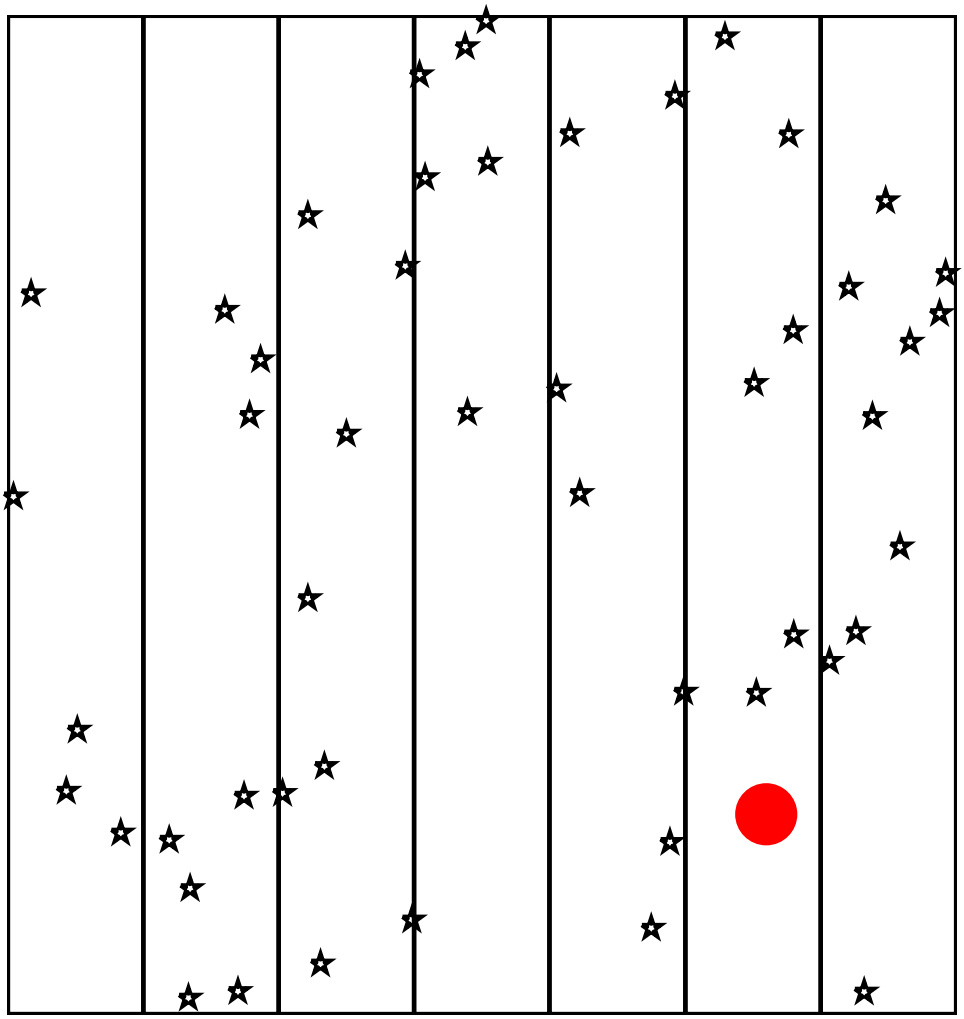

Fig. 6.— Illustration of the filters that cover the field of view during the SN spectrum measurement. The large red "●" indicates a SN under study; the 50 smaller "⋆" indicate stars used to measure the atmospheric extinction fluctuations. The seven bands are the filters with responses shown at the bottom of Figure 7.

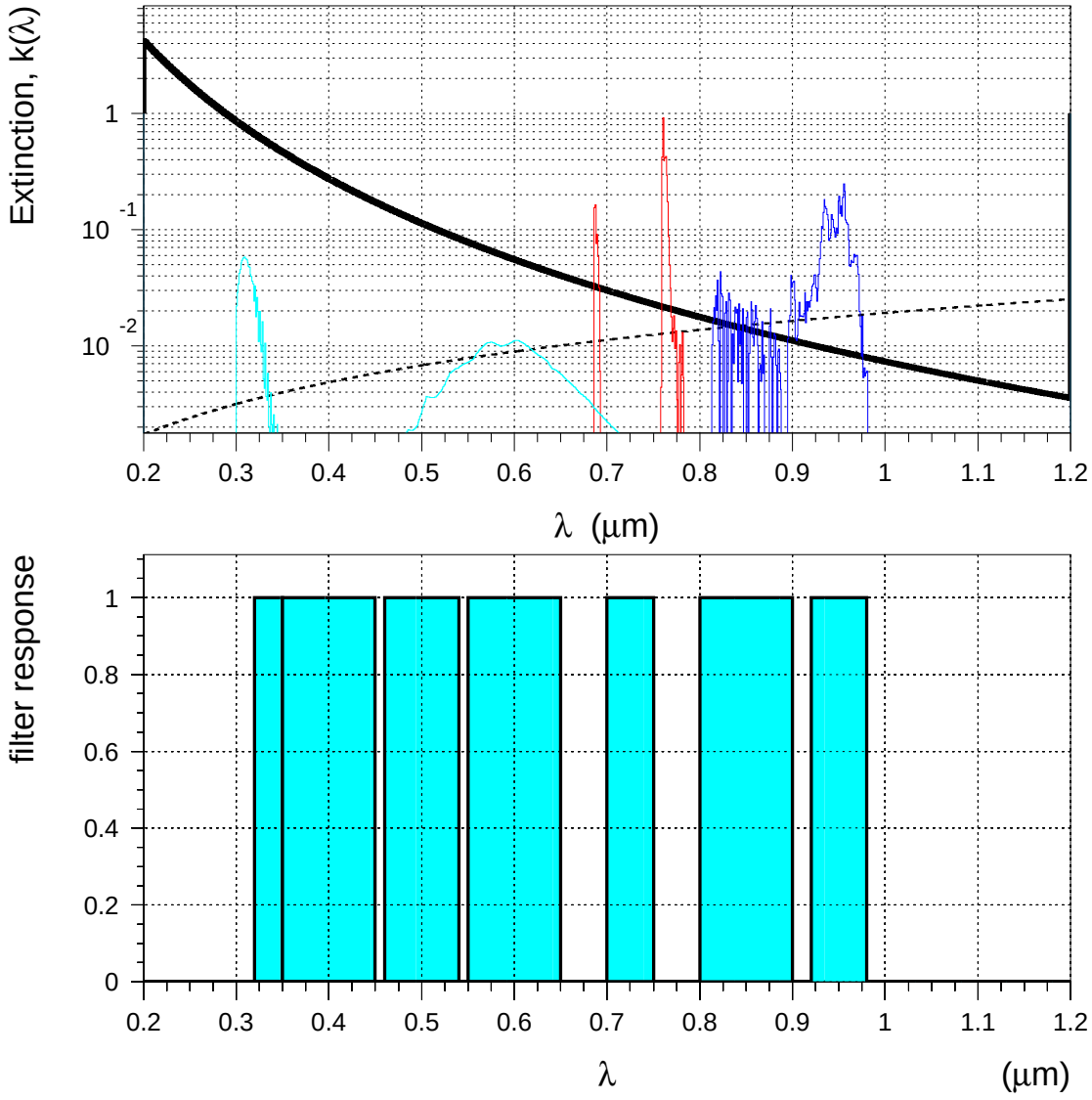

Fig. 7.— Top shows the extinction functions $k_i(\lambda)$ for: Rayleigh (thick), aerosols (dashed), water (0.8-1.0 μm), O_2 (narrow peaks at 0.69 and 0.75 μm) and O_3 (broad peaks at 0.3 and 0.6 μm). The bottom plot shows the responses of the seven filters used in this study.

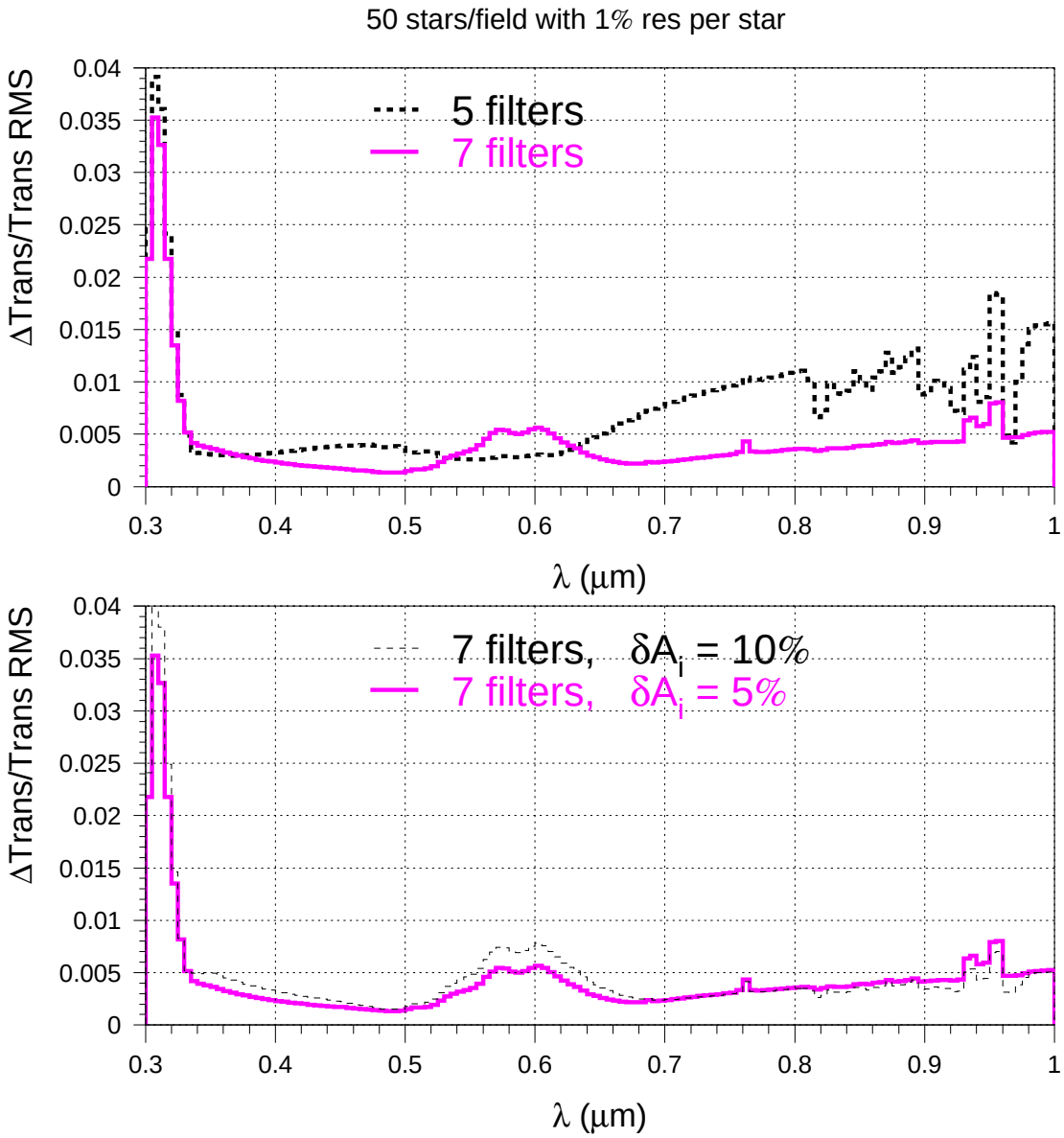

Fig. 8.— RMS of atmosphere transmission measurement vs. λ. The top plot compares the RMS for 7 vs. 5 filters; the seven filters are shown in the bottom plot of Fig. 7 and the result with five filters excludes the filters centered at 0.50 and 0.85 μm. Bottom plot compares the RMS when the a_i are drawn from gaussians with 5 and 10% width.

The above analysis shows that in principle the appropriate extinction as a function of wavelength can be determined from multicolor photometry of field stars taken *simultaneously* with spectrophotometric observations of a program object under non-photometric conditions. This method can be tested directly using such observations of spectrophotometric standard stars. More extensive Monte Carlo simulations, and up-to-date absorption spectral functions, are needed to validate the above analysis and to determine the best filters (central wavelengths, widths, and shapes) for the multicolor field-star monitoring.

3. The need to monitor system stability

So far it has been assumed that the $\phi(\lambda, t)$, $\xi_{\lambda_i}(t)$, and $D_I(\lambda, t)$ are constant over the entire one year period during which each supernova is observed. Moreover, even if parallel multicolor field-star observations are obtained to determine the extinction, the zero-point of the spectrograph, $\xi(\lambda, t)$, and the detector, $D_S(\lambda, t)$ must be known in order to obtain spectro*photometry* from the extinction-corrected spectra.

Before exploring a solution, the possible sources of zero-point change should be discussed. First, the telescope optics will collect dust and undergo cleaning and recoating. Dust accumulation alone can amount to 0.001 mag/day. The imaging filters, $\xi_{\lambda_i}(t)$ will have bandpasses that shift with temperature (and possibly humidity), and they will suffer degradation over time. The spectrograph optics should be fairly stable, however the dichroic beam-splitter can be expected to show changes with temperature, and to degrade over time. Finally, the $QE(\lambda)$ for the CCD detectors (D_S and D_I) will depend on cold-head temperature, and outgassing in the dewar will result in slow condensation of contaminants on the face of the detectors.

In the case of the spectrograph, regular observations of spectrophotometric standards on photometric nights will measure the product $C_S(\lambda, t) = \phi(\lambda, t)\xi(\lambda, t)D_S(\lambda, t)$ directly. Thus, if all sources of drift in the spectrograph zero-point are very slow, and photometric conditions occur sufficiently often, it may be possible to track $C_S(\lambda, t)$ for the spectrograph reasonably well. Sufficient standard stars will have to be observed to even ascertain whether or not conditions are photometric, unless there are other constraints on variations in $C_S(\lambda, t)$.

An approach using standard stars also might be considered for the imager. However, since the V's result from integrals over the spectral response of the imager and the unknown spectrum of the monitoring stars, shifts in filter wavelength — not just zero-point shifts — become an issue. In the parlance of ordinary photometry, this problem is one of a changing color term. In ordinary photometry, color terms are constrained by observation of stars having a wide range of spectra (colors), and such an approach might be possible here.

The careful reader will have noticed that with each new requirement needed to enable the use of non-photometric conditions, more and more of the observing time when conditions are photometric must be used for calibration. If calibration can not be done very quickly, observations described in this section will represent an undo burden. Moreover, the frequency of photometric conditions compared to expected changes in zero-points and color-terms is not yet known; if changes are fast compared to the frequency of photometric nights the calibration plan for using non-photometric nights may fail completely.

Young (1975) recommends that all precision photometry systems be monitored for stability using laboratory sources. This seems to be exactly what is required here. Since we are concerned with changes in both zero-points and color-terms, one solution would be to observe artificial stars produced by a suite of two or more stable lamps having different color temperature. The telescope response, $\phi(\lambda, t)$, is common to both the spectrograph and imager, and provided it is reasonably stable, the main outstanding calibration that is needed is that between the spectrograph and the imager.

3.1. Imager-to-Spectrograph scaling

In principle, a reference lamp observed simultaneously with the imager and the spectrograph will give the relative response of the spectrograph and imager. Imagine that the response of filters or spectral elements change only by scale factors, α_X, defined as follows:

$$C_I(\lambda, t_j) = \alpha_{C_I,t_j}\overline{C}_I(\lambda)\ (\text{imager}) \tag{4.11}$$

$$C_S(\lambda, t_j) = \alpha_{C_S,t_j}\overline{C}_S(\lambda)\ (\text{spectrograph}) \tag{4.12}$$

$$L(\lambda, t_j) = \alpha_{L,t_j}\overline{L}(\lambda), \tag{4.13}$$

where $L(\lambda)$ is the lamp spectrum. Simultaneous observations of the lamp with the imager and spectrograph at epoch t_1, $O_I(t_1)$ and $O_S(t_1)$ are given by:

$$O_I(t_1) = \int_0^\infty \alpha_{C_I,t_j}\overline{C}_I(\lambda)\alpha_{L,t_j}L(\lambda)d\lambda \tag{4.14}$$

$$O_S(t_1) = \alpha_{C_S,t_j}\overline{C}_S(\lambda_0)\alpha_{L,t_j}L(\lambda_0), \tag{4.15}$$

where λ_0 is arbitrary in this formulation. The ratio of these measurements yields:

$$\frac{O_I(t_1)}{O_S(t_1)} = \frac{\int_0^\infty \alpha_{C_I,t_j}\overline{C}_I(\lambda)\alpha_{L,t_j}L(\lambda)d\lambda}{\alpha_{C_S,t_j}\overline{C}_S(\lambda_0)\alpha_{L,t_j}L(\lambda_0)} = \omega_1\frac{\int_0^\infty \overline{C}_I(\lambda)L(\lambda)d\lambda}{L(\lambda_0)} \tag{4.16}$$

The values of ω_{t_j} thus track the relative sensitivity of the imager and spectrograph for any combination of imager filter and spectrograph wavelength, λ_0 (although it will be most sensible to compare at similar wavelengths, as will now be shown).

Of course it is likely that changes in the lamp spectrum will occur at different epochs unless care is taken to stabilize its response. How well must the lamp spectrum be stabilized? Following King (1952), the above integrals can be expanded as a Taylor series in derivatives of the lamp spectrum. The expansion is taken about the wavelength which is the 1st moment of the imager response (filter plus detector):

$$\lambda_0 = \mu_1 = \frac{\alpha_{C_I,t_j} \int_0^\infty \lambda \overline{C}_I(\lambda) d\lambda}{\alpha_{C_I,t_j} \int_0^\infty \overline{C}_I(\lambda) d\lambda} = \frac{\int_0^\infty \lambda \overline{C}_I(\lambda) d\lambda}{\int_0^\infty \overline{C}_I(\lambda) d\lambda} \tag{4.17}$$

(Note that λ_0 is immune to scaling changes in the imager response.)

The expansion given by King results in:

$$O_I(t_1) \approx \alpha_{C_I,t_j} \left(L(\lambda_0) \int_0^\infty \overline{C}_I(\lambda) d\lambda + \frac{dL(\lambda)}{d\lambda} \int_0^\infty (\lambda - \lambda_0) \overline{C}_I(\lambda) d\lambda + \frac{1}{2} \frac{d^2L(\lambda)}{d\lambda^2} \int_0^\infty (\lambda - \lambda_0)^2 \overline{C}_I(\lambda) d\lambda \right) \tag{4.18}$$

$$\approx \alpha_{C_I,t_j} \left(L(\lambda_0) \int_0^\infty \overline{C}_I(\lambda) d\lambda + \frac{1}{2} \frac{d^2L(\lambda)}{d\lambda^2} \int_0^\infty (\lambda - \lambda_0)^2 \overline{C}_I(\lambda) d\lambda \right) \tag{4.19}$$

$$\approx \tilde{\alpha}_{C_I,t_j} \left(L(\lambda_0) + \frac{1}{2} \mu_2^2 \left(\frac{d^2L(\lambda)}{d\lambda^2}_{|\lambda_0} \right) \right), \tag{4.20}$$

where μ_2 is the 2nd moment of the imager bandpass, and is defined in a manner analogous to μ_1. Note that the definition of λ_0 forces the 1st order term in the Taylor expansion to zero.

Now the earlier expression for the relative scaling of the imager and spectrograph can be rewritten as:

$$\frac{O_I(t_1)}{O_S(t_1)} = \tilde{\omega}_1 \frac{L(\lambda_0) + \frac{1}{2}\mu_2^2 \left(\frac{d^2L(\lambda)}{d\lambda^2}_{|\lambda_0} \right)}{L(\lambda_0)} = \tilde{\omega}_1 \left(1 + \frac{1}{2} \mu_2^2 \left(\frac{1}{L(\lambda_0)} \frac{d^2L(\lambda)}{d\lambda^2}_{|\lambda_0} \right) \right) \tag{4.21}$$

Here it is made clear that the observed flux ratio, $O_I(t_1)/O_S(t_1)$, tracks the relative response of the imager and spectrograph only if the normalized 2nd derivative of the lamp spectrum at the filter wavelength λ_0 is very small or the same from epoch to epoch. Therefore, a lamp with a linear spectrum (in photons), or a temperature-stabilized lamp is required. Since linear spectrum sources

aren't available (to our knowledge!), the required temperature stability has been investigated. For a filter having $\mu_2 \sim 400$Å, a NIST-calibrated FEL lamp stabilized at a color temperature of $T = 2856 \pm 8K$ (see Fig. 6) is just sufficient to keep color errors below 0.5% across the entire optical spectrum (the most stringent constraint is for $\lambda_0 < 4000$Å). A warmer lamp, with $T \sim 5000K$, would have an even smaller sensitivity. The ability to track the relative response of the imager and the spectrograph leads to a derived requirement for a stabilized lamp, preferably having as small of a normalized 2nd derivative as possible so that the stability of μ_2 is not a factor.

3.2. Imager wavelength shifts and bandwidth changes

In the above discussion, a characteristic wavelength, λ_0, was defined for each imager channel. For all glass and interference filters the characteristic bandpass is dependent on the ambient temperature. The wavelength response of the CCD can also change with operating temperature. The best solution for the latter problem is to stabilize the temperature to the requisite accuracy, as determined from laboratory tests. This leads to a derived requirement for laboratory tests of $dQE(\lambda, T)/dT$ for the CCD's, and temperature stabilized to the necessary accuracy (TBD).

The bandpass shifts for high-quality interference filters range from 0.015 nm/K to 0.025 nm/K across the optical. Colored glass filters have larger temperature coefficients, and so should be avoided for these purposes. Although the Mauna Kea site has good temperature stability, it seems sensible for the calibration procedure to be able to handle changes of $\pm 10\ K$. Filter temperature stabilization is possible, but presents a heat source in the imaging plane and thus may degrade the image quality. From Eqn. 23 we see that a shift in wavelength produces a term

$$\Delta O_I(t_1) = \tilde{\alpha}_{C_I,t_j} \frac{1}{L(\lambda_0)} \frac{dL(\lambda)}{d\lambda}_{|\lambda_0} \Delta\lambda_0 \tag{4.22}$$

For a NIST FEL lamp this amounts to no more than:

$$\Delta O_I(t_1) = \tilde{\alpha}_{C_I,t_j} 0.03\,\mathrm{nm}^{-1} \Delta\lambda_0 \tag{4.23}$$

and for the temperature coefficient of a high-quality interference filter this becomes:

$$\Delta O_I(t_1) = \tilde{\alpha}_{C_I,t_j} 0.03\,\mathrm{nm}^{-1}\, 0.025\mathrm{nm}/K \Delta T \tag{4.24}$$

$$= \tilde{\alpha}_{C_I,t_j} 0.00075\ K^{-1} \Delta T \tag{4.25}$$

Thus, a $\pm 10\ K$ temperature excursion can produce a calibration error of up to ± 0.75%, which is just at the level of being problematic. Fortunately, the filter temperature coefficient is only 0.015 nm/K in the blue, where the normalized derivative of the FEL lamp is largest, and so the expect error is more like ± 0.45%, which is acceptable.

Note that a wavelength shift for the imager will also change the V's, which must be stable over a period of 1 year. The effect on the V's will depend on the normalized slope of the star spectra. Thus, monitoring filter bandpass wavelengths and shapes should be chosen to give an imager response which is not effected by strong stellar absorption features. Unlike the case with the FEL lamp, different stars will present normalized derivatives with different signs, and so systematic errors in the V's could be small. This must be verified with simulations using realistic imager responses and stellar spectra.

A more proactive step would be to use lamps at two (or more) different operating temperatures to directly monitor the change in imager/spectrograph flux ratios as the normalized derivatives are changed. One lamp would have to be very stable for the reasons already cited. The normalized derivatives of the second lamp could be calibrated using the spectrograph observations of the stabilized lamp, and so they too would be known. It would be preferable to obtain a lamp temperature giving derivatives with opposite sign to a NIST FEL lamp. This requires a much hotter operative temperature, or perhaps a Cerenkov source such at that discussed by Young 1975. An alternative would be to place a gently sloping filter in front of the FEL lamp; drift in this filter would not be an issue since it's response would be calibrated using spectrograph observations of the lamp with and without the filter. Melles Griot sells "color temperature conversion filters" intended for just this purpose. Since O_I/O_S also depends on changes in μ_2, the filter width can be monitored independently of scaling and wavelength shift if a second color filter is added.

3.3. Location of photometric calibration sources

From a calibration point of view, it would be best if calibration lamps used to internally monitor the system were observed through the entire system, including the OTA. With a calibrated NIST FEL lamp, such observations would provide the correct wavelength-dependent flux calibration for the spectrograph, which is highly desirable both as an aid in data reduction and as a check on external wavelength-dependent flux calibration (within a scale factor) from spectrophotometric standard stars.

In this case, the telescope would have to directly view an artificial star constructed using a NIST FEL lamp and located on the dome. The standard procedure of illuminating a dome flat screen might work if a spectrally neutral screen material can be found. Of course in this case the absolute calibration of the NIST FEL lamp could not be exploited. Also, at this location, calibration observations would require that the telescope be open and pointed at the artificial star or screen. This may present operational difficulties, effecting when such calibration observations can be obtained. The advantage of this arrangement is that all the spectrograph and multicolor imaging observations can be obtained simultaneously with the multicolor filter in its regular

observing position. No instrument modifications would be necessary since the normal observing arrangement would be utilized.

If operational difficulties — or problems implementing an adequate artificial star or dome flat screen — prevent use of a totally external lamp, the relative imager/spectrograph calibration can still be obtained internal to the SNfactory instrument. This would require a beam splitter to direct the already-required spectral flat lamp to send light to the imager. The multicolor filter in the imager would have to be rotated in partial steps so that the beam-split light can be directed through each filter sequentially. Additional flat lamps or color temperature filters should then be added to the spectrograph calibration assembly.

Note that since a temperature stabilized lamp is a good choice for the spectrograph flat lamp, and since a beam-splitter is as simple as a mirror for the lamp pick-off mirror, it seems straightforward to implement the minimal internal flux calibration equipment within the SNfactory instrument. An external flux calibration module can then be pursued separately.

4. Multicolor imaging implementation

For a 2k×4k CCD with 15μm pixels on a 2.2-m f/10 telescope, the field is $6.1' \times 12.1'$. A 5-color filter (e.g., at wavelengths similar to those given in Table 1) would partition the field into $2.4' \times 6.1'$ regions. At the north Galactic pole about 6 stars are expected in a region this size down to $m_R = 19.5$. At R-band, the brightness of the faintest of these stars should be measurable to a few percent on a 2.2-m in a 300Å-wide filter in a 500 second exposure (the latter being typical of minimum spectroscopic exposures) for typical Mauna Kea seeing. Therefore, the surface density of useful stars is more than sufficient to overconstrain the series of equations needed to solve for temporal extinction variations.

A combination of observations of spectrophotometric standard stars and internal calibration should allow SNfactory calibration systematics to be kept below 1%. Reliance on only spectrophotometric standard stars will consume a non-negligible portion of observing time and is useful only under photometric conditions. We do not yet know the fraction of nights that are photometric to 1% on Mauna Kea, nor do we know how extensive spectrophotometric standard star observations must be to reliably establish a given night as photometric to 1%. Given these unknowns, and with an eye towards saving precious observing time, internal calibration should be provided to track sensitivity changes in the instrumentation.

Further observing time can be salvaged if non-photometric nights can be used. A method to determine the extinction correction to apply to the spectroscopy using simultaneous multicolor imaging of nearby field stars appears feasible. This method also requires an internal calibration

capability utilizing a stable lamp. The internal calibration is better able to characterize the imager if a filter to modify the color-temperature is available. (Alternatively a very blue lamp would work.)

These, and related derived requirements include:

A) The ability to determine whether or not a given night or smaller interval of time is photometric is required.

B) On photometric nights (estimated 50% of total), spectrophotometric standard stars must be observed close in time and sky location to target supernovae so that correction for atmospheric extinction can be determined. (Number, airmasses, and spectral types TBD.)

C) The optical telescope assembly (OTA), instruments and their detectors must be stable over the course of one week, as sufficient observations of standard stars to constrain both atmospheric variations (non-photometric conditions) and instrumental variations will not be possible. (Limits on stability TBD, but expected to be $< 0.5\%$.) If these specifications can not be met and validated, accurate internal calibration must be provided. An internal calibration method, possibly exclusive of the OTA, is described in this document.

D) On non-photometric nights a mechanism to determine the spectral scaling needed to correct for non-photometric conditions is required. A suggested solution using simultaneous multicolor imaging of field stars surrounding monitored SNe is described in this document.

E) Laboratory tests of $dQE(\lambda, T)/dT$ for the imager CCD, and temperature stabilization of the CCD's to a TBD accuracy.

F) The ability to internally monitor imager wavelength shifts and bandpass widths is desirable. Lamps with additional color temperatures, or color temperature filters, could be used for this purpose. Such lamps would have to be observable with the imager and spectrograph simultaneously.

G) The imager and the spectrograph must have a common shutter, or synchronized shutters. This is required so that atmospheric and calibration conditions are identical for both instruments.

Ångstrom, A., 1961, "Technique of Determining the Turbidity of the Atmosphere," Tellus, Vol. 13, pp. 214-231.

Burki, G., Rufener, F., Burnel, M., Richard, C., Blecha, A, and Beatschi, P. 1995, "The atmospheric extinction at the E.S.O. La Silla observatory," A&AS, 112, 383.

Hayes, D. S., and Latham, D. W. 1975, "A Rediscussion of the Atmospheric Extinction and the Absolute Spectral-Energy Distribution of Vega," ApJ, 197, 593.

Hill, F., *et al.* 1994, “The Global Oscillation Network Group Site Survey”, Solar Physics.

King, I., 1952, “Effective Extinction Values in Wide-band Photometry”, A.J., 57, 253.

Young, A. T. 1974, in “Methods of Experimental Physics: Volume 12-PartA, Optical and Infrared Astrophysics,” ed. N. Carleton, Academic Press, New York.

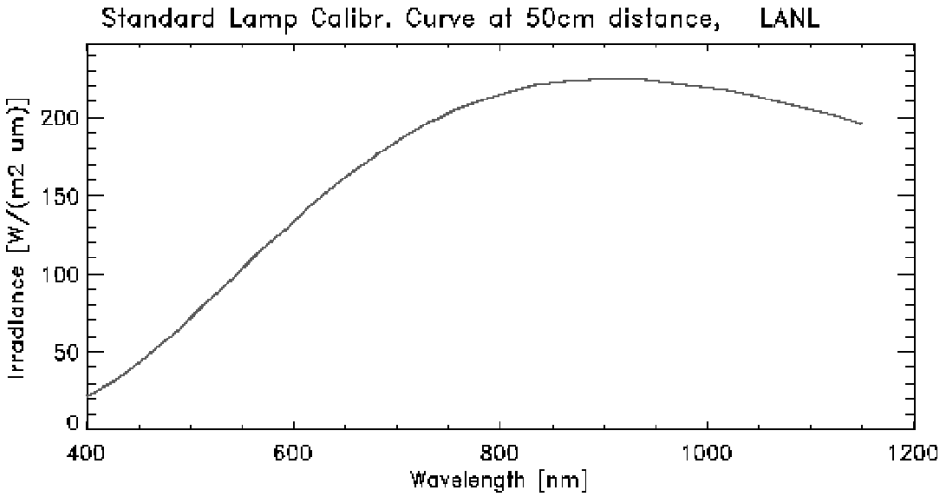

Fig. 9.— **The spectrum of an NIST-calibrated FEL lamp.** The lamp temperature is stable at $T = 2856 \pm 8K$. This stability is required to obtain a small, constant $\frac{1}{L(\lambda_0)} \frac{d^2L(\lambda)}{d\lambda^2}|_{\lambda_0}$. It also allows completely internal relative flux calibration of the spectrograph good to 1%.

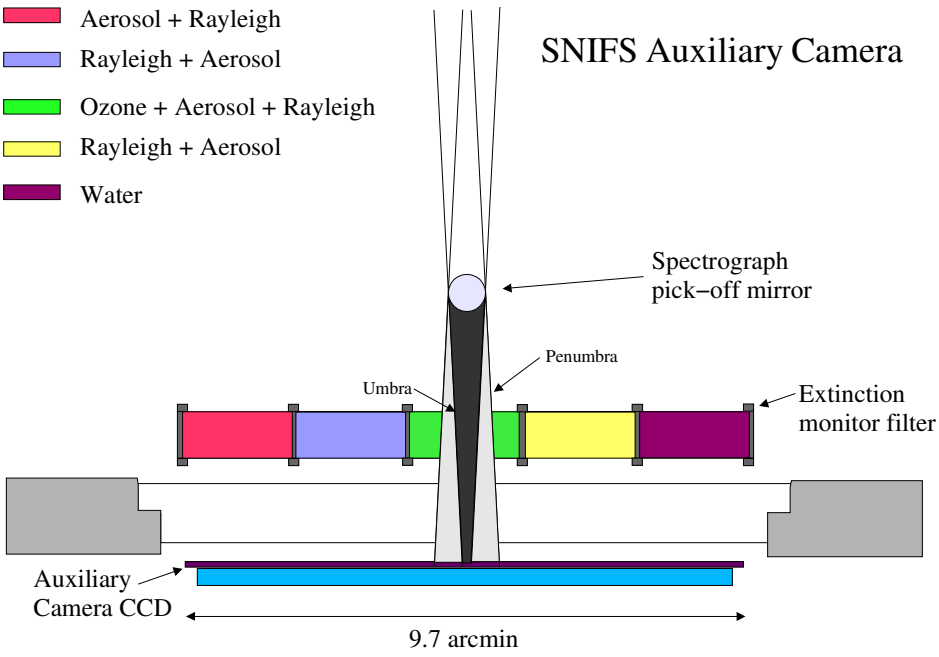

Fig. 10.— Possible layout for a multicolor extinction imaging filter.

Chapter 5

Operating mode

1. Detection

The Nearby Supernova Factory will find hundreds of supernovae a year by using images from automated nightly asteroid searches. We are currently in collaboration with the Near Earth Asteroid Tracking (NEAT) group, based at the Jet Propulsion Laboratory (JPL). They are conducting asteroid searches at two telescope, the 1.2m MSSS telescope at Haleakala, Maui and the 48” Oschin telescope at Palomar Observatory.

In their quest for asteroids, the NEAT group scans the skies every night and looks for objects which move over the time scale of an hour. They take three images of a given field in the sky, spaced fifteen minutes apart, and search for objects which move by more than a couple of arcseconds over this period. They do this for hundreds of fields every night. This strategy enables them to find hundreds of asteroids in the main asteroid belt of our solar system.

We use this data and compare the old (“reference”) and new (“search”) images of the same field spaced weeks apart by subtracting the reference image from the search image and looking for the objects which remain.

Fig. 1 shows an example of this process for a supernova in the NEAT dataset, 2001dd.

The subtraction step must be done with care. The computers use a sophisticated suite of image tools to do a good job with this, but until the present there remains a significant amount of human interpretation to tell the good supernovae candidates from the bad.

The specific details of implementation described below apply to our current plans and setup as of Spring 2002.

Starting in August of 2001 a systematic search for supernovae has been carried out with the

Palomar 48” Oschin telescope. The NEAT group, has outfitted this telescope with an automated system for control and observations and has added a 3-chip CCD camera at the spherical focal plane at the primary focus of this Schmidt reflector.

1. Obtain Reference Image
2. Reference Data Processing/Reduction
3. Obtain Search Image
4. Search Data Processing/Reduction
5. Subtractions
6. Automated Scanning
7. Human Scanning
8. Cross Checks
9. Obtain Confirmation Image

1.1. Reference Image

Using a dedicated telescope *NEAT* takes many images of the sky during the night over a range of RA and Dec. Ideally the fields obtained cover some simple rectangle on the sky to facilitate later searching images and to provide a complete set of references for future searches in later years. All sky fields are covered in at least three exposures spread over approximately an hour. For the *NEAT* groups’ purpose this spacing in time is to search for asteroids. For our purposes this helps us eliminate those same asteroids and to minimize the contamination due to cosmic rays.

1.2. Data Transfer from Palomar to LBL

The data is obtained from the telescope and stored at Lawrence Berkeley Laboratory (LBL) on the National Energy Research Supercomputing Center (NERSC) High Performance Storage System (HPSS). From there it is transferred to the Parallel Distributed Systems Facility (PDSF). This cluster comprises approximately 200 Dual 1 GHz PIII PCs with 2 Gigabytes (GB) of memory

and 50 GB of scratch disk space each. Processes are scheduled on the cluster using the Load Sharing Facility software package.

The data is uncompressed, converted to the standard astronomical FITS format, dark-subtracted, flat-fielded, and loaded into our image database. The actual image files are transferred to large-capacity local disks for use in 2-4 weeks when the search images are taken.

As each image comes off of the telescope it is saved in a compressed format to local disk space. There currently exist several hundred gigabytes of storage at the observatory for this purpose. This allows for the 20 GB/night (compressed) to be stored with space to buffer in cases of transmission failure.

A high-speed, 45 Megabit-per-second (Mbps) radio internet link has been established to the UC San Diego supercomputer center from the observatory to the UC San Diego internet connection. From there the bandwidth to LBL and NERSC is excellent.

The telescope goes through three pointings every four minutes. There are 3 CCD detectors on the current instrument so each pointing results in 3 images. These images are space about 1 degree apart in declination. Each image is 32 Megabytes (MB) in its raw form, but is compressed to $\sim$16 MB for transfer. This results in 144 MB of data to transfer every four minutes. Thus the telescope generates data at a rate of 4.8 Mbps. This is only one-tenth of the theoretical maximum bandwidth of the radio internet link so there is plenty of room for future expansion.

Each night the transfer script is initiated at 18:00 local Palomar time. The script looks in a known directory for files to transfer. It is keyed to images only from that night so if there are other files or images from other nights in that directory it ignores them. It keeps a list of files to be transferred and a list of files that have already been transferred. As new images appear they are added to the list of files to be transferred. The transfer to HPSS is accomplished through a scripted call to the standard RedHat GNU/Linux 'ftp'. We experimented with using 'scp' to transfer to our machines at LBL but found that 'ftp' gave better performance by a factory of two. The 'ncftp' program was also tried but we ran into problems in getting through the NERSC firewall with this program.

With the data rates given above, the transfer process is in almost real-time. The only delay comes from the few minutes it takes to compress the images for transfer. To allow for this the transfer script currently waits for six minutes after the creation of an image file to make sure it has been completely written to disk in it's compressed form to disk before adding to the list of image files to transfer. The transfer script for a given night runs continuously from 18:00 to 17:55 the next afternoon. It is then restarted with the information with the new night at 18:00.

At 09:00 every morning a script is run to verify the transfer of the previous nights images. It

compares a list of local image files from the previous night with the list of files in the appropriate directory on HPSS. If the file list names and sizes agree then an email is automatically sent to the LBL SNfactory system administrator (Michael Wood-Vasey <wmwood-vasey@lbl.gov>) and our NEAT collaborators at JPL indicating a successful transfer and giving a list of the images transferred and their compressed file sizes. If there is a discrepancy between what was transferred and what should have been transferred then an email is sent to the LBL SNfactory system administrator who then checks on the problem and reruns the check transfer script after the files have been resent. This has only happened a handful of times since August 2001.

This transfer setup has been working continuously since August 2001. Minor improvements in handling error conditions such as files of zero size were in made in September and October of 2001. It has been running unattended since January 2002.

1.3. Data Reduction of Palomar Images

Every morning at 08:30 (09:00 in the winter) a cron job runs on the PDSF cluster at NERSC. All of the images from the previous night are downloaded to local cluster disk space for processing. The images are split up in sets according to which dark calibration image they match. A dark images are taken with the same exposure time as science images, but with the shutter closed. Dark correction is needed since the CCDs are thermoelectrically cooled and therefore have non-negligible dark current. This grouping results in $20 - -30$ data reduction sets. These are submitted as jobs in the processing queue and complete three to five hours later, depending on the load on the cluster. After all of the images are reduced, they are saved back to long-term storage in their processed form.

It takes from four to five hours to retrieve and reduce all of the images for a night. A little under an hour of this time is spent retrieving the files from HPSS. This could clearly be improved by sending the files first to the cluster and then to HPSS, but this is harder from both a security and reliability standpoint. The security is a limitation as we are not allowed to run an FTP server on the cluster machines. We have found that FTP enables much transfer rates from Palomar than scp, so we have decided to use FTP. We have found that HPSS is much more reliable in having a higher percentage uptime. If we wish to move to a near-real-time processing scheme, however, something will have to be worked out to send the files directly to the processing machine.

Each data reduction set is processed by a separate job. Each job runs on it's own CPU. It begins by copying the images to be processed from the cluster central storage to local scratch space. All of the files are then decompressed and then converted from the NEAT internal image format to the astronomically standard Flexible Image Transport System (FITS) format (as defined

by NASA, <http://fits.gsfc.nasa.gov>). This is the format that all of our software is designed to understand for the processing of astronomical images.

Next the dark calibration image is subtracted from all of the other images in the data set. This removes the additional electrons which collect in each pixel of the CCD just by virtue of being on. It is important to remove this offset by using dark images from the same night as it varies from pixel to pixel as well as over time. We have observed, however, that the average value and deviation of the dark images remain relatively constant over a night.

The next important calibration step is accounting for the pixel-to-pixel variation caused both by variations in the sensitivity of each pixel and the different illumination coming to each pixel through the optics of the telescope. To correct for this difference in the effective gain of each pixel one must construct a “flatfield” image which has an average value of 1 and has the variation for the each pixel stored as the value of that pixel. One then divides one’s data images by this flatfield image to arrive at an image which have an effective even sensitivity for every pixel. We build out flatfield images by taking set of images of the sky at different positions and taking the median at each pixel to be the representative value. With a sufficiently large set (typically 21 images) this eliminates objects on the image. The median process involves some outlier rejection to attempt to recover a more representative median. For most of the past year flatfields have been built every night from the individual data sets. This results in flatfields which are most attuned for that night, but it also runs the risk of not having the best available flatfields. We suffered for a while from flatfields built with too few images, leading to residual objects and stars being clearly present in the flatfields. When images calibrated with these not-so-flat flatfields were used as references, false objects would appear in the subtractions. This became quite a problem when it was realized that only 70% of the images on some nights were being successful reduced due to problems in building flatfield images within a given data set. This often came from having data sets which were too small to reliably build a flatfield from, so we started using a generic flatfield, built from images from 27 May 2002 UT, to flatten all of our data. The current plan is to have generic flatfield which will be update approximately once a month based on the data from the previous month. This speeds up processing by about twenty minutes per data set (the time it takes to build the flatfield) and results in fewer bad flatfield images. This is not the ideal situation, however, as it clearly doesn’t use all of the available information from a given night to build the best flatfield possible. This is a complicated issue which we plan to study further in the summer of 2002.

The images are then split up into four quadrants – one for each of the four different amplifiers. Each CCD has four amplifiers to achieve the very fast 20-second readout times that are critical to this type of large-area variable object survey. This allows us to discard bad quadrants when they develop problems. This has happened several times for both the Haleakala and Palomar detectors so we have kept with this scheme. There is some areal coverage because there is more edge space

in this scheme. As the images are dithered a little space around the edges is always lost when the images are added together. This is proportional to the edge space and so is more expensive for small images. But there is no choice as dealing with non-rectangular images is not a viable option.

After splitting the images when then discard the aforementioned quadrants known to be bad. A list of bad quadrants, including dates, is kept in the reduction scripts and is referenced to decide which quadrants to eliminate.

The final step is to take the fully reduced images and register them with our image database and to rename them to match our canonical name format. After being renamed they are moved back to central cluster storage so that they can be accessed by other processes.

A PostgreSQL database is used to keep track of all of the reduction steps. This allows for reductions to be restarted and provides information in the case of a failed job. After all of the images have been processed and moved to central cluster storage they are saved to long-term storage on HPSS.

1.4. Search Image

The telescope observing program covers the same fields in the sky as often as possible while assuring full sky coverage from approximately -25 to $+25$ degrees in declination. In ideal conditions this can be as few as six days, but weather and the moon make for a more complicated observing pattern.

In general, though, repeat images suitable for searching will be taken in a little less than two weeks.

Once these images are taken they follow the same procedure in being transferred to LBL and the ensuing data processing. These images then will become the reference images for searches when we return again to these fields in another two weeks.

The search images are processed in an identical manner to the reference images. Once they are loaded into the database, a matching program is run to construct lists of matching fields for the reference and search nights to be used in generating files which describe the image subtractions to be done to look for supernovae. This matching takes about 10 minutes to compare all of the images for a night to all of the images from the previous year and generate appropriate subtractions to be done. Currently we are doing subtractions for three intervals: 10 ± 5 days, 25 ± 9 days, and 360 ± 120 days. Most of the subtractions from year-old references are against data from the Maui 1.2m MSSS telescope. As of June 2002 we are just starting to reach areas of the sky which were covered in the late summer of 2001 with the Palomar 48” telescope.

1.5. Subtractions

Almost a decade of work has gone into our subtraction software, and it is continually being improved and rewritten. We use the same software to search for deep supernovae ($z \geq 0.5$) as is used to search for nearby supernovae.

Our subtraction software takes the lists of images for the given subtraction and separately registers (aligns) each of the images to a common reference system. The images to be used as a reference are then added together after they have all been shifted to line up with each other. The list of images to be searched is split into two parts, 'new1' and 'new2', so that we can have two search images to run checks to make sure a possible candidate isn't an asteroid or cosmic ray.

One important weakness is that our current software ability to register images to each other is not as robust as we might like and fails more often than it should, particular when matching images with little overlap or with very different effect exposure times. It was designed for images which were well matched to each other in both exact region of the sky and brightness of objects. Another difficulty is the presence of one bad image in the image stacks. Just one bad image will cause the subtraction to fail. A future project is to be able to run a quick quality verification on all of the images processed and loaded into our database before attempting to use them in a subtrraction. The average percent of successful subtractions for the first nine days of June 2002 was 56%.

Once we have our coadded reference, new1, and new2 images, we try to match the aggregate point-spread-function, or "seeing", of each to the coadded image with the worst seeing. The coaddition process itself does not take this into account because there is no benefit, but when taken a subtraction we want objects to subtract to zero. If we didn't account for the seeing we would end up with donut-like positive and negative shapes in our subtractions that would have a net value of zero, but it wouldn't be obvious to the eye and it's more difficult to design an object-recognition program to understand that. It's much cleaner to properly match up the PSFs of the image so that objects which are at equal brightness subtract to zero and new object show up as consistent with a point source according to the point-spread-function of the coadded image with the worst seeing. There are a variety of ways to do this. We currently use several Gaussians which are allowed to vary separately in x and y to model the kernel to represent the convolution between any two of the coadded images. This has the advantage of speed, but it doesn't do a good job in all cases. A big project for the second half of 2002 is to improve the calculation of these convolution kernels to clean up the subtractions. This should significantly reduce the number of false objects in the subtracted images.

Once the images have been matched through the convolution kernel, the coadded reference image is then separately subtracted from the two search images and then these subtracted images

are added together to generate a final subtracted image.

1.6. Automated Scanning

After the subtraction is completed, an automated scanning program is run which takes the full subtractions and looks for objects in them. We apply a variety of cuts to objects found in the subtraction to eliminate cosmic rays, asteroids, clearly bad subtractions, and a variety of other effects which we have observed over the years.

Everything up to this point is completely automated and runs daily without almost no human intervention.

1.7. Human Scanning

The automated scanner then passes a list of flagged candidates on to a human scanner who then looks at the subtracted, search, and reference images and decides whether or a not a computer-flagged candidates indeed appears to be a real, variable object.

We are currently running with a very conservative set of cuts and so have to scan $20 - -40\%$ of the succesful subtractions for each night. During the academic Spring 2002 semester we had a team of six undergraduates who would scan the subtracted images. By the end of the semester they had all been trained sufficiently so that they were keeping up with the rate of subtractions when they each worked a few hours a week.

However, many of the supernovae discovered this spring have been found using very restrictive cuts suitable for only having to scan a dozen or so images a night. This happened after the undergraduates stopped working for the semester and also after the number of subtractions attempted and completed was increased by considering matching reference and search images from almost anything we had available in the database instead of limiting ourselves to our ideal intervals.

1.8. Cross Checks

To check for known causes of variable objects which are not supernovae we perform a number of cross-checks:

1. Check for known asteroids (MPEC Minor Object Catalog)

2. Check for classification of object as star/galaxy (POSS/APM catalogs)

3. Check year-old references to check for long-term variable object (variable star, nova, i.e. not a supernova) (we use our own references in addition to DSS/POSS images)

4. Examine automatically generated lightcurve of candidate

1.9. Confirmation Image

Once we have something we are happy with, we submit it to the target list of the telescope for the next night of observation (our current turn-around time is 2-days, we will decrease that to just 1-day, i.e. the next night after the search image was taken, by later this summer). Once that data comes in, we prioritize the images and subtractions to look at that same region of sky to verify that the variable object is still there.

1.10. Supernovae found to date by this method

Seven supernovae have been found and accepted by the International Astronomical Union (IAU) using the techniques described above. The following IAU designations have been given for these supernovae:

Supernova	UT Date of Discovery Data	PST Date Discovered	UT Date Confirmed	Type
2002bk	2002/02/09	2002/02/26	2002/03/03	Ia
2002cq	2002/04/20	2002/04/23	2002/04/29	—
2002cx	2002/05/12	2002/05/15	2002/05/16	Ia/91T
2002cz	2002/05/17	2002/05/18	2002/05/09	—
2002da	2002/05/16	2002/05/17	2002/05/18	—
2002dg	2002/05/31	2002/06/01	2002/06/03	—
2002dh	2002/06/04	2002/06/06	2002/05/28	II

Table 1: Supernova discovered in the Spring of 2002. The official IAU name for the supernova is given, along with the date of the data the supernova was discovered on, the date the supernova was scanned by a person and “found”, and the date of the confirmation image. Note that the date of the “confirmation” image can be before that of the discovery image in cases where there were large delays or gaps in active human scanning. This is the case for 2002cz and 2002dh.

2. Assessment of *NEAT* Data

Figure 2 shows the seeing distribution obtained with the *NEAT* camera at Palomar over a 200 day period beginning in July 2001. The seeing distribution has a typical log-normal distribution, but with some evidence of instrumental truncation at the good seeing end. This may be due in part to undersampling by the 1.01″ pixels.

Figure 3 shows the distribution of sky brightness values measured from the *NEAT* images taken at Palomar. shows a median seeing of 19.1 mag/□″with an unfiltered CCD bandpass zero-pointed to R-band magnitudes from the USNO catalog. Oddly examination of the sky brightness with time did not show much evidence of the lunar cycle, although that remains the best explaination for the bright sky values. Note that some values are probably spurious, being moonlit nights with cirrus (the very brightest nights) or cloudy nights with clouds low and close to the summit (the very darkest nights).

Overall, the quality of the data from Palomar are roughly what we would expect for an automated facility with minimal data quality-control. We hope to be able to implement checks on the image quality using the LBNL PC at the telescope to provide feedback on, e.g., the focus.

3. From Detection through Observation

Figure 4 illustrates the steps from discovery of a candidate supernova through observations at the telescope. There are several components which will be discussed in turn.

3.1. *A priori* Classification

The *a priori* classification step seeks to eliminate several possible sources of contamination. First, one needs to consider the likelihood that the detection of variability is real, but that the variable is a star, AGN, or an asteroid moving very slowly. There is no doubt that the *SNfactory* will discover far more variable stars than are presently known. Even at the relatively bright limiting magnitude of ROSTE more than 85% of the variable objects are newly discovered variable stars. One great advantage of having two years worth of *NEAT* archival data prior the beginning of *SNIFS* observations is that for any candidate a historical lightcurve can be calculated to look for past variability. This is our best hope for eliminating variable stars and AGN, and such a capability has been implemented in the current proto search pipeline.

Another powerful diagnostic of variable stars is whether the new light is perfectly centered on an unresolved “host” One diagnostic to reject AGN is the location of the new light — if it is

exactly on the core of a galaxy *and* shows only weak variability (such as an increase of less than 15% over one month) it is likely an AGN. In these cases, knowing whether the "host" is classified as a star or a galaxy is valuable extra information. Currently this information can be obtained from the APS or APM surveys; in the future SDSS can provide this information. It is also possible to obtain such classification from the *NEAT* dataset itself. None of these resolution features have been implemented yet, but there are obvious paths for doing so.

Main-belt asteroids at quadrature, and many Centaur asteroids can exhibit motions slow enough that the motion is not detected over the typical 30 minute span of a trio of *NEAT* images Jedicke(1996). The surest way to eliminate such asteroids is to consult the Minor Planet Electronic Catalog webpage to see whether a candidate is a know asteroid. This capability has been implemented, but requires some refinement. The only inexpensive alternative is to obtain further images. *NEAT* is happy to take images of any of our candidates on subsequent nights — the question is whether *NEAT* or other sources can check an object the *same* night. An *a priori* asteroid probability can also be assigned based on whether the candidate is located near quadrature or not — maybe this region will have to be avoided.

Finally, as more galaxy redshifts become available we may reach a point where redshifts are known in advance for some reasonable fraction (10%) of candidate host galaxies. Based on such a redshift, we may eliminate candidates with redshift beyond the *SNfactory* target range. Additional host-galaxy information, such as knowing that the host is an elliptical — based on SDSS colors or fits to the luminosity profile from the *NEAT* data — will be helpful in discriminating between thermonuclear and core-collapse SNe.

3.2. *A priori* Priority

Those candidates whose *a priori* classification doesn't rule out a SN will be carried to the next stage — the assignment of an *a priori* observing priority. This can be based on a number of factors including observability. Observability criteria will include whether the field can be followed for 2—3 months from Mauna Kea, whether there is a guide star and sufficient surrounding field stars for relative calibration, whether the Galactic extinction is high or whether a bright star ruins the field, etc.

Some measure of *desirability* will also enter into the *a priori* priority. For instance, candidates in elliptical hosts will be highly desirable because they are almost certainty SN Ia, will suffer little or not extinction by dust, and will be useful in exploring the low-stretch/old-progenitor part of SN parameter space. Similarly, candidates in very low-luminosity galaxies will be desirable since they are likely to be lower metallicity SNe, somewhat more analogous to SNe Ia at higher redshift.

3.3. Scheduling

The next stage is to update the observing schedule for both new candidates and those confirmed SNe already being followed. Recalculation of the schedule is a continuous process, involving periodic updates in the days leading up to one of our UH nights, and updates after each observation during the period when we are actually observing.

A vast array of input information is useful for this purpose — after all, during the night of observing we are basically asking a computer to replace the decision making skills of a professional astronomer. It is unlikely that human oversight can ever be replaced, but it is certainly in our interests to have the computer hand as much of the routine and tedious work as is possible.

The scheduler will need to know of astronomical constraints and parameters (sunrise/set, moon location and brightness), mechanical constraints and parameters (telescope limits, slew times, typical pointing accuracy, detector readout times, acquisition overheads), environmental parameters (seeing, wind direction and speed, whether it is photometric or raining and foggy, weather forecast for next hours and days), etc. With these inputs the schedule will know how much time is available and the quality of the conditions in general and in different regions of the sky.

This information must then be coupled with our estimate of the expense and importance of observing the various SNe and SNe candidates. One key ingredient will be an exposure time calculator — this module should pre-calculate the expense of current and future observations of a given SN based on the current best estimate of SN distance, lightcurve phase, stretch, etc. (These will be unknowns for most knew candidates). It would be ideal if this were scale free, but in practice we will often be working at the transition from the object-dominated noise regime and the sky-dominated noise regime. This may not matter much provided all the exposure time calculations are done in advance for a wide range of scenarios. In this case the scheduler can simply chose amongst options like observing a bright SN in bright time so that a fainter SN can be observed in dark time.

There will obviously be a premium placed on finishing SNe which are already begun. Although not completely decided yet, it is probable that the emphasis will be on observing the active SNe well rather than obtaining poorer data on more objects. For one thing, set-up inefficiencies will favor doing fewer targets well. Also, for those SNe which are unusual, one usually wants enough detail to examine that SN's specific characteristics. Fighting against this are the $\sqrt{N}$ gains in getting more SNe for cosmological constraints, and the $\sim N$ gain of having more template SNe to match one-to-one against high-z SNe from CFLS and *SNAP*.

There will also be efficiency hits due to weather uncertainties. For instance, in a worse-case scenario where we have to assume that future nights will be cloudy, we would be forced to observe

our best SNe every clear night in order to try to minimize the size of any lightcurve gaps caused by weather. Indeed, this one of the main reasons why the efficiency impact of bad weather does not enter simple in proportion in the amount of bad weather. The alternative here is to just live with large gaps in the lightcurves — more simulation is needed to estimate the real impact this would have on the *SNfactory* science goals.

Clearly implementing the scheduler will be some combination of determining just how well a computer can do the job and honing our preferences and how they are presented to the scheduler software. Based on the schedule available at any given time, the script must be generated which can tell the telescope and *SNIFS* what activities to perform and when. The next section discusses these activities in more detail.

4. SNIFS Observations

The first step in the observation of a new target will be the acquisition of the field. This involves an initial open-loop pointing based on the candidate coordinates (good to a few tenths of an arcsecond), and then improvement of the pointing. The nominal pointing accuracy of the UH 2.2m is 6 arcseconds RMS, thus the typical open-loop pointing will place our targets off the microlens array. As seen on the imager, most targets will lie in the shadow of the pick-off-prism.

After the open-loop pointing, it will be necessary to secure a guide star so that no telescope drift occurs during the acquisition phase.

Once the guide star is secured, *SNIFS* will obtain a short image of the field — probably in a broadband filter, but possibly through the multifilter. This image will be compared to the *NEAT* discovery image (or previous *SNIFS* images) to *transfer* the location of the SN candidate on the discovery image to the location of the SN candidate on the acquisition image. This comparison involves Robert Quimby's QUICKMATCH code. While this comparison is going on, we may consider using the time to update the focus (using a method TBD). The transferred location of the SN candidate on the acquisition imager will be compared with the location of the shadow of the pick-off-prism (or its virtual location off the acquisition image) and an offset calculated and sent to the *guider software*. The guider will then move the telescope to the correct location.

Once the field is acquired and focused, the necessary spectral calibrations will be taken in order to accurately location the positions of the microlens spectra and determine their point-spread-function(s). In principle the calibration could be obtained immediately after the open-loop pointing so that the necessary mechanical operations can be executed during the slew phase. The drawback there is that any calibration is wasted if an acquisition fails completely (hopefully a very rare event!). The observing sequence is as follows:

- target ra, dec, epoch presented to telescope
- move telescope to target location
- ingests TCS info to check on location (HA, Dec, UT)
  - ◇ calculate offsets based on internal pointing model
  - ◇ send offsets
  - ◇ iterate
- rotate to correct auxiliary camera acquisition filter
- acquire star in guider camera
- if outdated focus, execute focus sequence (requires encoded focus & temperature)
- if current focus, check image quality and focus if needed
- begin guiding (monitor guiding / seeing / star flux)
- acquisition
  - ◇ auxiliary camera takes an image (30 sec readout)
  - ◇ optional overscan subtraction of auxiliary camera image
  - ◇ optional flatfielding (requires queued flatfield image)
  - ◇ surface auxiliary camera image
  - ◇ generate object catalog
  - ◇ X-match with input catalogs (requires NEAT or other object catalog)
  - ◇ calculate offsets
  - ◇ send offsets
  - ◇ ingest TCS info to check on location
- rotate to correct auxiliary camera science filter
- if all OK, start science exposures
  - ◇ flush CCDs
  - ◇ open imager/ifu shutter to telescope
  - ◇ close imager/ifu shutter to telescope
  - ◇ read out blue, red, and auxiliary detectors in parallel (80 sec)
- science exposure assessment
- calibration (as needed) for each arc, flat, x-calibration
  - ◇ turn on lamp X
  - ◇ flush CCDs
  - ◇ open shutter on calibration unit
  - ◇ close shutter on calibration unit
  - ◇ read out red, blue, and optionally auxiliary camera (40-80 sec)

According to the UH 2.2m TCS guide, the telescope maximum slew rates are 0.8°/sec in RA and 1.0°/sec in Dec. The dome rotates at up to 1.5°/sec. Typical slew times are 50 sec for 15°, 70 sec for 30°, 90 sec for 45°. Offsets require 2–4 seconds for 1-10″ and 7–10 seconds for 20-100″. The CCD readout time in acquisition mode should be well less than 30 seconds since readout noise is not an issue and the spatial scale is so fine that on-chip binning is sensible. The science exposures should be read more slowly in order to achieve the lowest readout noise. For

LBNL CCDs, a 40s readout (100 kpixels/sec) gives a readout noise of 3 e^-, while a 80s readout gives 2 e^- readout noise. The Marconi CCD is expected to have similar performance (the quoted readout noise of 1.9 e^- for our chip was measured at a readout of 45 kpixel/sec). It may be possible to execute faster readouts of the science CCDs for arc and possibly for flat calibration exposures. The times for movement of the filter wheel and calibration mechanisms are TBD. Note that some operations, such as calibration readouts and setups, can be performed in parallel with slewing of the telescope and dome. It also may be possible to perform focus checks while the acquisition data are being processed. It will be the job of the scheduling software to arrange such parallel operations.

To be implemented
Observation and calibration sequences
Emmanuel + Yannick

5. Global monitoring and data flow

It is envisioned that the amount of useful information that may need to be available for effective human intervention should problems arise during *SNIFS* observations is considerably more than one monitor can display, and that the information may need to arranged in unforeseeable ways such that scrolling through a status webpage would be ineffective. Thus, to make human intervention most effective, it may be necessary to consider setting-up command and control centers at the three institutions which simultaneously display a wider range information on multiple screens and which are equipped with tele- and video-conferencing capabilities with preprogrammed hot-lines to key UH sites and to the other institutions. One such station could be manned during normal nighttime operations of *SNIFS*— 5 hrs every 2nd and 5th night (daytime in France). One can envision displays for the UH 2.2m TCS; *SNIFS* mechanical, electronics and detector components; weather data and images; current data (acquisition images, spectra); *NEAT* reference data, guider seeing and transparency data, spectral classifier output and template fits, listing of the current schedule and execution status, schedular feedback, target sky locations and observing bounds, etc. If we attempt fast turn-around, status on the *NEAT* observations, the detection pipeline operations will also prove useful.

On top of monitoring and control facilities, the analysis of the overall information required to plan the observations will require a specific attention. At the core of the data flow will be the *scheduler*. It will collect information from *NEAT*, *SNIFS* and the different results of the data processing to be able to setup the *SNIFS* observation and send feed back to *NEAT* if needed. The relative weight of human and automatized intervention in the *scheduler* will evolve with time.

5.1. *SNfactory* running

In the first stage of the *SNfactory* development the effort will be put in the implementation of communication, monitoring , data transfer and control channels. Each of this four kinds of channel will have specific objectives and technical constraints. These channels will have to be setup between the different *SNfactory* sites and people involved :

- the *NEAT* observatory
- the *NEAT* data reduction center and SN candidate search
- the *SNIFS* instrument
- the *SNIFS* data processing center
- the *SNfactory* observers
- the *SNfactoryscheduler*

Communication channels

The goal of this communication channel will be to put the different people involved in the *SNfactory* data taking (*SNfactory* observers) in contact. Not only mail but also phone and multi-media video-conferencing will be implemented. On top of selecting the required software (see for example http://www.vrvs.org/) a central “phone book” with real time information (who is around, who is doing what, who is on-call for what...) will have to be implemented.

Monitoring channels

All the sites where data will be collected and processed will require a monitoring. The data transfer between the production and processing centers will also have to be monitored. In the implementation of the monitoring , special care on the readability of the informations and on the network or computing load will have to be taken into account. To be really useful and robust, a special care should be taken in the way the monitoring information will be distributed as many people at the same time, but from different sites, may want to access the same information. The remarks above is in favor to implement in each site a *monitoring data server* which will interact with the local monitoring to get the useful informations or collect itself this interesting information and will make it available for interrogation. Indeed when a problem is detected a direct interaction

(login on the site , browsing of files ...) with the local monitoring by the *SNfactory* observer(s) will be possible. To reduce the load on the monitored site and to have an universal access to the monitoring, this *monitoring data server* may use a web server do distribute its informations.

Control channels

The control of the systems in each sites will require action/interaction from the other sites / *SNfactory* observers. The control will require more care than the monitoring itself, to avoid for example contradictory requests. It will be considered than only a limited number of control channel for a given site can be open at the same time. For this last reason the software associated to this control channel will be less constrained from the point of view of computing resources and network band width than the pure monitoring operation. A special care will be taken in the development on the SNIFS control. A GUI interface allowing to control all the systems at UH will have to be developed. It will be possible to launch it from any site.

Data channels

Two main data channels are needed by the project :

- the data transfer from *NEAT* to the NERSC (the computer center at LBL)
- the data transfer from *SNIFS* to the CCIN2P3 (the french computer center)

Specific radio network link between the Palomar to the UC San Diego supercomputer has been setup and provide a network band width 10 times bigger than what is needed to transfer in realtime the 20 GB/night of *NEAT* data to the NERSC. This data channel is used with success in real condition since July 2001.
The amount of *SNIFS* data to transfer between UH and France is at least 10 time smaller than what is required for *NEAT*. Due to high energy physics collaboration on both side of the atlantic, high network capability exist between the CCIN2P3 and the US (up to 500 GB/day are transfered between SLAC and the CCIN2P3). Even with the limited band width between Hawaii and the French network access to the US, there is a factor 4 in the available network band width and the *SNIFS* data-flow. Test of the network stability as been performed for a few month and shows good result.

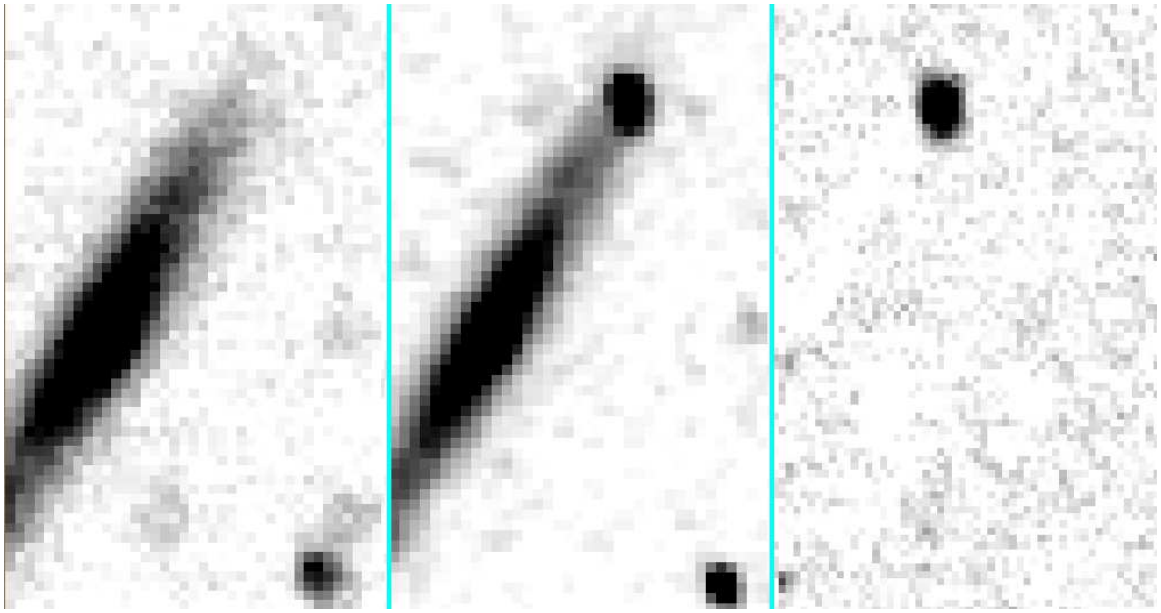

Fig. 1.— (a) A reference image shows an anonymous galaxy. (b) A search image shows the same galaxy with brighter region. (c) Subtracting the reference image from the search image yields a new object, which was confirmed to be a Type Ia supernova.

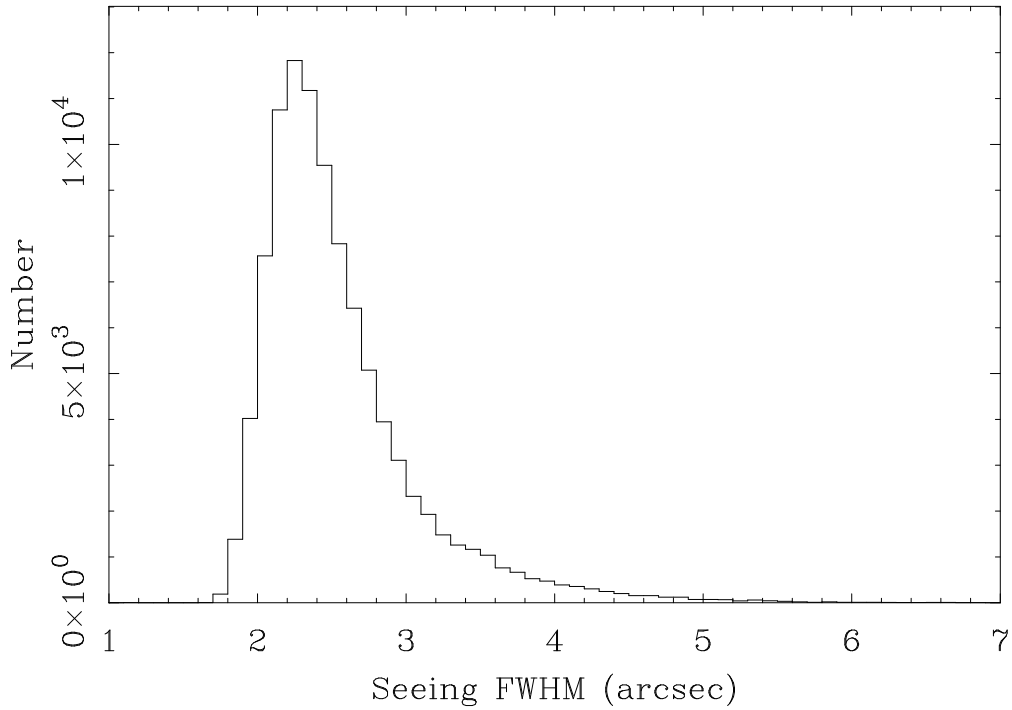

Fig. 2.— ***NEAT* seeing distribution at Palomar:** A histogram of seeing values measured from the *NEAT* images taken at Palomar shows a median seeing of 2.4″. The steep cut-off below 2″suggests the presence of some instrumental performance limits, and merits further investigation. It many be due in part to the pixel scale of 1.01″/pixel which will set a minimum image quality because of undersampling.

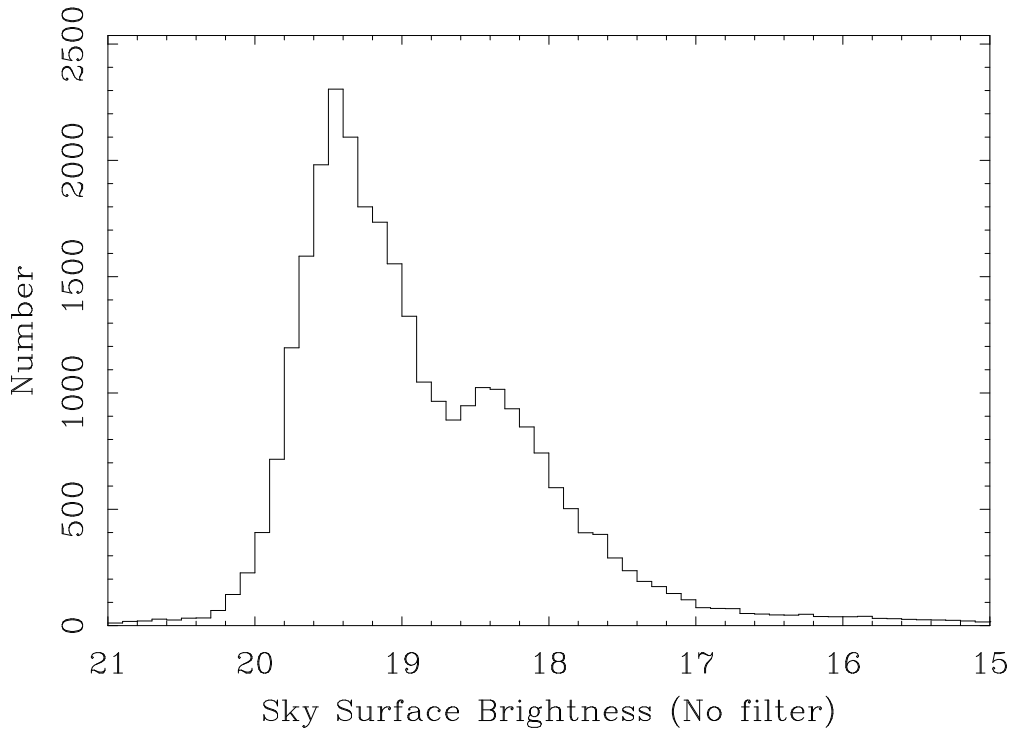

Fig. 3.— ***NEAT* sky brightness distribution at Palomar:** A histogram of sky brightness values measured from the *NEAT* images taken at Palomar.

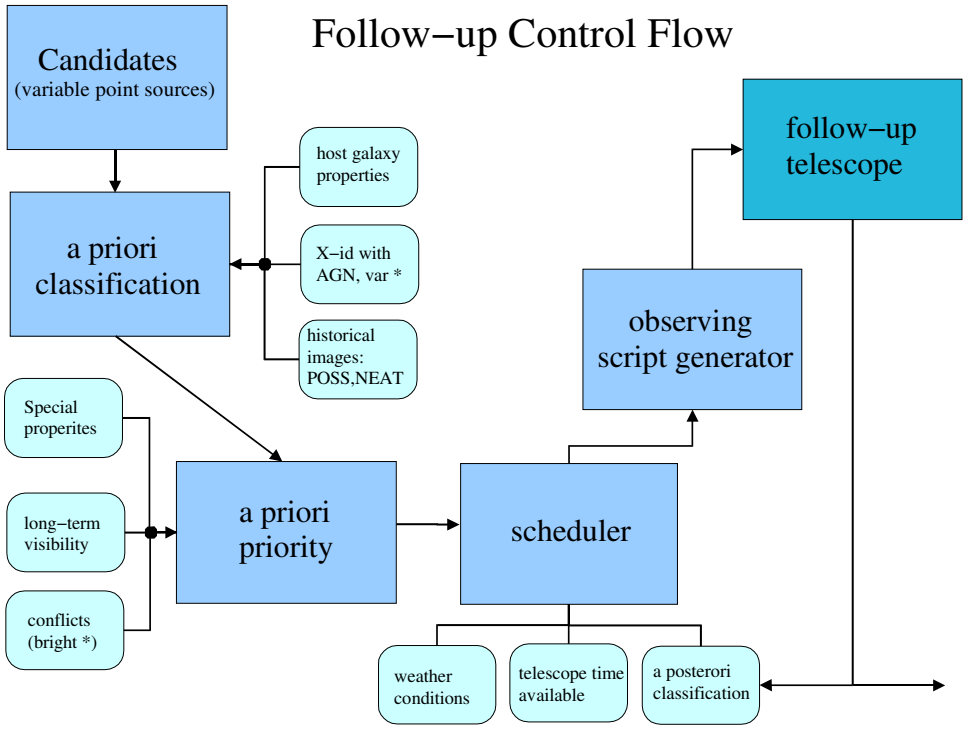

Fig. 4.— ***SNfactory* Processing from Discovery to Observation:** Search of a supernova candidate is but the first step before an object is cleared for follow-up observations. Indeed, although discovery of a variable object suggests a supernova, there are many other possibilities which must be eliminated if possible before valuable telescope time is dedicated to further observations. If a candidate passes all the tests and there is observing time available, the telescope (principally the UH 2.2-m) will be directed to observe the candidate with *SNIFS*. As the survey progresses we will learn a great deal more about variable objects, and this knowledge can be fed back into the process of target selection.

Chapter 6

Software and Data analysis

1. Computers and related hardware

1.1. *NEAT* related computing

The *SNfactory* operates a dual 1 GHz PIII PC at Palomar Observatory which operates as our interface between the NEAT data-taking computer and disk storage and the HPWREN wireless internet. There is 300 Gb of disk space serving as a data buffer in the event of interruption in the wireless connection. The data (currently roughly 50 Gb/night) are archived on the 2 Pbyte tape vault of the High Performance Storage System (HPSS). The *SNfactory* image processing of the NEAT data is performed on the 390+ node Parallel Distributed Systems Facility (PDSF) at NERSC. Our "share" is made up of 5 high bandwidth machines comprised of dual 1 GHz PIII processors with 2 Gbyte memory and three 0.5 Tbyte RAID5 disk vaults. Scanning of computer-detected candidates is performed using the network of ~ 15 desktop workstations used for general supernova research at LBNL.

1.2. *SNIFS* related computing

For the supernova follow-up spectrophotometry at the Hawaii 2.2m telescope, the telescope control is performed by a PII PC connected to I/O cards and a 3-axis Galil motion control card driving the two telescope axes and the dome axis via the original power amplifiers and motors. Data acquistion for the three CCD cameras at the UH 2.2-m will use one Linux PC per camera. The *SNIFS* instrument and the guider software will run on another PC, with all the PC's on one network. The ensemble of four PC's will be configured so that the duties of a defunct machine can be assummed by the other machines.

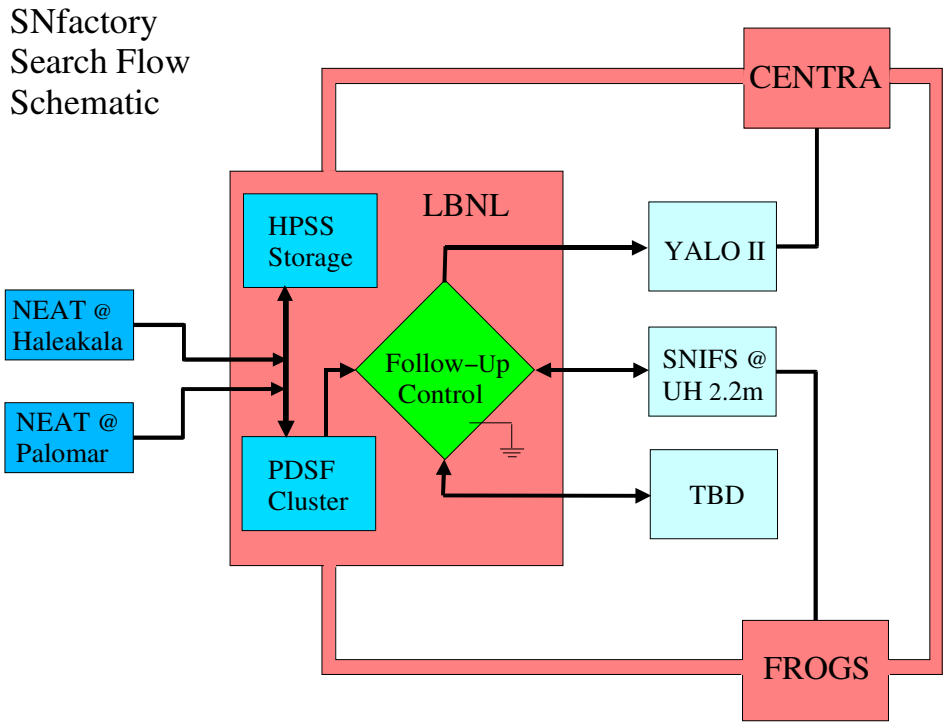

Fig. 1.— **Schematic of *SNfactory* Data and Information Flow:** All the collaborations share operational and science information through the salmon-colored "ground-plane." Imaging data for the search arrives from Palomar and Haleakala observatories and is archived at HPSS and processed at PDSF. A schedule of follow-up observations is sent to the follow-up telescopes and the schedule is executed. (See Fig. 4 of more details on the follow-up control.) The results of the observations are sent to the collaboration for processing, science analysis, and feedback into the follow-up control.

In France the spectral reductions, analysis, and archiving will use the the computing center at CCIN2P3. *SNIFS* raw data will be backuped with a double copy security in HPSS at the CCIN2P3. The data processing will use the linux farm facility of the computer center. The resources allocation will be controled to allow an "online" reduction of the *SNIFS* data when they will be collected. For processing *SNfactory* should be allowed to use when needed , up to 10 % of the linux farm (this 10 % corresponds today to 20 PIII 700 MHz and 20 PIII 1 GHz). For reprocessing more computing power could be requested if needed.

2. Detection Software

The data transfer from Palomar is implemented using PERL, while the data processing uses heritage C and C++ code from the Supernova Cosmology Project, with a small (and shrinking) amount of heritage *IDL* code. The image subtractions also use C and C++ with a human scanning interface implemented in *IDL*.
To be further implemented
Subtraction algo
Greg
The processed information is maintained in a *PostGres SQL* database. Effort is underway in coordination with the *SNAP* computing group to implement the processing pipeline in *OPUS* — a pipeline developed at the Space Telescope Science Institute and now in use on numerous space missions.

3. Scheduler software

Scheduling of the follow-up observations will be challenging, since the goal is to replace the observer at the telescope. In coordination with the *SNAP* computing group we will experiment with *SPIKE*. *SPIKE* is another space telescope product and has been in use for several years for space missions and the scheduling of ground-based telescopes. Other options include the *ASPEN* and *CASPER* packages from JPL (see http://casper.jpl.nasa.gov). Full environmental monitoring is being installed and linked to the telescope control system at the UH 2.2-m.

4. UH software

The telescope control software is provided by UH. A detailed description is available at www.ifa.hawaii.edu/88inch/TCS2. The target acquistion software is being written at LBNL — the field recognition stage is now complete and a Monte Carlo image simulator is in development. The guider software consists of DSP code supplied by GL Scientific.

5. SNIFS software

see the *SNIFS Technical Design Report* for a complete description of the SNIFS software.

To be implemented
Spectral resolution, spectra extraction (sky, SN, galaxy)
Yannick

6. Automated SN Classification

An automated SN classification program called `fitgtw` has been designed for use in the Supernova Factory. The program simultaneously finds the best fit SN template spectrum while subtracting host galaxy light over a range of redshifts.

Supernovae (SNe) are divided into four broad categories based on features in their spectra: Ia, Ib, Ic, and II. Type I SNe have no hydrogen lines, while the spectra of Type II SNe do show hydrogen. SNe Ia show Si near maximum light, while Ib and Ic SNe have no strong Si. Type Ib supernovae have strong lines of helium, while Type Ic SNe do not. Type II SNe can be further divided into IIn, IIb, II-L, and II-P. SNe IIn show narrow lines of hydrogen superimposed on a broader base, while SNe IIb show hydrogen at an early epoch which fades over the first few weeks after explosion, causing them to look like a Ib SN. Type II-L and II-P SNe are subdivisions of the Type II class based upon the appearance of the light curve. Type II-P SNe have a plateau in the light curve lasting for tens of days, while SNe II-L have a lineraly declining light curve. See Filippenko et al. (1997) for a review of SN spectra and classification.

There is considerable evidence that Type Ia SNe represent thermonuclear explosions of an accreting white dwarf (WD) in a binary system (Hoyle & Fowler 1960). All other SNe are believed to be the core collapse of single massive stars, though binary systems may play a role for some unusual core collapse SNe. It is thought that the amount of hydrogen and helium envelope left on the star at the time of explosion determines its subtype. SNe II-P have a large outer layer of hydrogen, while II-L have less, IIb have only a very small layer of hydrogen, Ib have no hydrogen but do have helium, and SNe Ic are bare stellar cores devoid of hydrogen and helium layers. The narrow lines in SNe IIn arise when the SN ejecta interacts with circumstellar material cast off by the last phases of mass loss of the progenitor star. For all types of SNe peculiar individual cases exist and are denoted by, ‘pec,’ as in IIpec.

Historically, identification of SN spectra has required a trained observer — one that has a working knowledge the spectra of hundreds of supernovae. This can lead to problems because such trained observers are often in short supply. Also, the eye is subjective, and human beings are slow – they can only classify on spectrum at a time. Here we introduce an automated SN classification system that is quantifiable, reproducible, and relatively fast.

6.1. General Approach

After experimentation with various classification schemes, including wavelet analysis and cross correlation, fitting of the observed SN to a library of template spectra was found to be the most accurate and robust method. The main principle behind the program, called `fitgtw`, is to minimize the square of the deviations between the input and template spectra. This is similar to a χ^2 fit, although errors are not usually used, since most SN spectra do not come with an associated error spectrum. Since observed SN spectra are often the combination of the intrinsic SN spectrum and the spectrum of its host galaxy, it is useful to minimize the difference between the observed spectrum and the combination of template SN and template galaxy light. A line of the form $y = a + bx$ may also be subtracted from the observed spectrum to correct for tilts that may arise from reddening or calibration errors. Each point may also be weighted by a different amount. Here we represent quantity to be minimized as S. The parameters which are varied to achive minimization are a, b, c, and d. Then, if the observed spectrum is O, the template SN spectrum is T, the galaxy spectrum is G, the wavelength is x, the weights are ω, and each of these are evaluated at each pixel i, then:

$$S = \sum_i \omega_i (O_i - cT_i - a - bx_i - dG_i)^2.$$

To minimize this function, we take partial derivatives with respect to each of the parameters to be minimized and get:

$$\frac{\partial S}{\partial c} = -2 \sum_i \omega_i T_i (O_i - cT_i - dG_i - a - bx_i)$$

$$\frac{\partial S}{\partial a} = -2 \sum_i \omega_i (O_i - cT_i - dG_i - a - bx_i)$$

$$\frac{\partial S}{\partial b} = -2 \sum_i \omega_i x_i (O_i - cT_i - dG_i - a - bx_i)$$

$$\frac{\partial S}{\partial d} = -2 \sum_i \omega_i G_i (O_i - cT_i - dG_i - a - bx_i).$$

If we define

$$[f] \equiv \sum_i \omega_i f_i,$$

and set the above equations to zero, we get:

$$\begin{pmatrix} [OT] \\ [O] \\ [xO] \\ [GO] \end{pmatrix} = \begin{pmatrix} [T^2] & [T] & [Tx] & [TG] \\ [T] & [1] & [x] & [G] \\ [Tx] & [x] & [x^2] & [Gx] \\ [TG] & [G] & [Gx] & [G^2] \end{pmatrix} \begin{pmatrix} c \\ a \\ b \\ d \end{pmatrix}. \tag{6.1}$$

This matrix is solved for the parameters a, b, c, and d. This is a specific implementation that works well, but methods have been tested that include no line subtraction, a linearly variable scale factor over the wavelength range, no galaxy subtraction, and other variations.

6.2. Program specifics

The preceeding section outlined the general method for the determination of the best match to a given SN template T using a given galaxy template G at a given redshift. The procedure must be iterated over all SN templates, all galaxy templates, and the entire specified redshift range. We will now discuss the specific program used to do this, `fitgtw`.

`Fitgtw` was written in IDL. At the command line a user can supply various keywords. These are:

- `o`: The observed SN spectrum.
- `w1`: The starting wavelength. If no starting wavelength is specified then the starting wavelength of the data is used.
- `w2`: The ending wavelength. If no ending wavelength is specified then the ending wavelength of the data is used.
- `disp`: The dispersion, or binning, to use in Angstroms. The default is 20.
- `zl`: The lowest redshift interval to search.
- `zu`: The highest redshift interval to search.
- `zi`: The increment to use when iterating the redshift.
- `weight`: A weight spectrum. For example, it is convenient to weight out strong night sky lines.

- `dir`: The directory for the results. If no directory is provided then the results are put into the same directory as the input spectrum.
- `gspec`: The spectrum of the host galaxy. If none is provided then a list of galaxy template spectra are used.
- `noline`: Switch to be set (e.g. /noline) to avoid subtracting a line from the data.

The program first reads in an ascii input spectrum and it is rebinned into bins of size `disp` so that it starts at wavelength `w1` and ends at `w2`. All templates and weight spectra are rebinned to the same binning. The input spectrum and all templates are scaled to have a median value of 1 over the input wavelength range.

Beginning at the starting wavelength specified by `zl`, the minimization routine is called for each SN template and galaxy template. The redshift is then incremented by `zi` and the templates are searched again. This procedure is repeated until the final redshift, `zu` is reached. For each SN template, the host galaxy template and redshift that produced the minimum valuse of the "goodness-of-fit" criteria, S, is recorded in the output file.

6.3. SN templates

SN templates are specified in an IDL save file. The templates can be changed by editing the file `templates.list` and running the IDL program `tempsetup`. The current template list has 161 SN templates, including 81 SN Ia templates from 8 different SNe spanning the full range of stretch over epochs from 14 days before maximum to 105 days after maximum. The more diverse set of Ib/c SNe has 75 representative spectra from 26 individual objects taken from Matheson et al. (2000). There is only one Type II supernova with 5 spectra.

6.4. Galaxy templates

If a host galaxy spectrum is supplied with the keyword `gspec`, then it is used in the procedure outlined above. Otherwise SN templates represending E, S0, Sa, Sb, Sc, SB1, SB2, SB3, SB4, SB5, and SB6 galaxies are used. SB1-6 are starbust galaxies. Like SN templates, galaxy templates are specified in an IDL save file. The templates can be changed by editing the file `gal.list` and running the IDL program `tempsetup`.

6.5. Weighting functions

A weight spectrum can be specified with the keyword `weight`. Some common weighting functions are `no77.weight`, which sets the weights of values near the strong 780 nm night sky line to zero, and `gmos.weight`, which gives zero weight to gaps in Gemini GMOS spectra. If errors exist for a spectrum, one should construct a weight function from the inverse of the variance. If no weight spectrum is specified then all weights are set to unity.

6.6. Run time

The run time of `fitgtw` varies greatly based on the number of templates used, whether or not a host galaxy spectrum is specified, the binning of the spectrum, and the redshift interval studied. For narrow redshift searches at $z = 0.1$ with a binning of 20 Angstroms, searching all galaxy templates, the program takes roughly 5 minutes to run on a Pentium 4 800 Mhz machine. More extensive searches of wavelength space, e.g. from $z = 0$ to $z = 1$ in increments of $z = 0.01$ can take several hours to complete.

6.7. Program output

The output is stored in a text file, which is given the root name of the input file with a `.out` suffix. The best fit SNe are listed in order, along with the value of S, the redshift, the galaxy subtracted, and the SN and galaxy scale factors derived. The template files are named such that the SN template filename gives the SN name and relative to maximum light, e.g. 'SN 1991bg.p01.dat' represents SN 1991bg at 1 day after maximum light.

6.8. Plotting the results

Plotting of the results is done with a second IDL program, `plotgtw`. It is necessary to give the plotting program the observed SN spectrum, the redshift, and the template SN spectrum to use. If an input galaxy spectrum is not given, the program tries all template galaxy files to find the best fit. The use of a second program for plotting allows minor tweaking of the inputs, for example the binning, or starting and ending wavelengths, without running having to rerun the `fitgtw` program again.

`Plotgtw` can take as input the following parameters, which are identical to those of `fitgtw: o, w1, w2, disp, weight, gspec,` and `noline`. It also takes the additional parameters:

- `z`: The redshift of the best fit.
- `psfile`: The name of the output postscript plot. If one is not specified, then no postscript is generated.
- `ymin`: The minimum value of the y-axis. If not provided, IDL defaults are used.
- `ymax`: The maximum value of the y-axis. If not provided, IDL defaults are used.
- `keep`: If set, data from the program is retained in separage output files. These have the same root name as the input file, with different extentions: `.obs` is the scaled, binned input observation used by the program. `.temp` is the scaled, binned SN template. `.gal` is the scaled, binned galaxy template, and `.sub` is the observation after the template galaxy has been subtracted.

6.9. Limitations

While `fitgtw` in general produces excellent results. If the input specrum is similar to one of the SNe in the template library, then the program will find the best match without fail. One limitation is that the program will only attempt a match for those templates that overlap the input spectrum in wavelength space. This means that at low redshift, for most supernovae, more than 100 templates are compared to the input. At high redshifts, only those SNe with ultraviolet spectra are compared. This limitation is necessary to ensure that the "goodness-of-fit" criteria, S, has the same meaning from template to template. This limitation will not be a problem for the SN factory where only $z < 0.2$ SNe will be studied.

Comparisons are also limited by the quality and completeness of the template library. While this is constantly being improved by the addition of new templates, the best solution is to observe a wide range of SNe during the early days of the SN factory to ensure a consistent data set with full wavelength coverage.

A final limitation is that extinction is not properly treated in the version of the program outlined here. However, Lifan Wang has created an program based upon the same principles that treats extinction with a better approximation. This improvement will be added to future versions.

`Fitgtw` was designed to be flexible enough to use at high and low redshift. When it is incorporated into the SN Factory reduction pipeline, it will be trivial to modify it for the specifics of low redshift SN Factory data.

Chapter 7

Project Timeline and Management

1. Timeline

The *SNfactory* began in mid-1999 after the highly successful nearby search and follow-up program carried out by the Supernova Cosmology Project in the spring of 1999. Following several months of discussions, France joined the projected (with official agreement reached in Jan 2001) and planning for *SNIFS* was begun. Tentative agreement with University of Hawaii on the use of the 2.2-m was reached in fall 2000, and was finalized in summer 2001. Work on exploring how to establish the necessary telecommunications with Palomar Observatory was begun in summer 2000, and the installation of wireless internet was completed in summer 2001. *SNIFS* is now in the construction phase, with completion expected in early 2003. Full operation of the *SNfactory* will begin a few months thereafter, once the instrument is shipped to Hawaii and installed at the UH 2.2-m. In the meantime, the software pipelines for searching and data reduction and analysis are being written.

The top-level milestones for the project are enumerated in Table 1, while construction milestones are given in Table 2. The project timetable is driven by more than our eagerness to understand dark energy. First, the *SNfactory* has a unique window of opportunity to use the UH 2.2-m before it is torn down to make room for a larger telescope; second, the *SNfactory* needs to have results for use by the upcoming ground-based programs; and finally, we want *SNfactory* in time to serve as input into the final mission planning for *SNAP*.

Table 1: *SNfactory* Major Project Milestones

Date	Milestone
Summer 1999	Project inception
Spring 2003	*SNfactory* operations begin
Spring 2006	Discovery stage completed (final refs continue)
Spring 2007	Observing operations completed
Spring 2008	Analysis operations completed

Table 2: *SNfactory* Project Construction Milestones

Date	Milestone
Summer 2000	*SNIFS* conceptual design begun
Summer 2001	Agreement for use of UH 2.2-m reached
Summer 2001	Palomar telecommunications established
Fall 2001	Preliminary search pipeline operational
Summer 2002	Preliminary spectral reduction pipeline operational
Summer 2002	Final search pipeline operational
Fall 2002	Completion of *SNIFS* CCD cameras
Fall 2002	Completion of *SNIFS* optical fabrication
Winter 2003	*SNIFS* integration & test (Lyon)
Winter 2003	Final data reduction pipeline operational
Spring 2003	*SNIFS* integration & test (Hawaii)

2. Management

Greg Aldering (LBNL) serves as the *SNfactory* Project Leader. The *SNfactory* Executive Committee, comprised of Greg Aldering, Reynald Pain (spokesperson of the French consortium) and Saul Perlmutter (LBNL), oversees and coordinates the overall effort. In France, Emmanual Pecontal serves as the *SNIFS* Project Scientist. Jean-Pierre Lemmonier serves as *SNIFS* Project Manager and Pierre Antilogus serves as the Computing Scientist. At LBNL, Stewart Loken serves as Supernova Factory Project Manager with responsibility for schedule and budget. He also serves as liaison with the LBNL Computing Sciences Directorate which includes the NERSC computing facilities as well as the computer science and software engineering programs. There are two monthly technical meetings, one on instrumentation and one on software. In addition, there is an annual collaboration meeting and frequent face-to-face meeting of group members as part of other

conferences and workshops.

Chapter 8

Conclusion

The *SNfactory* will revolutionize all phases of experimental work on supernovae. The rate of discovery for Hubble-flow supernovae will exceed the current rate by an order of magnitude, the discovery biases will be lessened (and traceable), and the quality and quantity of follow-up data will exceed that of current programs by a large factor. With such data, it is expected that great strides can be made in improving supernovae as cosmological distance indicators. In addition, the *SNfactory* study of the peculiar velocities of supernova host galaxies should provide strong dynamical constraints on the value of Ω_M.

REFERENCES

N. Arkani-Hamed et al., Phys. Lett. B **480**, 193 (2000) 1

Baggett W. E., Baggett S. M., Anderson K. S. J.; AJ, **116**, 1626 (1998). 4.2, 6

Bely P.; PASP, **99**, 560 (1987). 4.5

R. Caldwell, R. Dave, and P.J. Steinhardt, Phys. Rev. Lett. **80**, 1582 (1998) 1

Colley, W. N., Gott, J. R. I., Weinberg, D. H., Park, C., & Berlind, A. A., Ap. J., **529**, 795 (2000). 5, 4

Cross, N. & Driver, S. P., MNRAS, **329**, 579 (2002). 2.1

S. Courteau & A. Dekel, "Astrophysical Ages and Time Scales," ASP Conf. Series 245, ed. T. von Hippel, N. Manset, and C. Simpson (2001). 4

Filippenko, A. V., 1997, ARA&A, 35, 309

M. Hamuy *et al.*, Astron. J., **112**, 2391 (1996). 3, 4.1

Horne K., PASP, **98**, 609 (1986). 4.4

Hoyle, F., & Fowler, W. A. 1960, ApJ, 132, 565

Jansen, R. A., Fabricant, D., Franx, M., & Caldwell, N., ApJ Suppl., **126**, 331 (2000). 1

Jedicke, R., Astron. J., 111, 970 (1996). 3.1

Knop, R. A., and the Supernova Cosmology Project, *in prep.*. 2

Matheson, T., Filippenko, A. V., Li, W., Leonard, D. C., Shields, J. C. 2001, AJ, 121, 1648

A. G. Riess *et al.* Astron. J. **116**, 1009 (1998). 1

L. Silberman, A. Dekel, A. Eldar & I. Zehavi, Ap. J. **557**, 102 (2001). 4

S. Perlmutter *et al.*, Ap. J. **483**, 565 (1997). 1, 4.1

S. Perlmutter *et al.*, Nature **391**, 51 (1998). 1

S. Perlmutter *et al.*, Ap. J. **517**, 565 (1999). 1, 1

Phillips, M. M., Lira, P., Suntzeff, N. B., Schommer, R. A., Hamuy, M., & Maza, J. ; Astron. J., **118**, 1766 (1999). 2

Rocca-Volmerange, B. & Guiderdoni, B.; A&A Supp., **75**, 93 (1988). 4.2, 5

Umeda, H., Nomoto, K., Yamaoka, H., & Wanajo, S. 1999, ApJ, 513, 861 3

I. Zlatev, L. Wang and P. J. Steinhardt, Phys. Rev. Lett. **82**, 896 (1999) 1

List of Figures

1 Cosmological constraints from Type Ia supernovae 10
2 The importance of low-redshift SNe Ia for near-future dark energy probes 13
3 The importance of low-redshift SNe Ia for next-generation dark energy probes . . . 14
4 Photometric and Spectral Time Evolution of Type Ia supernovae 17
5 Gravitationally-induced peculiar velocities 20

1 Distribution of host luminosities for SNe Ia 25
2 Relative error contributions with redshift 27
3 Luminosity function and SN Ia rate 28
4 *NEAT* sky coverage 29
5 Galaxy and sky spectra 30
6 Galactic surface brightness 31
7 Sky spectra for different conditions 32
8 SN Ia/galaxy/sky relative contributions 33
9 Influence of the host galaxy characteristics on the S/N spectrum 38
10 Influence of the SN Ia parameters on the S/N spectrum 39
11 Influence of the observing conditions on the S/N spectrum 40

1 Telescope Facilities Participating in the *SNfactory* 42
2 Measured QE of LBNL red-enhanced CCD 46

3 Mock-up of *SNIFS* spectrograph . . . 48

4 Spectroscopic channel transmission . . . 50

5 Transmission details . . . 51

6 Photometric channel transmission . . . 52

1 The extinction, in magnitudes per airmass, typical of Mauna Kea. . . . 59

2 The variation in the Ångstrom aerosol extinction parameter . . . 61

3 The frequency distribution of water vapor typical of Mauna Kea. . . . 62

4 Representative Mauna Kea water vapor monitor readings, from CSO. . . . 63

5 Histogram of Ozone over Mauna Loa . . . 64

6 Illustration of the filters that cover the field of view during the SN spectrum measurement. The large red "●" indicates a SN under study; the 50 smaller "⋆" indicate stars used to measure the atmospheric extinction fluctuations. The seven bands are the filters with responses shown at the bottom of Figure 7. . . . 70

7 Top shows the extinction functions $k_i(\lambda)$ for: Rayleigh (thick), aerosols (dashed), water (0.8-1.0 μm), O_2 (narrow peaks at 0.69 and 0.75 μm) and O_3 (broad peaks at 0.3 and 0.6 μm). The bottom plot shows the responses of the seven filters used in this study. . . . 71

8 RMS of atmosphere transmission measurement vs. λ. The top plot compares the RMS for 7 vs. 5 filters; the seven filters are shown in the bottom plot of Fig. 7 and the result with five filters excludes the filters centered at 0.50 and 0.85 μm. Bottom plot compares the RMS when the a_i are drawn from gaussians with 5 and 10% width. . . . 72

9 The spectrum of an NIST-calibrated FEL lamp . . . 81

10 Possible layout for a multicolor extinction imaging filter. . . . 81

1 (a) A reference image shows an anonymous galaxy. (b) A search image shows the same galaxy with brighter region. (c) Subtracting the reference image from the search image yields a new object, which was confirmed to be a Type Ia supernova. . . 99

2 *NEAT* seeing distribution at Palomar . . . 100

3 *NEAT* sky brightness distribution at Palomar . . . 101

4 *SNfactory* Processing from Discovery to Observation 102

1 Schematic of *SNfactory* Data and Information Flow 104

List of Tables

1 *NEAT* Search Facilities 28

2 Spectro-photometric observation strategy #1 35

3 Spectro-photometric observation strategy #2 36

1 UH 2.2-m: Monthly Time Lost 43

2 Current specifications of *SNIFS* 56

3 POSS I B-band Star Counts at High-Latitude 57

1 Extinction components per airmass at various wavelengths 65

1 Supernova discovered in the Spring of 2002. The official IAU name for the supernova is given, along with the date of the data the supernova was discovered on, the date the supernova was scanned by a person and "found", and the date of the confirmation image. Note that the date of the "confirmation" image can be before that of the discovery image in cases where there were large delays or gaps in active human scanning. This is the case for 2002cz and 2002dh. 90

1 *SNfactory* Major Project Milestones 114

2 *SNfactory* Project Construction Milestones 114